Identification and Quantification of Environmental Radionuclides and the use of Monte Carlo Codes for Gamma-ray Detector Optimisation

Mistura Bolaji Ajani

A thesis submitted to the Faculty of Science, University of the Witwatersrand, Johannesburg, in fulfilment of the requirements for the degree of Doctor of Philosophy,

September, 2020

School of Physics

University of the Witwatersrand

Identification and Quantification of Environmental Radionuclides and the use of Monte Carlo Codes for Gamma-ray Detector Optimisation

Mistura Bolaji Ajani

Ph.D. thesis

Supervisor

Prof. I. T. Usman

School of Physics
University of the Witwatersrand, Johannesburg

Co-Supervisor

Dr. P. P. Maleka

Department of Subatomic Physics

iThemba Laboratory for Accelerator Based Sciences, Cape Town

Declaration

I, Ajani Mistura Bolaji, hereby declare that this research is my original work which to the best of my knowledge has not been submitted to any other university for the purpose of awarding a degree. Where the work of other authors has been used, they are duly acknowledged in the form of references.

_____

Signature

_____

Date

Abstract

The study to determine the radioactivity levels and elemental concentrations of soil samples collected in Chad was undertaken. The objective was to ascertain possible contribution to the enhancement of naturally occurring and/or man-made radionuclides, including toxic heavy metals in the area. Moreover, the HPGe gamma-ray counting system was efficiency calibrated using standard sources and verified by Monte Carlo simulations to correct for the summing effect. A low background Hyper Pure Germanium detector was used to determine the radioactivity levels in 20 soil samples collected from Chad in Central Africa. The following radionuclides, ^{238}U, ^{235}U, ^{232}Th, ^{137}Cs and ^{40}K were identified and their activity concentrations were determined. The results show that samples S1-S16 with an average activity concentration range of 2.4 to 35.3 Bq/kg is lower compared to sample S17-S20 with range of 130.9 to 239.3 Bq/kg for ^{235}U. For ^{232}Th and ^{40}K, the observation was not similar to the trend as shown with ^{235}U. The distribution of activity concentrations in the samples were found to be relatively lower in sample S1-S16 while sample S17-S20 were found to be relatively higher. Additionally, the results obtained for ^{238}U, ^{232}Th and ^{40}K were compared with the world average value 35, 30 and 400 Bq/kg, respectively, specified by UNSCEAR (2000). In order to evaluate the radiological hazard of the natural radionuclides, the radium equivalent activity, external and internal hazard indices, annual effec-

tive dose equivalent (AEDE) and excess lifetime cancer risk (ELCR) have been calculated with average of 111 (Bq/kg), 0.30 and 0.54, 0.41 (mSv/y) and 1.42 ($\times 10^{-3}$) respectively. Correlation between ^{238}U vs ^{232}Th, ^{40}K vs ^{238}U, and ^{40}K vs ^{232}Th were investigated, the result showed good correlation for ^{238}U vs ^{232}Th and ^{40}K vs ^{238}U while ^{40}K vs ^{232}Th gives poor correlation. From the 20 samples collected in Chad, 10 samples were selected for further analysis using Inductively Coupled Plasma-Mass Spectrometry (ICP-MS). The uranium and potassium results were correlated with the data from gamma-spectroscopy and the uranium were found to have strong positive correlation while potassium have poor correlation. ICP-MS analysis revealed the presence of various toxic elements, Cu (3-225 mg/kg), Mo (0.15-15.50 mg/kg), Co (1-35 mg/kg), Sn (0.29-8.89 mg/kg), Sb (BDL-1.01 mg/kg), Se (0.04-0.44 mg/kg), As (0.41-6.09 mg/kg); U (0.19-64.37 mg/kg); Pb (4-59 mg/kg); Cd (0.004-1.896 mg/kg) and Hg (0.07-5.57 mg/kg), respectively. Some of the elemental concentrations for Cu, Mo and Hg were higher than the Maximum Allowable Limit (MAL) for some samples, while others were within the safe limit. The observed Hg with average of 2 mg/kg was found to be higher than the FAO/WHO recommended/safe limit of 0.93 mg/kg. To validate the experimental results due to coincidence summing effect and efficiency calibration, GEANT4 and FLUKA Monte Carlo codes were utilised to test these parameters. For the full-energy peak efficiency, the following reference sources ^{40}K, ^{22}Na, ^{137}Cs, ^{60}Co and ^{152}Eu were used, while both the ^{60}Co and ^{22}Na were further employed to validate coincidence summing corrections. This comparison shows how two different Monte Carlo codes agree with experimentally obtained efficiency of the detector and ultimately applied GEANT4 for coincidence summing corrections. Also, coincidence summing correction factor were calculated for

both ^{238}U and ^{232}Th using EFFTRAN software and the correction factors show 65-100% confidence level.

Dedication

This thesis is dedicated to my late father Ajani Rafiu Owoyemi. Dad, you left without seeing me achieve my doctoral degree as you would have loved to. For all you laboured and strive for has come to reality. I am sure you are proud and happy wherever you are now. I miss you so much Dad. Continue to rest in peace. I love you!!!

Acknowledgements

I thank Almighty Allah for my life and for seeing me through all the challenges I encountered during the course of this research.

My sincere appreciation goes to Prof. Iyabo Usman, who encouraged and motivated me throughout the duration of this research. She took me like her daughter and provided the necessary supports; financial, moral and physical supports. In fact, your efforts made were of great importance in making this research a success, "*Jazakumullah Khaira*".

Also, to my Co-supervisor Dr. Peane Maleka for his constant constructive criticism. He never for once got tired of me even when I had many shortcomings. He made sure I got the necessary support and motivation to aid my work, "*Ke ya leboga*".

My gratitude also goes to University of the Witwatersrand for the Postgraduate Merit Award (PMA) and NRF-iThemba LABS for providing Top-up funds. This went a long way in supporting me financially.

To my environmental radiation group Avuyile Bulala, Refilwe Setso and Sizwe Mhlongo and all my iThemba LABS colleagues I couldnt mention their names. You are all appreciated.

My university colleague Dr. Sunday Olorunfunmi thanks for always helping me sort things out from the University, and Samafo Penabei thanks for getting the

samples for me.

Much appreciation to my mentors Dr. Maboob Adekilekun and Alhaji Jimoh Kehinde Adekilekun for their moral support. I am also indebted to Prof. Pedro's family for their guidance and spiritual supports. Also to my lovely friends Modupe Adebawo and Pheladi Molema who provided supports when I needed them. Thanks a lot.

And to the family of Usman, Maryam and Mardiya for always giving me a warm reception each time I visited. I really appreciate all you do for me.

To my lovely mother Taiwo Kudirat Ajani, my siblings Aishat Bolade Ajani, Maimunat Yetunde Ajani, Hameed Eniola Ajani and Abdulrafiu Adekilekun Ajani. Thank you for the supports. I could not have done this without you.

Last but not the least, my loving husband Omoyemi Hameed Babarinde for his patience and encouragement during difficult times and my adorable son Faahiz Akorede Babarinde who served as source of inspiration during this research. I love you !!!

Contents

Declaration ii

Abstract iii

Dedication vi

Acknowledgements vii

List of Figures xxiii

List of Tables xxv

1 Introduction 1

1.1 Background 1

1.2 Problem Statement 3

1.3 Naturally Occuring Radioactive Materials 3

1.4 Radiometry 5

1.5 Heavy Element Detection Technique 6

1.6 Monte Carlo Methods 6

1.7 Aim and Scope of the Study 7

2 Theoretical Aspects 10

2.1 Natural Radioactive sources 10
2.1.1 Radiation Concentration and Exposure 15
2.2 Radioactive Decay Modes 16
2.2.1 Alpha Decay 16
2.2.2 Beta Decay 18
2.2.3 Gamma Decay 23
2.3 Decay Chains of ^{235,238}U, ^{232}Th 23
2.4 Radioactive Equilibrium 29
2.4.1 Transient Equilibrium 29
2.4.2 Secular Equilibrium 30
2.4.3 Non-Equilibrium Decay 30
2.5 Law of Radioactive Decay 31
2.5.1 Bateman Equation (BE) 33
2.6 Interactions of Gamma-rays with Matter 34
2.6.1 Photoelectric Absorption 35
2.6.2 Compton Scattering 38
2.6.3 Pair Production 40
2.6.4 Gamma-rays Attenuation 42
2.6.5 Attenuation Correction 44
2.7 Gamma-ray Detection 45
2.8 Coincidence Summing Process 46

3 Monte Carlo Methods **50**

3.1 Introduction 50
3.2 Monte Carlo Method for Radiation Transport 51
3.3 Monte Carlo Code: GEANT4 54

3.3.1 Physics List . . . 58
3.3.2 Primary Particle Component . . . 60
3.3.3 Environmental Radioactivity Laboratory Detector System Setup . . . 61
3.3.4 Reproduction of Source . . . 64
3.4 Monte Carlo Code: FLUKA . . . 64
3.4.1 Extracting Information from FLUKA . . . 68

4 Experimental Setup **69**
4.1 Sample Collection and Preparation . . . 69
4.1.1 Study Area and Sample Collection . . . 69
4.1.2 Sample Preparation . . . 72
4.2 HPGe Gamma-ray Detector System . . . 73
4.3 Gamma Spectroscopy Data Analysis . . . 77
4.3.1 Energy Calibration . . . 77
4.3.2 Determining the Full Energy Efficiency . . . 79
4.3.3 Background Counting . . . 82
4.3.4 Activity Concentration Calculation . . . 84
4.4 Estimation of Radiation Protection Quantities . . . 85
4.4.1 Gamma Dose Rate . . . 86
4.4.2 Activity Concentration of $Ra_{equivalent}$ (Ra_{equ}) . . . 86
4.4.3 External Hazard Index . . . 87
4.4.4 Internal Hazard Index . . . 87
4.4.5 Annual Effective Dose Equivalent (AEDE) . . . 87
4.4.6 Excess Lifetime Cancer Risk (ELCR) . . . 88
4.5 Inductively Coupled Plasma Mass Spectrometry Overview . . . 88

4.6 ICP-MS Sample Preparation 90
4.7 Benchmark Tests 91

5 Results and Discussion **93**
5.1 Monte Carlo and Experimental Results: Benchmark Exercise . . . 94
5.1.1 Coincidence Summing corrections (GEANT4) 94
5.1.2 Comparison of Experimental Data with GEANT4 and FLUKA 100
5.2 Radionuclide Identification and Quantification: HPGe 104
5.2.1 Activity Concentration 105
5.2.1.1 Activity Concentration of ^{238}U 106
5.2.1.2 Activity Concentration of ^{232}Th 118
5.2.1.3 Activity Concentration of ^{235}U, ^{137}Cs and ^{40}K . . 130
5.2.1.4 Summary of Activity Concentration 132
5.2.2 Correlations of Activity Concentration of ^{238}U, ^{232}Th, ^{40}K 133
5.2.3 Radiation Health Risk Assessment 135
5.3 Elemental Concentration: ICP-MS 137
5.4 Comparison of ICP-MS and HPGe Data: U and K 141

6 Conclusion and Future Work **144**
6.1 Conclusion 144
6.2 Future Work 146

Appendices **148**

A Gamma-ray Transitions and Data Analysis **149**

B Elemental Analysis Data **153**

Bibliography 158

List of Figures

1.1 Sources of radiation 2

2.1 Decay scheme of ^{40}K showing the singel emitting energy and the daughter nuclides formed during beta-minus (β^-) and Electron Capture (EC) decay processes 14

2.2 The inverse relationship between alpha decay half-life and decay energy illustrated for even-Z and even-N nuclei 18

2.3 Production of Characteristic X-ray emission and electron capture from K-shell 22

2.4 Schematic decay chain of ^{238}U (4n+2). The weak decay branches are from ^{218}Po, which decay by beta through ^{218}At to ^{218}Rn, also the daughter nuclides decay alpha back to the main chain. The grey shaded circles indicated gamma-ray emitting radionuclides and the blue shaded circle are radionuclides in gaseous form. 26

2.5 Schematic decay chain of ^{235}U (4n+1). From ^{231}Th nuclides seen above, there is a weak decay branch, which may decay by alpha into ^{227}Ra before decaying beta back to main branch. The grey shaded circles indicated gamma-ray emitting radionuclides and the blue shaded circle are radionuclides in gaseous form. 27

2.6 Schematic decay chain of ^{232}Th (4n). The nuclides in the decay chain will be in the samples that contain thorium, but if the samples is left to undergo an equilibrium for a long time with ^{232}Th, then the ^{220}Rn may escape the sample as it's a noble gas. The grey shaded circles indicated gamma-ray emitting radionuclides and the blue shaded circle are radionuclides in gaseous form. 28
2.7 Example of the β^- decay of ^{210}Bi into ^{210}Po which corresponds to a relative activities of parent and daughter nuclides undergoing the non-equilibrium decay process 31
2.8 Schematic diagram of photoelectric absorption mechanism 36
2.9 Linear attenuation coefficient of a materials relevant to gamma-ray spectrometry as a function of gamma-ray energy 37
2.10 Schematic diagram of Compton scattering mechanism 40
2.11 Schematic diagram of pair production mechanism and annihilation. 41
2.12 The three important γ-ray interaction processes 42
2.13 Schematic diagram of decay scheme for ^{152}Eu 47
2.14 Schematic Decay scheme of a nuclide decaying from X to Y 49

3.1 A schematic diagram showing workflow of radiation transport applied in Monte Carlo simulations 53
3.2 Simplified flow chat of GEANT4 simulation 55
3.3 A screenshot of GEANT4 display ran on Ubuntu-16 operating system 56
3.4 A screenshot of material definitions during GEANT4 simulation. . 57
3.5 A screenshot of how the photon interactions are defined 59
3.6 A screenshot of Boson-Lepton particles constructor definitions. . . 59
3.7 This illustrates how the General Particles Source (GPS) is defined 61

3.8 Acquired image of HPGe dectector constructed with GEANT4 . . 63
3.9 A screenshot diagram showing how the geometry was constructed 63
3.10 HPGe detector geometry surrounded with Lead shielding constructed using FLUKA code. 66
3.11 Example of geometry specifications used in FLUKA. 67
3.12 Screen shot assigning materials to various regions in FLUKA. . . 67
3.13 Screen shot illustrating the Physics list used in FLUKA. 67

4.1 Schematic diagram illustrating the spacing between the composite sampling points. 71
4.2 Map of sample collection location. 72
4.3 Sample preparation process used for this study. 73
4.4 Schematic diagram of Hyper-Pure Germanium detector setup, showing the electronics accessories. 76
4.5 Experimental set-up for Environmental radioactivity laboratory HPGe detector system. 76
4.6 HPGe detector with liquid nitrogen cross-section diagram 77
4.7 Energy versus channel relationship for energy calibration using ^{232}Th standard source 79
4.8 Full energy peak efficiency curve from ^{238}U, ^{232}Th and ^{40}K reference source. 82
4.9 A background spectrum measured with empty lead castle (closed) for 3 days 83
4.10 Schematic diagram of ICP-MS 90

5.1 Measured and simulated spectra with coincidence summing using ^{60}Co point source placed at a surface of the detector. 96

5.2 Measured and simulated spectra with coincidence summing using ^{22}Na point source placed at a surface of the detector. 96
5.3 Corrected simulated spectra without coincidence summing, using ^{60}Co point source. The source was placed at -20.5 cm from the surface/front of the detector as to observe the effect of additional peak due to coincidence summing. 97
5.4 Corrected simulated spectra without coincidence summing, using ^{22}Na point source. The source was placed at -20.5 cm from the surface/front of the detector as to observe the effect of additional peak due to coincidence summing. 98
5.5 Simulated and measured spectra using ^{152}Eu point source placed at surface of the detector. 99
5.6 Top: shows the GEANT4 simulated and measured spectra for ^{60}Co point source ; Bottom: shows the FLUKA simulated spectra for ^{60}Co point source. 102
5.7 Experimental (blue), GEANT4 (red) and FLUKA (green) full energy peak efficiency as a function of gamma energy. 104
5.8 Sample S1: Activity concentrations as function of gamma-ray energy for various radionuclides (^{234m}Pa, ^{226}Ra, ^{214}Bi and ^{214}Pb) in the ^{238}U series. 108
5.9 Sample S2: Activity concentrations as function of gamma-ray energy for various radionuclides (^{234m}Pa, ^{226}Ra, ^{214}Bi and ^{214}Pb) in the ^{238}U series. 108

5.10 Sample S3: Activity concentrations as function of gamma-ray energy for various radionuclides (^{234m}Pa, ^{226}Ra, ^{214}Bi and ^{214}Pb) in the ^{238}U series. 109
5.11 Sample S4: Activity concentrations as function of gamma-ray energy for various radionuclides (^{234m}Pa, ^{226}Ra, ^{214}Bi and ^{214}Pb) in the ^{238}U series. 109
5.12 Sample S5: Activity concentrations as function of gamma-ray energy for various radionuclides (^{234m}Pa, ^{226}Ra, ^{214}Bi and ^{214}Pb) in the ^{238}U series. 110
5.13 Sample S6: Activity concentrations as function of gamma-ray energy for various radionuclides (^{234m}Pa, ^{226}Ra, ^{214}Bi and ^{214}Pb) in the ^{238}U series. 110
5.14 Sample S7: Activity concentrations as function of gamma-ray energy for various radionuclides (^{234m}Pa, ^{226}Ra, ^{214}Bi and ^{214}Pb) in the ^{238}U series. 111
5.15 Sample S8: Activity concentrations as function of gamma-ray energy for various radionuclides (^{234m}Pa, ^{226}Ra, ^{214}Bi and ^{214}Pb) in the ^{238}U series. 111
5.16 Sample S9: Activity concentrations as function of gamma-ray energy for various radionuclides (^{234m}Pa, ^{226}Ra, ^{214}Bi and ^{214}Pb) in the ^{238}U series 112
5.17 Sample S10: Activity concentrations as function of gamma-ray energy for various radionuclides (^{234m}Pa, ^{226}Ra, ^{214}Bi and ^{214}Pb) in the ^{238}U series. 112

5.18 Sample S11: Activity concentrations as function of gamma-ray energy for various radionuclides (^{234m}Pa, ^{226}Ra, ^{214}Bi and ^{214}Pb) in the ^{238}U series. 113
5.19 Sample S12: Activity concentrations as function of gamma-ray energy for various radionuclides (^{234m}Pa, ^{226}Ra, ^{214}Bi and ^{214}Pb) in the ^{238}U series. 113
5.20 Sample S13: Activity concentrations as function of gamma-ray energy for various radionuclides (^{234m}Pa, ^{226}Ra, ^{214}Bi and ^{214}Pb) in the ^{238}U series. 114
5.21 Sample S14: Activity concentrations as function of gamma-ray energy for various radionuclides (^{234m}Pa, ^{226}Ra, ^{214}Bi and ^{214}Pb) in the ^{238}U series. 114
5.22 Sample S15: Activity concentrations as function of gamma-ray energy for various radionuclides (^{234m}Pa, ^{226}Ra, ^{214}Bi and ^{214}Pb) in the ^{238}U series. 115
5.23 Sample S16: Activity concentrations as function of gamma-ray energy for various radionuclides (^{234m}Pa, ^{226}Ra, ^{214}Bi and ^{214}Pb) in the ^{238}U series. 115
5.24 Sample S17: Activity concentrations as function of gamma-ray energy for various radionuclides (^{234m}Pa, ^{226}Ra, ^{214}Bi and ^{214}Pb) in the ^{238}U series. 116
5.25 Sample S18: Activity concentrations as function of gamma-ray energy for various radionuclides (^{234m}Pa, ^{226}Ra, ^{214}Bi and ^{214}Pb) in the ^{238}U series. 116

5.26 Sample S19: Activity concentrations as function of gamma-ray energy for various radionuclides (^{234m}Pa, ^{226}Ra, ^{214}Bi and ^{214}Pb) in the ^{238}U series. 117
5.27 Sample S20: Activity concentrations as function of gamma-ray energy for various radionuclides (^{234m}Pa, ^{226}Ra, ^{214}Bi and ^{214}Pb) in the ^{238}U series. 117
5.28 Sample S1: Activity concentrations as function of gamma-ray energy for various radionuclides (^{208}Tl, ^{212}Bi and ^{228}Ac) in the ^{232}Th series. 120
5.29 Sample S2: Activity concentrations as function of gamma-ray energy for various radionuclides (^{208}Tl, ^{212}Bi and ^{228}Ac) in the ^{232}Th series. 120
5.30 Sample S3: Activity concentrations as function of gamma-ray energy for various radionuclides (^{208}Tl, ^{212}Bi and ^{228}Ac) in the ^{232}Th series. 121
5.31 Sample S4: Activity concentrations as function of gamma-ray energy for various radionuclides (^{208}Tl, ^{212}Bi and ^{228}Ac) in the ^{232}Th series. 121
5.32 Sample S5: Activity concentrations as function of gamma-ray energy for various radionuclides (^{208}Tl, ^{212}Bi and ^{228}Ac) in the ^{232}Th series. 122
5.33 Sample S6: Activity concentrations as function of gamma-ray energy for various radionuclides (^{208}Tl, ^{212}Bi and ^{228}Ac) in the ^{232}Th series. 122

5.34 Sample S7: Activity concentrations as function of gamma-ray energy for various radionuclides (^{208}Tl, ^{212}Bi and ^{228}Ac) in the ^{232}Th series. 123
5.35 Sample S8: Activity concentrations as function of gamma-ray energy for various radionuclides (^{208}Tl, ^{212}Bi and ^{228}Ac) in the ^{232}Th series. 123
5.36 Sample S9: Activity concentrations as function of gamma-ray energy for various radionuclides (^{208}Tl, ^{212}Bi and ^{228}Ac) in the ^{232}Th series. 124
5.37 Sample S10: Activity concentrations as function of gamma-ray energy for various radionuclides (^{208}Tl, ^{212}Bi and ^{228}Ac) in the ^{232}Th series. 124
5.38 Sample S11: Activity concentrations as function of gamma-ray energy for various radionuclides (^{208}Tl, ^{212}Bi and ^{228}Ac) in the ^{232}Th series. 125
5.39 Sample S12: Activity concentrations as function of gamma-ray energy for various radionuclides (^{208}Tl, ^{212}Bi and ^{228}Ac) in the ^{232}Th series. 125
5.40 Sample S13: Activity concentrations as function of gamma-ray energy for various radionuclides (^{208}Tl, ^{212}Bi and ^{228}Ac) in the ^{232}Th series. 126
5.41 Sample S14: Activity concentrations as function of gamma-ray energy for various radionuclides (^{208}Tl, ^{212}Bi and ^{228}Ac) in the ^{232}Th series. 126

5.42 Sample S15: Activity concentrations as function of gamma-ray energy for various radionuclides (^{208}Tl, ^{212}Bi and ^{228}Ac) in the ^{232}Th series. 127
5.43 Sample S16: Activity concentrations as function of gamma-ray energy for various radionuclides (^{208}Tl, ^{212}Bi and ^{228}Ac) in the ^{232}Th series. 127
5.44 Sample S17: Activity concentrations as function of gamma-ray energy for various radionuclides (^{208}Tl, ^{212}Bi and ^{228}Ac) in the ^{232}Th series. 128
5.45 Sample S18: Activity concentrations as function of gamma-ray energy for various radionuclides (^{208}Tl, ^{212}Bi and ^{228}Ac) in the ^{232}Th series. 128
5.46 Sample S19: Activity concentrations as function of gamma-ray energy for various radionuclides (^{208}Tl, ^{212}Bi and ^{228}Ac) in the ^{232}Th series. 129
5.47 Sample S20: Activity concentrations as function of gamma-ray energy for various radionuclides (^{208}Tl, ^{212}Bi and ^{228}Ac) in the ^{232}Th series. 129
5.48 Activity correlation between: (a) ^{40}K vs ^{238}U, (b) ^{40}K vs ^{232}Th and (c) ^{238}U vs ^{232}Th. 134
5.49 Estimated radiation hazard indices showing the Ra_{equ} (blue), ELCR (red), H_{int}(green) and H_{ext} (yellow) for the study area. 137
5.50 The comparison of concentration level of Cu, Mo and As in the selected samples. The horizontal lines represent the average and Maximum Allowable Limit (MAL) 140

5.51 Comparison of concentration level of Hg, Cd and Pb in the selected samples. The horizontal lines represent the average and Maximum Allowable Limit (MAL) 141
5.52 Uranium correlations for HPGe and ICP-MS data 142
5.53 Potassium correlations for HPGe and ICP-MS data 142

B.1 Bar charts of elemental concentration for major elements. 156
B.2 Bar charts of elemental concentration for Essential trace elements. 157

List of Tables

2.1 Natural origin of cosmogenic radionuclides. 12

2.2 Examples of single occuring primordial radionuclides. 15

3.1 HPGe detector modelled specifications using GEANT4 [Ger] . . . 62

4.1 Technical specifications of HPGe detector system used in this study 75

4.2 List of gamma-energies and channel numbers obtained for ^{232}Th and ^{40}K standard sources. 78

4.3 Gamma-ray transitions and the corresponding full energy efficiency for ^{238}U, ^{232}Th and ^{40}K 81

5.1 Coincidence summing correction factor for gamma energy 100

5.2 Comparison of measured and simulated peak efficiencies with the corresponding ratios for GEANT4 and FLUKA codes 103

5.3 Activity concentrations (weighted average) for ^{238}U in all samples 107

5.4 Activity concentrations (weighted average) for ^{232}Th in all samples 119

5.5 Activity concentration of ^{235}U, ^{137}Cs and ^{40}K 131

5.6 Activity concentration values in all samples compared with some other countries across the world 133

5.7 Result of radiological hazard risk factors measured for all samples collected from Southern area of Chad. 136

5.8 Activity concentration and elemental concetration results obtained from HPGe detector and ICP-MS. 143

A.1 The gamma-ray transitions used for activity concentration 149

A.2 Activity concentration results for sample S1 to S10 151

A.3 Activity concentration results for sample S11 to S20 152

B.1 Elemental concentrations 153

B.2 Elemental concentrations 155

Chapter 1

Introduction

1.1 Background

Reliable estimates and representative studies of environmental radioactive elements that have inherently heterogeneous distributions have remained a well-established problem for earth and environmental scientists. The environment in which we live contains quantities of radioactive (unstable) elements or radionuclides (radioisotopes) derived from primary, secondary and cosmic sources (extraterrestrial space) at various concentrations in every part of the surface of the earth and in the tissues of a living being. They can be found in product and by-products, such as soil, public water supplies, oil and gas even in human food and drinking water. The anthropogenic sources are related to industrial use of man-made nuclear materials, for instance nuclear power plants and nuclear medicine. However, with all the artificial utilisation of radionuclides, up to 85% of an average individuals radiation exposure received from world population are mostly from exposure related to natural radionuclides (see Fig. 1.1) [WNA19]. Still, there are other non-nuclear industrial activities that result in enhancement of

NORMs (Naturally Occurring Radioactive Materials) [Ala14], or sometimes referred to as Technologically-Enhanced Naturally Occurring Radioactive Materials (TENORMs). Hundred years ago, Henri Becquerel discovered that metallic uranium and all salts of uranium emit radiation which is spontaneous and has similar properties with Roentgen rays [Gen95]. The same phenomenon was also observed with thorium, using their energies and penetrating abilities as the new analytical tool that led to the discovery by curies of two substances considerably more active than uranium, which they called polonium and radium [Nao97]. Such nuclei are subjected to investigations of radiations emitted from a radioactive nuclides indicating the existence of gamma energy whose identification and quantification are essential source of information about the nucleus [Kra88]. However, potassium and carbon radionuclides are found in human being, thus radiation emitting radionuclides could not be ignored [Tho98].

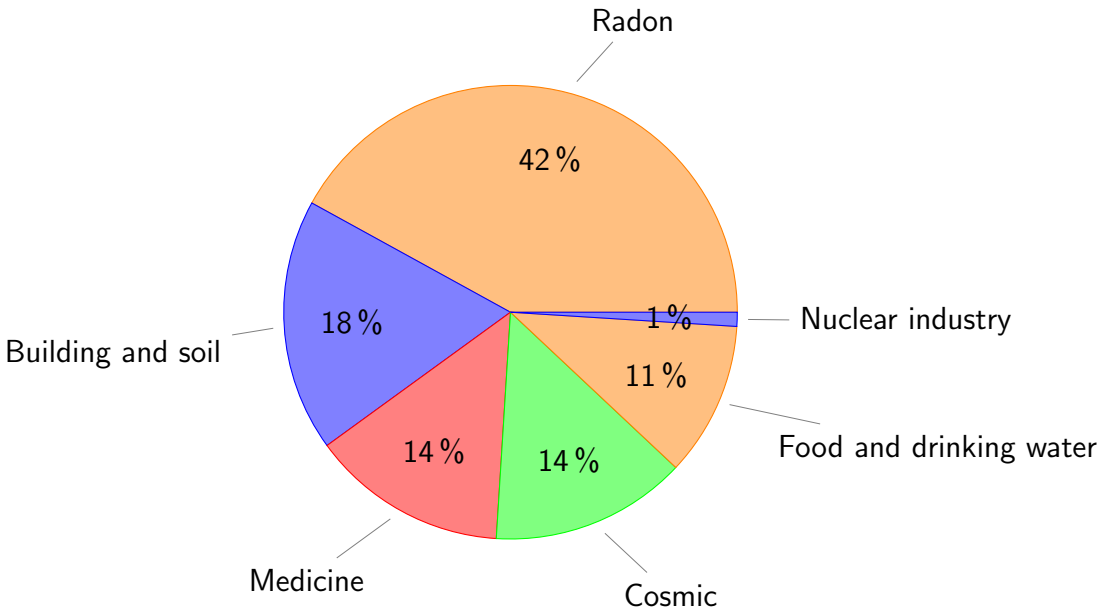

Figure 1.1: Sources of radiation [Uns00].

1.2 Problem Statement

Humans are exposed to heavy metals which are toxic to health, due to the increase in the use of these metals in recent years as they are introduced into industrial products and processes. Human exposure to heavy metals is generally absorbed daily in small doses through ingestion from various components such as food and water. And in rare cases, through chemical accidents that can occur in industries around us. The transformation of heavy metals through human intervention changes the concentration of these heavy metals in industrial and agricultural activities. This transformation makes heavy metals more toxic and harmful to health and the environment. Among the regulated pollutants are heavy metals, in particular arsenic, cadmium, mercury, and lead. The other elements individually pose much less of a problem, either because they remain rare in soils (this is the case of tin, selenium and metals which are sometimes very toxic but of specific use), or because in the forms in which they are found, they would only be toxic to humans in exceptional amounts and that ecosystems adapt to them, this is the case of copper, zinc, nickel which are essential trace elements, and even chrome. However, they can be harmful to agro-systems and by transfer to aquatic systems.

1.3 Naturally Occuring Radioactive Materials

Radionuclides that made up the naturally occuring radioactive materials (NORMs) decay by emision of various particles, α, β and γ-rays. Technologically Enhanced NORMs (commonly referred to as TENORMs) has also become a widely recognised problem in the oil and gas industry, coal industry, fertiliser/phosphate industries and so on [Lan13]. For instance, NORMs will chemically separate from

other piped material in the process of the extraction of oil, resulting in high concentrations of radioisotopes in a density caked layer on inner surface of the piping [Zie99, Lan13]. Radium and radon is one of the common radioisotope elements found in NORMs. Gamma radiation emitted from radium isotopes are able to penetrate the pipelines and other oil and gas installation causing an external dose of ionising radiation to the general public and field workers. Technically, NORMs can be used to differentiate natural radioactive sources from the artificial radioactive sources, such as ^{137}Cs.

In the last decade, the amount of research on environmental radioactivity has increased. Exposure to ionizing radiation has been shown to increase the incidence of cancer and leukemia in humans [Hus17]. The risk of radiation-induced cancers has been demonstrated by numerous experimental and epidemiological studies [Uns00]. These studies have shown that people exposed to ionizing radiation such as the survivors of the bombings in Hiroshima and Nagasaki, patients who received doses of radiation for therapeutic or diagnostic purposes, certain professional groups such as radiologists, workers in the nuclear, uranium miners, etc. and certain populations exposed to the environment (domestic radon, etc.). For this reason, it is therefore important to carry out studies of environmental radioactivity measurements that are representative not only in terms of absolute quantity, but also have meaning in terms of relationship with the lateral and vertical spatial distributions underlying activity. This work focuses on the measurement of environmental radioactivity through the following two techniques: (1) Gamma spectroscopy and (2) Inductively Coupled Plasma-Mass Spectrometry (ICP-MS).

To validate the experimental results of coincidence summing and efficiency calibration, GEANT4 and FLUKA Monte Carlo codes were employed to test the characterisation of the efficiency of peaks obtained from ^{40}K, ^{22}Na, ^{137}Cs, ^{60}Co and ^{152}Eu while ^{60}Co and ^{22}Na were used to correct for the sum of coincidences that occurs in environmental samples. Also, coincidence summing correction factor were calculated for both ^{238}U and ^{232}Th using EFFTRAN software.

1.4 Radiometry

Radiometry is a widely used measurement technique to identify and quantify radiations that are present in samples. These radiations are of three types namely; gamma-ray, beta and alpha particles. Various methods are available by which these radiations can be measured, either in a laboratory or in the field. These methods include Neutron Activation Analysis (NAA), Sodium Iodide (NaI), fundamental physics research, environmental analysis, alpha particle detection, inductively coupled plasma mass spectrometry (ICP-MS), Geiger Mueller and so on. Hyper Pure Germanium (HPGe) detectors are used for non-destructive counting of gamma emmiting radionuclides and can also be used on the field if these crystals are handled properly and with care in order to avoid damages. Furthermore, due to the high sensitivity and good energy resolution capabilities of HPGe detector, it has been widely used in determining the level of NORMs through direct on-field measurements.

1.5 Heavy Element Detection Technique

Heavy elements can be detected using different analytical techniques, for instance, Neutron Activation Analysis (NAA), Proton Induced X-Ray Emission Spectroscopy (PIXE), X-Ray Fluorescence Spectroscopy (XRF), Inductively Coupled Plasma-Mass Spectrometry (ICP-MS), and others. In the present investigation, the capability of ICP-MS was harnessed in identifying and quantifying the presence of heavy toxic metals in the collected environmental soil samples. Inductively Coupled Plasma-Mass Spectrometry (ICP-MS) was developed in the early 1960 as a commercial analytical techmique and has become the most widely used detection technique in determination of heavy metals for both routine analyses and in research area [Ndl16]. The main reasons for using this technique is its ability to determine low detection limit, less interference and also to carry out rapid multi-elemental analysis.

1.6 Monte Carlo Methods

Monte Carlo is the term given to the method of solving problems using random events. The term was created in 1945 by Stanislaw Ulam, Los Alamos National Laboratory, as he had an uncle who frequented the Casino of Monte Carlo. Whilst working on solving the problems of nuclear diffusion in fissionable materials, a computer program based on random numbers was constructed and executed on the first electronic computer, ENIAC [Mey56, Ula87]. Random events may be generated in many ways other than through the use of computer algorithm. Thus, the concept of Monte Carlo calculation has increased user group doing research in various fields like applied physics, medical physics, high energy physics and so

on. There are many Monte Carlo codes that have been developed for particle transport which include GEANT4 [Ago03], FLUKA [Fer05], MCNPX [Pel08], e.t.c. All Monte Carlo radiation transport codes follow the same proceedure for calculation (see more details about Monte Carlo in Chapter 3).

1.7 Aim and Scope of the Study

There is a noticeably higher concentration of radionuclides present in the environment due to industrial activities. TENORMs are formed in the process of mining including, phosphate production, where the end goal is to concentrate on high quantity of natural and artificial radionuclides (if found). Natural sources are known to be the main contributor to the external dose of the world population [Uns00]. These doses are generally correlated with relatively high activity concentrations of natural radionuclides of ^{238}U, ^{232}Th and ^{40}K, which in turn depend on local geological and geographical conditions [Uns00, Ahm14, Mal14]. The present study examines the existence of radionuclides in soil samples collected from Yapala, Mayo-Dallah region in Chad. The Mayo-Dallah region is one of the sub-region that is rich in mineral resources [Pen18]. Previously mining activities were undertaken in a random way without following the international standards [Pen18]. However, such activities are always accompanied by disturbances of ecological factors in the environment. In 1970, a study was carried out which was funded by United Nations Development Programme (UNDP) with the help of IAEA which revealed evidence of uranium in the region [Oya20]. Additional studies to assess the radiological condition were done by Penabei et al., [Pen18] and IAEA [IAEA03] and these studies have proven the presence of gold, iron, uranium, thorium, potassium, chromium (Cr), nickel (Ni), copper (Cu). By def-

inition, chromium (Cr), nickel (Ni) and copper (Cu) are heavy metals which are basically toxic metals, irrespective of their atomic mass or density. Techniques used in this study to identify and quantify radionuclides present in samples is by gamma-ray spectrometry complemented by ICP-MS elemental analysis.

This study will provide an overview information on radiological map of Mayo-Dallah region that can be integrated to project the future radiological map of Chad. The results also present the estimation of radiation dose to assess the potential radiological risk associated with the soil samples by evaluating the radium equivalent activity, external radiation hazard index, internal radiation hazard index, annual effective dose equivalent (AEDE) and Excess lifetime cancer risk (ELCR). The work also provides a baseline for activity concentration for the defined region which can be used to determine the future of increased activity concentration levels.

However, Monte Carlo simulation codes (GEANT4 and FLUKA) were also used to determine the coincidence summing that occurs in the environmental samples and the full-energy peak efficiency for Hyper-Pure Germanium (HPGe) detector. This codes takes detector characteristics into concederations including sample position, Physics list and the Full-Width-Half Maximum of the detector. Furthermore, the present work aim at investigating and to develope methods to correct the measured ^{60}Co, ^{137}Cs, ^{22}Na, ^{152}Eu and ^{40}K activity by Monte carlo simulations. From the above statement, a detailed study was carried out on how this effects affect the accuracy of efficiency values. The placement of sample that makes the radionuclide and sample density distributed heterogeneous is also considered. Also, ^{60}Co and ^{22}Na were used for the coincidence summing correction and the result

obtained from simulations were compared with experimental data.

The research project is organised as follows:

• Chapter 2 describes the theoretical aspect of natural radioactive source, law of radioactive decay, radioactive equilibrium, radioactive decay modes,decay chains of ^{235,232}U and ^{232}Th, interactions of gamma-ray with matter, gamma-ray detection and Coincidence Summing process.

• Chapter 3 presents the Monte Carlo Methods of radiation transport, GEANT4 and FLUKA overview applications and implementations.

• Chapter 4 describes the experimental setup which illustrate the sample collection and preparation, the HPGe gamma-ray detector, gamma spectroscopy data analysis and Inductively Coupled Plasma Mass Spectrometry (ICP-MS) overview and benchmark tests.

• Chapter 5 presents the experimental results for both HPGe detector and ICP-MS together with comparison of experimental data with Monte Carlo codes.

• A summary of the conclusions and future work are detailed in Chapter 6.

Chapter 2

Theoretical Aspects

This chapter presents the theoretical aspects of natural radioactive source, decay chains of radionuclides of interests, law of radioactive decay, radioactive equilibrium, radioactive decay modes and physical interactions of gamma-ray with matter. In addition, coincidence summing effect that occurs in some of the radionuclides of interest will be explored.

2.1 Natural Radioactive sources

Natural radionuclides fall into two categories:

- Cosmogenic radionuclide and
- primordial radionuclide.

Cosmogenic radionuclides are natural radionuclides that originate from various nuclear reactions during which high-energy cosmic radiation passes through the earth's atmosphere, by producing secondary radionuclides such as ^{14}C, ^{3}H and ^{7}Be [Eis97]. The cosmic radiation goes through the earth atmosphere and inter-

acts with particulate constituents and gases to produce a variety of cosmogenic radionuclides [IAEA20]. Example of such cosmogenic radionuclides are listed in Table 2.1, with half-lives ranging from few days to few million years, exhibiting relatively low atomic numbers. The concentration and rate of production of cosmogenic radionuclides are strongly dependent on altitude. For instance, the production rate of ^{7}Be is 70% in the stratosphere layer whereas only 30% of the total is produced in the lower altitudes troposphere. The most important radionuclides produced by cosmic rays are ^{14}C via (n,p) reaction on ^{14}N and ^{81}Kr via (n,γ) reaction on ^{80}Kr [Kat98]. Moreover, ^{14}C that serves as an important ingredient during carbon cycle, oxidises to form carbon dioxide which can be further utilised by plants and later follows the pathway as animal food. Excretory waste and decomposing bodies of animals and plants put organic ^{14}C into terrestrial and aquatic environment where it remains in the active reservoir in the food chain [Kat98]. The production of ^{14}C is quite low and therefore these nuclides have little radiological impact [IAEA20, Ali08]. Small amount of primary radionuclides are ^{59}Mn. ^{56,57,58,60}Co, ^{53,54}Mn, ^{51}Cr, ^{48}V,^{46}Sc, ^{26}Al and ^{22}Na which are related to spallation on heavier materials and added to the environment through extraterrestrial dust and meteorites [Kle82, Kat98].

Primordial radionuclides usually originate from fusion reaction in the interior of supernovae. They have been present since the formation of the planet 4.6x10^{9} years ago and possess long half-lives, which decay through beta emitters with a few alpha emitters [Uns00]. Most of them are not yet completely decayed, hence they are still being detected. One of the most common single primordial radionuclides is ^{40}K with half-life of 1.28$\times$10^{9} years which is widely distributed in the earth's

crust and present in measurable quantities in many building materials [Uns00]. The amount of ^{40}K is estimated to be 0.1% in limestone and 4% in some granite rocks [Ali08]. Natural isotopic abundance of potassium (^{40}K) is 0.0118% with specific activity of 31.4 Bq/g [Ens20, Kat98].

Table 2.1: Natural origin of cosmogenic radionuclides [Uns00, Kat98].

Nuclide	Half life	Decay mode and discete	Gamma energy (keV)
^{3}H	12.32 yrs	β^- (100%)	*
^{7}Be	53.22 days	EC (100%), γ	477
^{10}Be	1.51×10^{6} yrs	β^- (100%)	*
^{14}C	5730 yrs	β^- (100%)	*
^{22}Na	2.60 yrs	β^+ and γ (100%)	1275
^{26}Al	7.17×10^{5} yrs	EC (100%)	*
^{32}Si	153 yrs	β^- (100%)	*
^{32}P	14.26 days	β^- (100%)	*
^{33}P	24.4 days	β^- (100%)	*
^{35}S	87.37 days	β^- (100%)	*
^{36}Cl	3.01×10^{5} yrs	EC (1.9%), β^- (98.1%)	*
^{37}Ar	35.04 days	EC (100%)	*
^{39}Ar	269 yrs	β^- (100%)	*
^{81}Kr	2.29×10^{5} yrs	EC (100%)	*

The decay of potassium (^{40}K) goes to a stable product of ^{40}Ca through β^- decay of 89.25(17)% while β^+ and electron capture(EC) goes to a stable product of ^{40}Ar and releases the remaining 10.55(11) %. The identification and quantification of potassium by gamma spectrometry is attainable via the detection of gamma-ray

at 1460 keV, following deexcitation to 2^+ state, which is the first excited state of ^{40}Ar. As illustrated in Fig. 2.1, the ^{40}K has a single distinct gamma-ray emission, this decay can be utilised to calculate the initial energy calibration of a system. For a proper energy and efficiency callibration, a source with multiple energy peaks is recommended to cover the energy range of interest. Some of the single occuring radionuclides are given in Table 2.2.

Some radionuclides like ^{235,238}U and ^{232}Th [Kra88] decays in multiple steps, resultig in a decay chain with daughter radionuclides to reach a stable isotope. Majority of the atoms were initially radioactive but they have decayed to form stable nuclides. This chains undergo a complicated succession of alpha and beta decays.

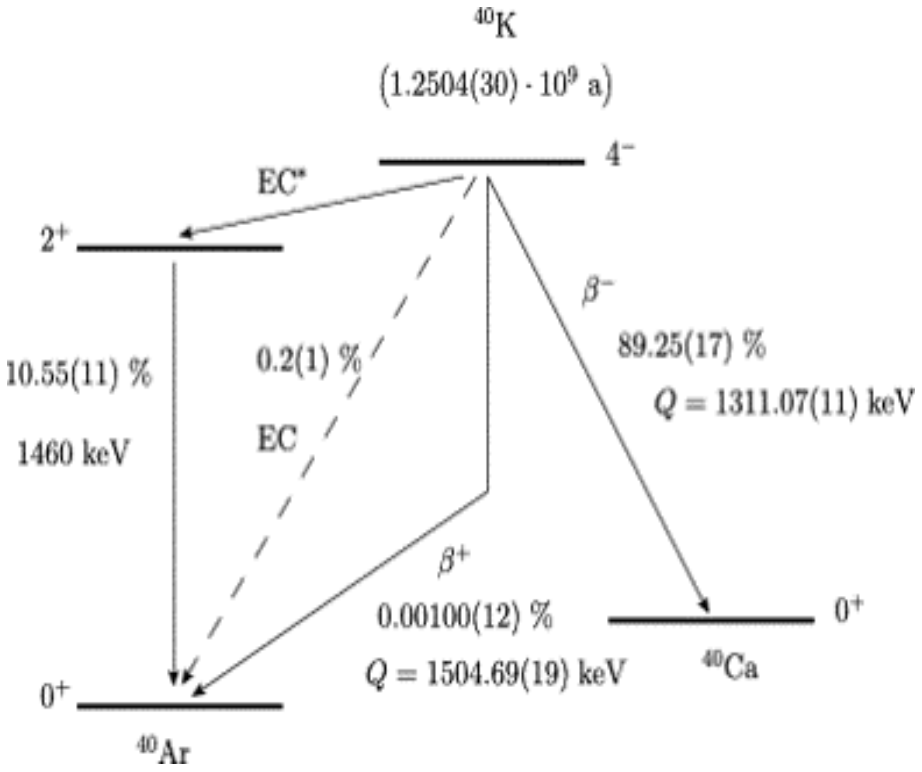

Figure 2.1: Decay scheme of ^{40}K showing the single emitting energy and the daughter nuclides formed during beta-minus (β^-) and Electron Capture (EC) decay processes [Pra13].

Table 2.2: Examples of single occuring primordial radionuclides [Uns00, Kat98].

Nuclide	Half life	Decay mode	Isotopic abundance(%)	Gamma-ray energy (keV)
^{40}K	1.28×10^{9} yrs	β^+, EC, β^-	0.0117	1461
^{87}Rb	4.8×10^{10} yrs	β^-	27.83	336
^{113}Cd	8×10^{15} yrs	β^-	12.2	*
^{115}In	4.4×10^{14} yrs	β^-	95.7	497
^{138}La	1.02×10^{11} yrs	EC, β^-, β^+	0.089	1436, 789
^{144}Nd	2.29×10^{15} yrs	α	23.8	*
^{147}Sm	1.06×10^{11} yrs	α	14.99	*
^{148}Sm	7×10^{15} yrs	α	11.24	*
^{152}Gd	1.08×10^{14} yrs	α	0.2	*
^{176}Lu	3.76×10^{10} yrs	β^-	2.599	88, 202
^{174}Hf	2×10^{15} yrs	α	0.16	*
^{187}Re	4.33×10^{10} yrs	β^-	62.60	*
^{190}Pt	6.5×10^{11} yrs	α	0.0122	*

2.1.1 Radiation Concentration and Exposure

Environmental exposure to radiation is usually caused by some activities being carried out in nuclear related industries that warrant government regulations in order to minimise any potential health risk to the surrounding population. The main concern for scientist is to calculate the amount of dose and the source of ionising radiation. This dose level depends on the specific environment or occupation. The dose received by a person in a general public may be lower than the

people working in a radition facility or nuclear industry. However, uranium, thorium and potassium are the natural occurring nuclides that are found everywhere which could be responsible for external expposure to human being [Uns00].

2.2 Radioactive Decay Modes

Radioactive decay is a random process and therefore follows the statistical procedures in which an unstable nucleus loses energy by emitting ionising particles and radiation. The decay or energy loss results in an atom of one type known as parent nuclide, which either left as a stable daughter nuclide or as an unstable nuclide. The three principal modes of decay are alpha (α), beta (β) and gamma-ray (γ) decays. These decays are further discussed in details in the next subsections.

2.2.1 Alpha Decay

Alpha decay is a type of radioactive decay characterised by the emission of a ^{4}He nucleus i.e., a bound system of two protons and two neutrons, which are generally emitted by heavy nuclei in order to remain stable [Leo87]. It has short range and low penetration power because of high ionisation and potential, can deposit energy within a short distance. The emission of such nucleon as a whole rather than the emission of a single nucleons is the most preferred and advantageous because of the high binding energy of alpha (α) particle. During this process, the mother nucleus (Z, A) loses four units of mass and two units of charge, and the reaction is thus transformed through

$$^{226}_{88}Ra \rightarrow ^{222}_{86}Rn + ^{4}_{2}He \tag{2.1}$$

For instance, Radium(Z=88) decayed to Radon (Z=86), releasing a quantity of energy. This process was first explained by Gamow & Condon and by Gurney [Leo87] as tunnelling of alpha particle through the potential barrier of the nucleus. A fixed quantity of energy released during the decay process is known as Q-value, which equals to the difference in mass between initial nuclide and the final products.

$$Q = [m_N(^{A}_{Z}X) - m_N(^{A-4}_{Z-2}Y) - m_\alpha]c^2 \tag{2.2}$$

where m_N are the mass of the initial nuclide and the final product. The Q-value is conveyed in "MeV" while the mass is conveyed in atomic mass unit or amu (1 amu = 931.5 MeV/c^2) and c is the speed of light. This indicates that the transition of alpha decay is a process of exothermic process (Q>0), and can occur spontaneously.

- **Geiger-Nuttall Alpha-Decay Law**

One landmark in modern Physics, shaping the developments that leads to Quantum mechanics, was the formulation of Geiger-Nuttall (GN) law in 1911 [Cho12]. According to GN rule which states that there is a dramatic decrease in the alpha decay lifetime with increasing decay energy. The alpha half-life ($T_{1/2}$) is expressed by:

$$\log T_{1/2} = aQ_\alpha^{-1/2} + b \tag{2.3}$$

where a and b are constant, since different expression have been proposed to calculate $\log T_{1/2}$ using A, Z and Q-value. The adjustment of constant a and b was realised on the total experimental results of alpha decay half-lives [Cho14, Pai13]. A lot of works have been done on trying to generalise the GN law for a universal description of all detected alpha decay events. The reason why these

approaches have been successful is due to the alpha particle formation probability which usually varies from nucleus to nucleus. In the half-life scale of GN law, the differences in the formation probabilities are usually small fluctuations along the lines predicted by the law for different isotopic chains, illustrated in Fig. 2.2.

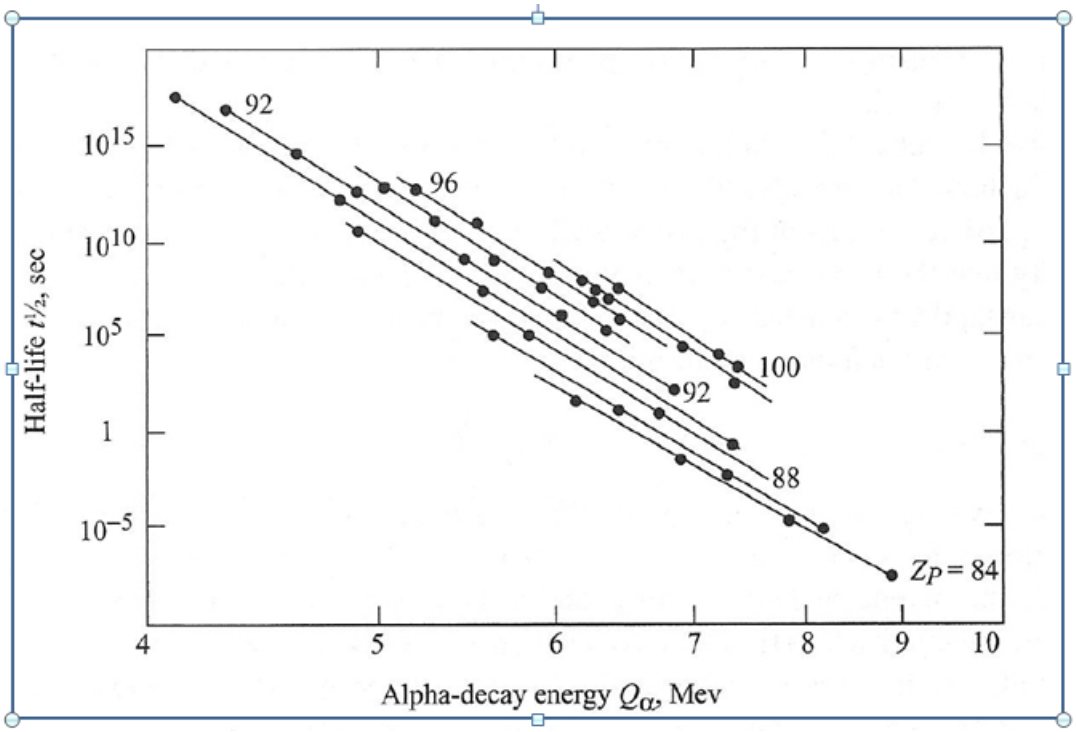

Figure 2.2: The inverse relationship between alpha decay half-life and decay energy illustrated for even-Z and even-N nuclei [Lil01].

2.2.2 Beta Decay

Beta particles are fast electrons or positrons [Leo87]. They have a penetration power of about 100 times more than alpha-particles, and are spin (1/2) fermions [Kra88]. This is the most common type of radioactive decay, and all nuclides lying beyond the valley of stability are unstable against this type of transition. Beta-decay has three processes, namely; β^-, β^+ and electron capture:

• **Beta-minus (β^-) Decay (Negatron)**

In a β^--decay, a neutron changes into proton while electron and anti-neutrino particles are emitted. The β^--particle is a single negatively charged (-1.6×10^{-19} C), with a relatively small mass compared to a proton or neutron (5.5×10 $^{-4}$ amu). Anti-neutrinos are undetectable because of a low probability of interaction with matters. The daughter nucleus (recoil) will appear with an extremely low recoil energy because of its large mass, and not commonly detected by a conservational detectors. Because of the three body nature of decay, beta-particle or an electron has a range of energies from zero up to an end-point energy, which can be theoretically estimated based on the mass-energy relation for a particular beta transition. The beta-radiation average energy is about 30 - 40 % (end-point) of the maximum energy for most of the beta emitters [Kno99].

This has a maximum beta end-point energy for a beta-particle of 1.16 MeV (^{210}Bi) and most of the betas kinetic energies are smaller than the average energy. (≈ 390 keV or about 33% of maximum energy). This process of decay can be written as:

$$ {}^{1}_{0}n \rightarrow {}^{1}_{1}H + {}^{0}_{-1}\beta + \bar{v}, \tag{2.4} $$

where $\bar{v}$ is the anti-neutrino. The beta-particle can also be written in mono-energetic way:

$$ m_n = m_p + m_\beta + Q, \tag{2.5} $$

Where Q-value is given by the following equation,

$$ Q = (m_n - m_p - m_\beta)c^2. \tag{2.6} $$

- **Beta-plus (β^+) Decay (Positron)**

The existence of anti-particle to an electron was first suggested by Fermi- Dirac in 1928, after four years Carl D. Anderson observed a particles with mass of electron and opposite charge in an experiments performed by using cloud chamber and cosmic-ray [Kra88]. He also named the particle as positron and was later awarded a Nobel prize in 1936 for this discovery. The positron has a positive charge of $1.6 \times 10^{-19}\ C$ and the same mass as an electron of 5.5×10^{-4} amu. Inside a nucleus, a proton spontaneously decays into a neutron, β^+-particle and neutrino. This process is impossible for free proton but for a proton in an unstable nucleus, that can supply more energy for the reaction [Leo87]. The atomic number of the daughter product is one less than the parent and also produced a neutrino according to the following equation:

$$ {}^{1}_{1}H \rightarrow {}^{1}_{0}\, n + {}^{0}_{1}\, \beta + v, \tag{2.7} $$

where v is the neutrino. Losing one proton from the nucleus leads to another vacant of an orbital electron from the daughter nucleus which happens after nuclear transition. The mass-energy conservation equation is giving in atomic masses as:

$$ m_p = m_n + m_{\beta^+} + m_{\beta^-} + Q \tag{2.8} $$

where $m_n, m_p, m_{\beta^-}, m_{\beta^+}$ are the masses of the daughter nucleus, parent nucleus, electron and positron, while Q is the energy released from the reaction. Therefore, in order for the positron to be emitted from the nucleus, the Q value is written as:

$$ Q = (m_p - m_n - 2m_\beta)c^2. \tag{2.9} $$

This can combine atomic electron, both the electron and positron can annihilate two(2) gamma-rays results, whose two energies are equal to the mass of both

electron and positron (1022 keV). Equation 2.9 is very important because if the threshold Q-value is reached, the positron can be emitted and the remaining electron will combine with proton, which will result in neutron being produced.

- **Electron Capture(EC)**

The suggestion that β^+ emission might decay by an alternative process of electron capture (EC) was first discovered by Yukawa based on the consideration of Fermi's theory of β-ray emission [Kra88]. This theory states that the electrons and positrons are created at the moment they are ejected during the neutron-proton transition. The continuous β-ray spectrum and the spin conservation are well described by a simultaneous emission of electron and neutrino. One may represent the electron and positron transition by Eqs.(2.4, 2.7). The Dirac's theory states that the positron is the *hole* that left the continuum of negative energy electrons when one of the electrons gives a positive energy by an addition of at least $2mc^2$ [Alv38]. The proton in Eq.2.7 does not transform into a positron and neutron, but captures the negatively charged electron and turns into neutron, leaving the hole in the positron or negatron energy. The electron comes mostly from K-shell and the process can be written as:

$$ {}^{1}_{1}H + {}^{0}_{-1}e \rightarrow {}^{1}_{0}n + v. \tag{2.10} $$

Furthermore, a proton in the nucleus is changed to neutron following the capture of one of the K of L-shell electrons. The capturing of electron occurs based on the wave motion of an orbital electrons which brings them to an unstable nucleus, such that the electron capture results in a reduction of the number of proton in the nucleus. As a result, the possibility of electron capturing in the K-shell is much higher than that of any other shells. The equation for conservation of energy for

K-shell electron is given as:

$$m_p + m_e = m_n + E_b + Q \tag{2.11}$$

where m_n and m_p are the nucleus masses of neutron and proton, m_e is the mass of electron captured, E_b is the electron binding energy and Q is the energy released from the reaction [Gil08]. The process of electron moving to a lower level of energy or orbitals produces the characteristic X-ray emitted with the daughter nucleus as depicted in Fig. 2.3.

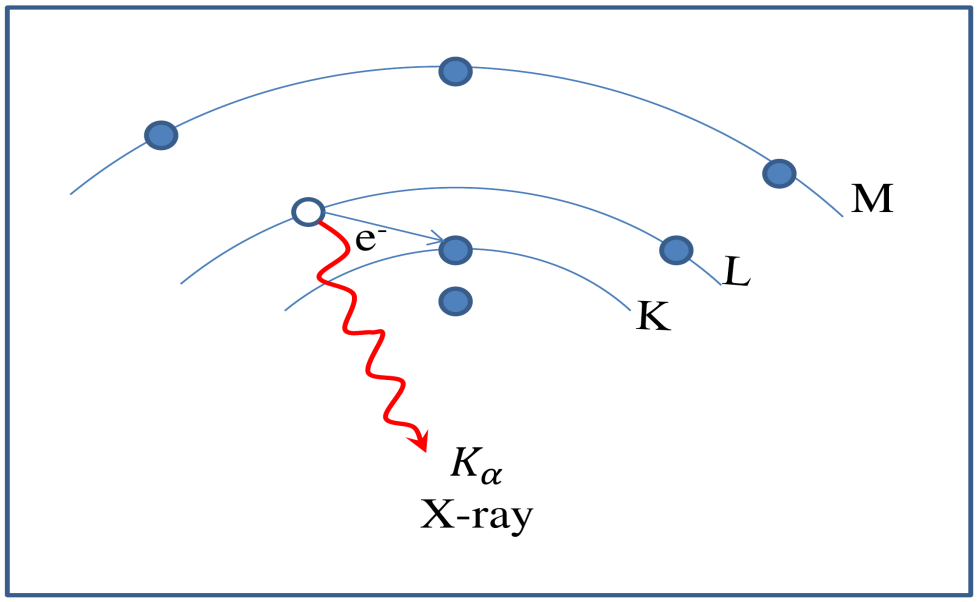

Figure 2.3: Production of Characteristic X-ray emission and electron capture from K-shell.

Also, the characteristic of X-ray does not escape from the atom but interacts with one of the electrons in the outer electron shells.

2.2.3 Gamma Decay

The gamma-decay, unlike alpha, beta or spontaneous fission, does not involve any particle, rather consist of energy emitted from an unstable nucleus. Gamma-ray photon is electrically neutral and travels at the speed of light. Gamma-rays (photon) can travel 100 m in air before undergoing interaction and attenuated. Gamma-rays evolved through a radioactive transformations from the excited state of daughter nuclides, and does not effect or change the atomic number or neutron number of the atom following gamma-ray emission. Each gamma-decay is mono-energetic, and consists of a photon with the energy ΔE of the difference between the initial excited state E_i and the final state E_f. From the conservation of energy, the energy released during the process of transition is expressed by the following [Kra88]:

$$\Delta E = E_i - E_f = E_\gamma + E_R = E_\gamma + \frac{E_\gamma}{2mc^2} \tag{2.12}$$

where $E_\gamma \sim 1$ MeV, $mc^2 \sim$ A$\times$GeV, thus recoil term

$$\frac{E_\gamma}{2mc^2} \ll\sim E_\gamma \tag{2.13}$$

where E_R is the final nucleus product recoil energy and in most of the cases is considered to be negligible. From Eq. 2.12, E_γ is equal to the de-excitation energy (ΔE), which is approximately equal to the energy difference between the initial and final states. Nuclei in an excited state decay to the ground state through the emission of one or more gamma-ray.

2.3 Decay Chains of ^{235,238}U, ^{232}Th

Most naturally occurring radioactive materials decay in chain series of transformation rather than decaying in a single step. The radionuclides found naturally

on earth can be grouped into three decay chains starting with, ^{238}U (half-life 4.5 bn years),^{235}U (half-life 0.7 bn years) or ^{232}Th (half-life 14 bn years). Natural uranium consist of three radioisotopes in various abundances, ^{238}U (99.3%), ^{235}U (0.7%) and ^{234}U (5×10^{-3}%) [Wey08]. However, ^{234}U and ^{238}U appear on the same uranium decay series, while the ^{235}U is on the actinide series [Cem08]. The distribution of these radionuclides within the geographical components (in liquid, solid and gas forms) can be determined by their geographical characteristics [Jon19].

Naturally, thorium is four times higher in abundance than uranium and it is 100% of ^{232}Th [Gil08]. The three members of the group can be simply distinguished by dividing their mass number by four. The nuclides that has mass number that can be formed by 4n+2, 4n+1 and 4n, these belongs to the uranium, actinium and thorium series, respectively. Radioactive nuclei in the chain emit various types of radiation, usually beta or alpha particles, and this process continues until it ends in a stable nuclide. The decay chain has been extensively studied, for many years, through series of α, β and γ decay of naturally occurring radioactive materials (NORMs). Usually, the activity of parent isotopes decrease as the decay progresses, while at the same time, that of their daughter nuclides increases [Eur19]. Figure 2.4 shows the ^{238}U decay chain, which passes through eighteen intermediate stages up to a stable ^{206}Pb. The ^{226}Ra from ^{238}U decay series decays to ^{222}Rn gas which might escape the matrix and thus disturbing the secular equilibrium. Therefore, the activity of the daughter nuclei will not be the same as their parent. Figure 2.5 gives the actinium series starting with ^{235}U and producing fifteen daughter radionuclides and ends at stable ^{207}Pb. In addition, thorium decay chain starts with ^{232}Th and ends at stable ^{208}Pb, including ten daughter nuclides (see

Fig. 2.6). The disturbance of secular equilibrium due to ^{220}Rn (thoron) is less due to its short half-life. The so called decay chains are created and end only when a non-radioactive (stable) nuclide is formed.

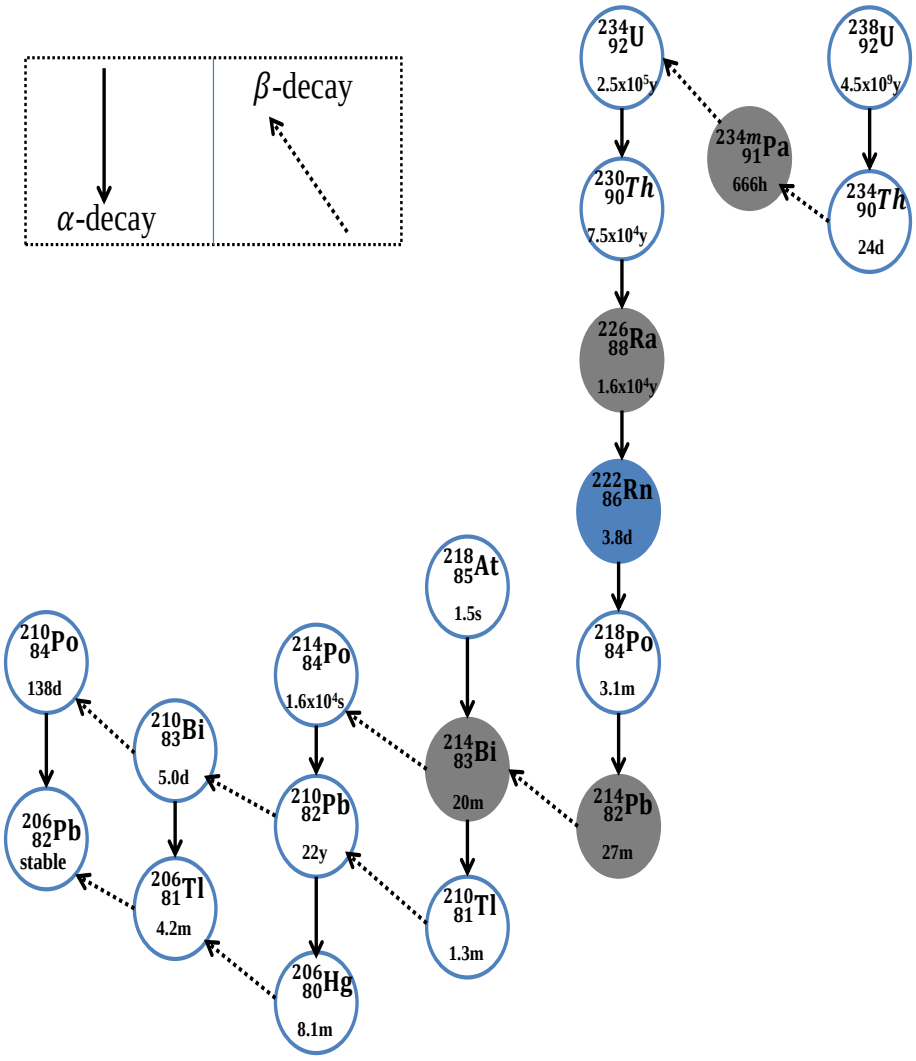

Figure 2.4: Schematic decay chain of ^{238}U (4n+2). The weak decay branches are from ^{218}Po, which decay by beta through ^{218}At to ^{218}Rn, also the daughter nuclides decay alpha back to the main chain. The grey shaded circles indicated gamma-ray emitting radionuclides and the blue shaded circle are radionuclides in gaseous form [Fir96].

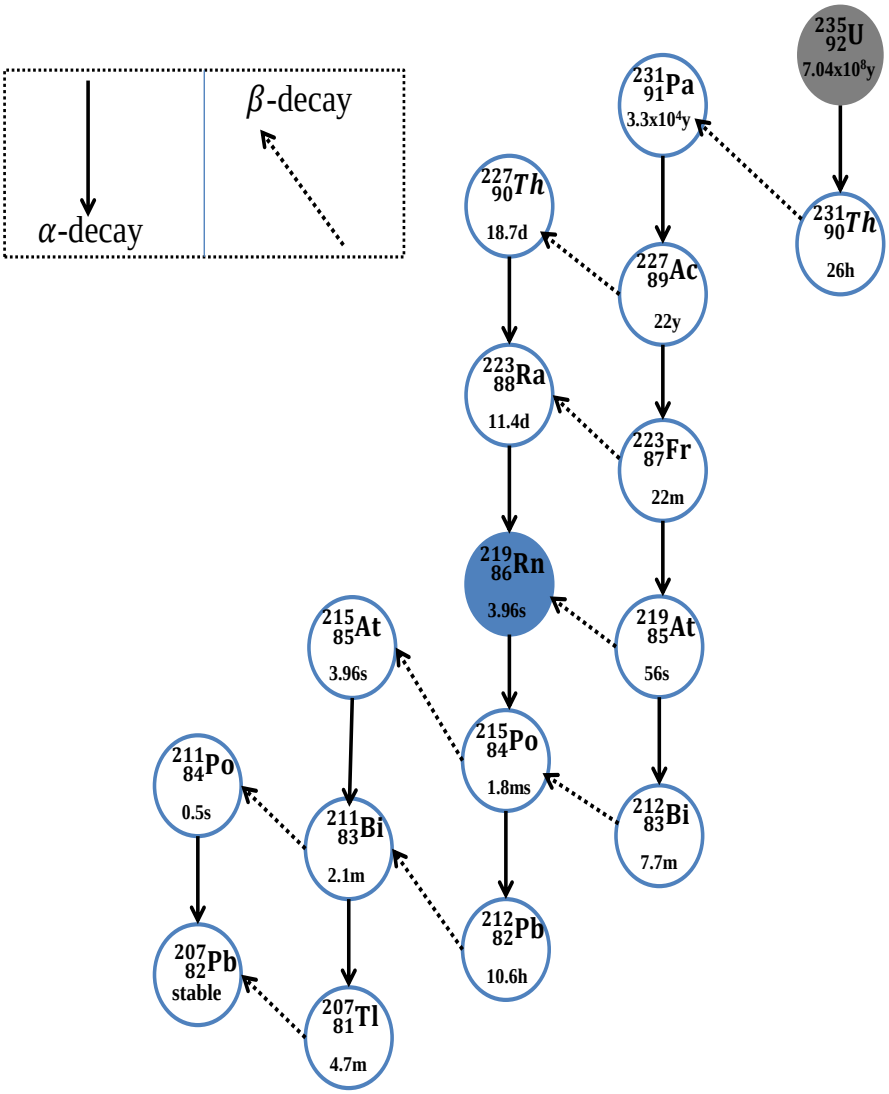

Figure 2.5: Schematic decay chain of ^{235}U (4n+1). From ^{231}Th nuclides seen above, there is a weak decay branch, which may decay alpha into ^{227}Ra before decaying beta back to main branch. The grey shaded circles indicated gamma-ray emitting radionuclides and the blue shaded circle is radionuclides in gaseous forms [Fir96].

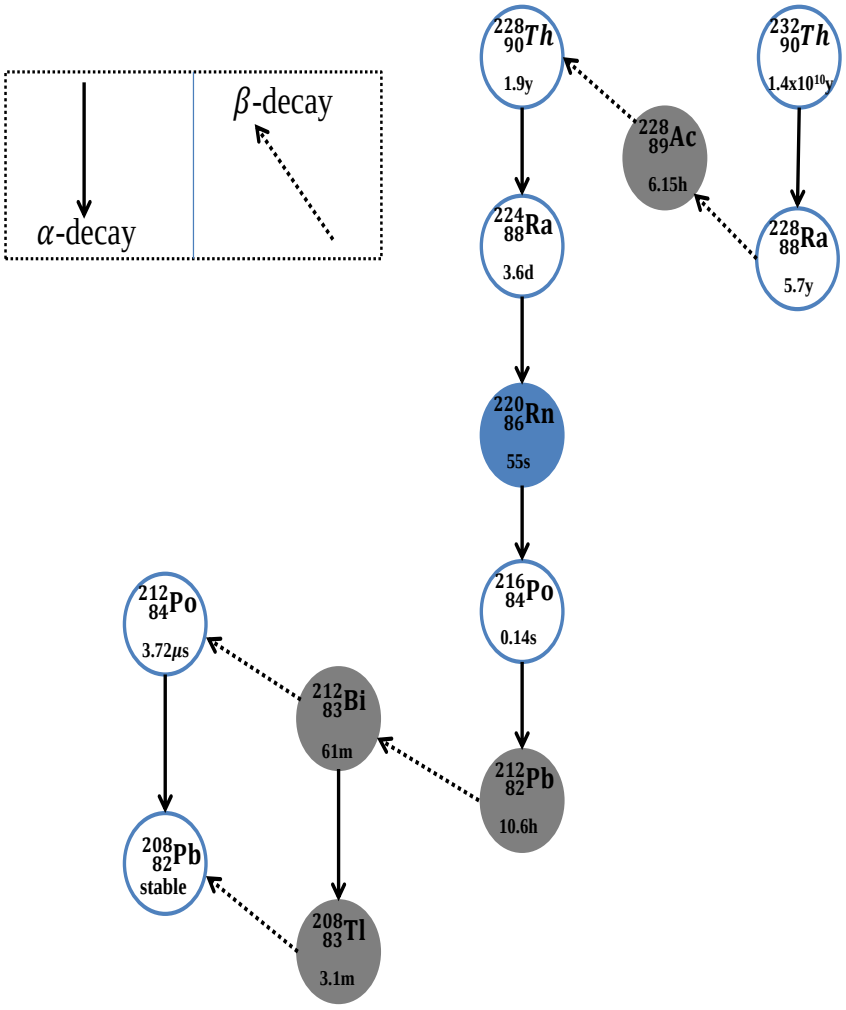

Figure 2.6: Schematic decay chain of ^{232}Th (4n). The nuclides in the decay chain will be in the samples that contain thorium, but if the samples is left to undergo an equilibrium for a long time with ^{232}Th, then the ^{220}Rn may escape the sample as it's a noble gas. The grey shaded circles indicated gamma-ray emitting radionuclides and the blue shaded circle is radionuclides in gaseous form [Fir96].

2.4 Radioactive Equilibrium

It is possible to have many radioactive generations for a particular isotope, where each decay transforms the nuclide through different decay channels or particles. The parent isotope decays into the daughter isotope. Sometimes the daughter isotope is unstable as well, and it also decay. Radioactive equilibrium is used to describe the relative activity of each radionuclide in a decay chain, therefore, it can be classified into three general conditions: Transient equilibrium, Secular equilibrium and Non-equilibrium decay.

2.4.1 Transient Equilibrium

Transient equilibrium is said to be attained when the activity of the daughter nucleus is in constant ratio with that of parent nucleus and also decays with half-life of the parent [Gil08]. The decay of the parent is unaffected by the presence or absence of the daughter and also the growth of the daughter activity. The sum of the daughter and the parent activities is equal to the total activity in the system. For example, ^{212}Pb (with half-life of 10.64 h) decays to ^{212}Bi (with half-life of 60.55 m) in the thorium series because the parent's half-life is slightly longer than that of the daughter. For $\lambda_d > \lambda_p$ or $(t_{1/2})_d < (t_{1/2})_p$: ^{212}Pb ($t_{1/2}$=10.64 h)$\rightarrow$ ^{212}Bi ($t_{1/2}$=60.55 m), therefore, the relationship between the daughter and the parent activities can be expressed by:

$$\frac{A_d}{A_p} = \frac{\lambda_d}{\lambda_d - \lambda_p} \tag{2.14}$$

2.4.2 Secular Equilibrium

Secular equilibrium is said to exist when half-life of a parent nuclide is much longer than that of the daughter nuclide. Since the half-life of the parent is much longer, then the rate of loss is lower than the rate of formation, so the daughter build up its activity continuously until its equal to that of the rate of loss. Activities in secular equilibrium in terms of number of atoms can be written by the general formula:

$$\lambda_p N_p = \lambda_d N_d \tag{2.15}$$

Equation 2.15 is the activity of the parent which is equal to the daughter, N_p is the number of nuclei of the parent and N_d is the number of nuclei of the daughter.

2.4.3 Non-Equilibrium Decay

Assuming the half-life of the daughter nuclide is longer than that of the parent nuclide, then the parent will decay completely, leaving the daughter behind. Figure 2.7 shows how ^{210}Bi (with half life of 5.013 d) decays into ^{210}Po (with half-life of 138.37 d) in the uranium series, where non-equilibrium decay is established. Then the decay curve will be that of a grown-in daughter [Gil08]. For $\lambda_d < \lambda_p$ or $(t_{1/2})_d > (t_{1/2})_p$: ^{210}Bi ($t_{1/2}$=5.013 days)$\rightarrow$ ^{210}Po ($t_{1/2}$=138.37 days), then, the relationship between the daughter and parent is expressed by the equation:

$$\frac{A_d}{A_p} = \frac{\lambda_d}{\lambda_d - \lambda_p}(1 - e^{-(\lambda_d - \lambda_p)t}) \tag{2.16}$$

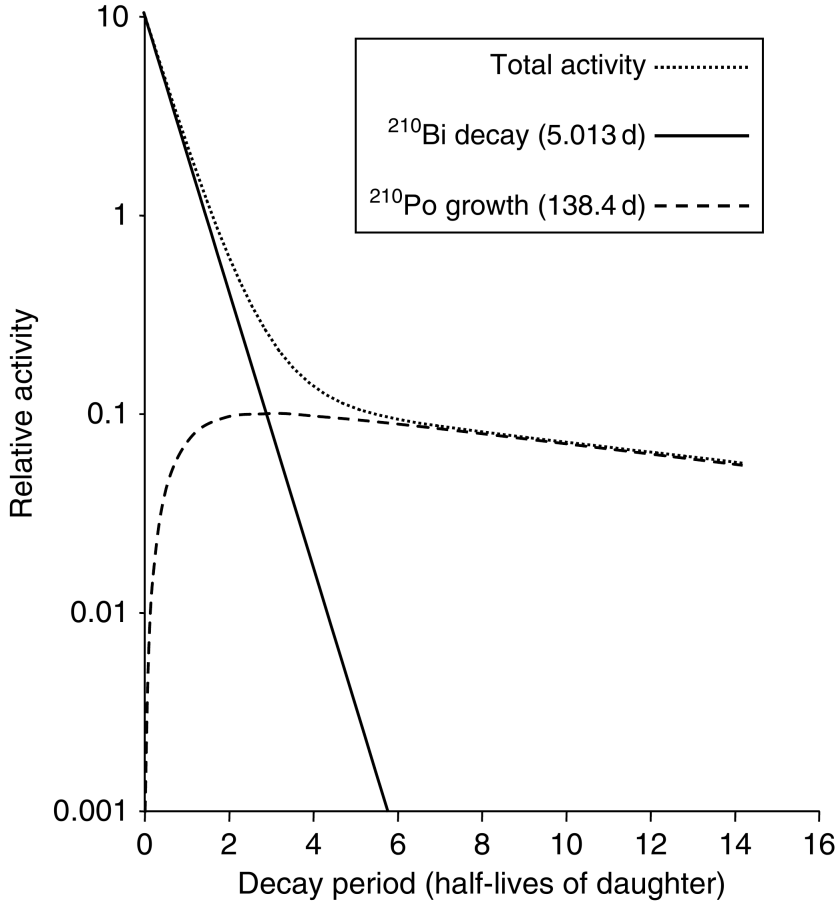

Figure 2.7: Example of the β^- decay of ^{210}Bi into ^{210}Po which corresponds to a relative activities of parent and daughter nuclides undergoing the non-equilibrium decay process [Gil08].

2.5 Law of Radioactive Decay

Radionuclides are generally unstable; hence they seek to attain stability by releasing part of their mass or excess binding energy through series of decay processes. By releasing this mass energy, these nuclei can obtain a more energetically proportion of protons and neutrons, and reach a minimum and more stable state of

energy [But72]. If a sufficiently great number of radioactive atoms are observed for sufficient long time, the law of radioactive decay is expressed as:

$$A = -\frac{dN}{dt} = \lambda N, \tag{2.17}$$

where A is the activity of a given radionuclide species (i.e., the number of decays per unit time), N is the number of atoms of a certain radionuclide, λ is the decay constant (per second) and -dN/dt is the disintegration rate. The negative sign is very important because N decreases as the time (t) increases. Equation 2.17 is the probability measurement of radioactive decay [Kno99,Lil01]. Integrating both sides of Eq. 2.17 leads to exponential law of radioactive decay which relates the number of atoms $N(t)$ at a time (t) and half-life ($t_{1/2}$):

$$N(t) = N_o e^{-\lambda t}, \tag{2.18}$$

where N_o is the number of radioactive atoms at time $t = 0$. It is more important to use half-life ($t_{1/2}$) frequently than the decay constant (λ). This is the time after which half of the original amount of radioactive atom present have decayed. To determine the $t_{1/2}$ in terms of λ, this is expressed from Eq. 2.18 at time $t = t_{1/2}$:

$$\frac{N_o}{2} = N_o e^{-\lambda t_{1/2}}, \tag{2.19}$$

By taking the natural logarithm in both sides, this yields

$$-\lambda t_{1/2} = ln(1/2) = -ln2, \tag{2.20}$$

therefore:

$$t_{1/2} = \frac{ln2}{\lambda} = \frac{0.693}{\lambda}, \tag{2.21}$$

and

$$N = N_o(1/2)^{t/(t_{1/2})}, \tag{2.22}$$

If the time t is small compared with half-life of radionuclide ($t << t_{1/2}$), therefore, the following approximation can be used:

$$e^{-\lambda t} = 1 - (ln2)\frac{t}{t_{1/2}} + \frac{(ln2)^2}{2}\left[\frac{t}{t_{1/2}}\right]^2 - ... \tag{2.23}$$

The average lifetime τ is related to the decay half-life by:

$$\tau = \frac{1}{\lambda}. \tag{2.24}$$

Furthermore, the number of radioactive atoms can be replaced with activity and represented as:

$$A = A_s e^{-\lambda t}, \tag{2.25}$$

Also, the ratio of activity (A_s) and the total mass (m) of an element (sum of radioactive and stable isotopes) known as *specific activity* (A) are related as:

$$A_s = \frac{A}{m}(Bq/kg) \tag{2.26}$$

2.5.1 Bateman Equation (BE)

The evolution of nuclide concentrations undergoes linear or serial decay chain governed by a set of first order differential equation known as Bateman equation [Cet06]. The solution to Bateman equations for radioactive decay in linear-chain is given by H. Bateman [Bat10]. If $N_i(0)$ is the number of i^{th} isotope of the series at time t = 0, and assuming zero concentrations of all daughters at time zero [Cet06] , then:

$$N_1(0) \neq 0 \quad \text{and} \quad N_i(0) = 0 \quad \text{when} \quad i > 1 \tag{2.27}$$

The general Bateman Equation takes the form:

$$N_i(t) = \lambda_1\lambda_2....\lambda_{i-1}N_1(0)\sum_{j=1}^{i}\frac{e^{-\lambda_j t}}{\prod_{k\neq j}(\lambda_k - \lambda_j)}, \tag{2.28}$$

By applying the BE for the 2nd isotope in a series, this gives [Cet06]:

$$N_2(t) = \lambda_1 N_1(0)\left[\frac{e^{-\lambda_1 t}}{\lambda_2 - \lambda_1} + \frac{e^{-\lambda_2 t}}{\lambda_1 - \lambda_2}\right] = \frac{\lambda_1 N_1(0)}{\lambda_2 - \lambda_1}(e^{-\lambda_1 t} - e^{-\lambda_2 t}), \tag{2.29}$$

and

$$\begin{aligned} A_2(t) = \lambda_2 N_2(t) = N_1(0)\frac{\lambda_2\lambda_1}{(\lambda_2 - \lambda_1)}(e^{-\lambda_1 t} - e^{-\lambda_2 t}) = A_1(0)\frac{\lambda_2}{\lambda_2 - \lambda_1}(e^{-\lambda_1 t} - e^{-\lambda_2 t}) \\ = A_1(0)\frac{1}{1 - \frac{\lambda_1}{\lambda_2}}(e^{-\lambda_1 t} - e^{-\lambda_2 t}) \quad = A_1(t)\frac{\lambda_2}{\lambda_2 - \lambda_1}(1 - e^{-(\lambda_2 - \lambda_1)t}) \end{aligned}, \tag{2.30}$$

also, for the 3rd isotope in a series:

$$N_3(t) = \lambda_1\lambda_2 N_1(0)\left[\frac{e^{-\lambda_1 t}}{(\lambda_2 - \lambda_1)(\lambda_3 - \lambda_1)} + \frac{e^{-\lambda_2 t}}{(\lambda_1 - \lambda_2)(\lambda_3 - \lambda_2)} + \frac{e^{-\lambda_3 t}}{(\lambda_1 - \lambda_3)(\lambda_2 - \lambda_3)}\right], \tag{2.31}$$

$$\begin{aligned} A_3(t) = \lambda_3 N_3(t) = \lambda_3\lambda_1\lambda_2 N_1(0)\left[\frac{e^{-\lambda_1 t}}{(\lambda_2 - \lambda_1)(\lambda_3 - \lambda_1)} + \frac{e^{-\lambda_2 t}}{(\lambda_1 - \lambda_2)(\lambda_3 - \lambda_2)} + \right. \\ \left. \frac{e^{-\lambda_3 t}}{(\lambda_1 - \lambda_3)(\lambda_2 - \lambda_3)}\right] = \lambda_3\lambda_2 A_1(t)\left[\frac{1}{(\lambda_2 - \lambda_1)(\lambda_3 - \lambda_1)} + \frac{e^{-(\lambda_2 - \lambda_1)t}}{(\lambda_1 - \lambda_2)(\lambda_3 - \lambda_2)}\right. \\ \left. + \frac{e^{-(\lambda_3 - \lambda_1)t}}{(\lambda_1 - \lambda_3)(\lambda_2 - \lambda_3)}\right] \end{aligned}. \tag{2.32}$$

Therefore, both the number of atoms and the activity concentrations of 1^{st}, 2^{nd} and 3^{rd} decaying isotopes in the series can be well estimated using Bateman Equation.

2.6 Interactions of Gamma-rays with Matter

Gamma-ray is an electromagnetic radiation with wave-like particle and can also interact with matter. Gamma radiation have greater penetration power and a longer range in matter than most other types of radiation [Gil08]. The transitions between nuclear energy states from excited nuclear states to the nuclear ground

states result in gamma-ray emission. There are various interaction mechanisms for gamma-rays, however only three are the most important that play a significant roles in radiation measurements, namely: Photoelectric absorption, Compton scattering and Pair production [Gil08, Kno99].

2.6.1 Photoelectric Absorption

Photoelectric absorption occurs when an incident gamma-ray photon transfers all its energy to a bound electron. An electron may be ejected from the shell usually from K-shell, and the photon disappears (see Fig. 2.8). The vacancy will be filled through capture of a free electron from other shells of the atom. About 80% of photoelectric absorption processes take place in K-shell of the atom since the photon energy ($E_\gamma = h\upsilon$), usually exceeds the binding energy of the K-shell electron [Gil08, Kno99]. If sufficient energy is not available to eject a K electron, then L or M electrons will be ejected instead. This gives rise to sharp discontinuities (K, L or M edges) in the photoelectric absorption curves with respect to the binding energies of the K, L and M electron shells. These absorption curves occur at binding energies corresponding to the electron shells. As an illustration, the curve in Fig. 2.9 shows the K and L absorption edges spectra obtained from HPGe and Caesium iodide (CsI) detectors, which occurs at 11.1 keV (K-absorption) and CsI have two edges, one corresponds to iodine K-electron (33.16 keV) and the other to caesium K-electron (35.96 keV) [Gil08]. Below this energies, only L and higher electrons can be photoelectrically ejected.

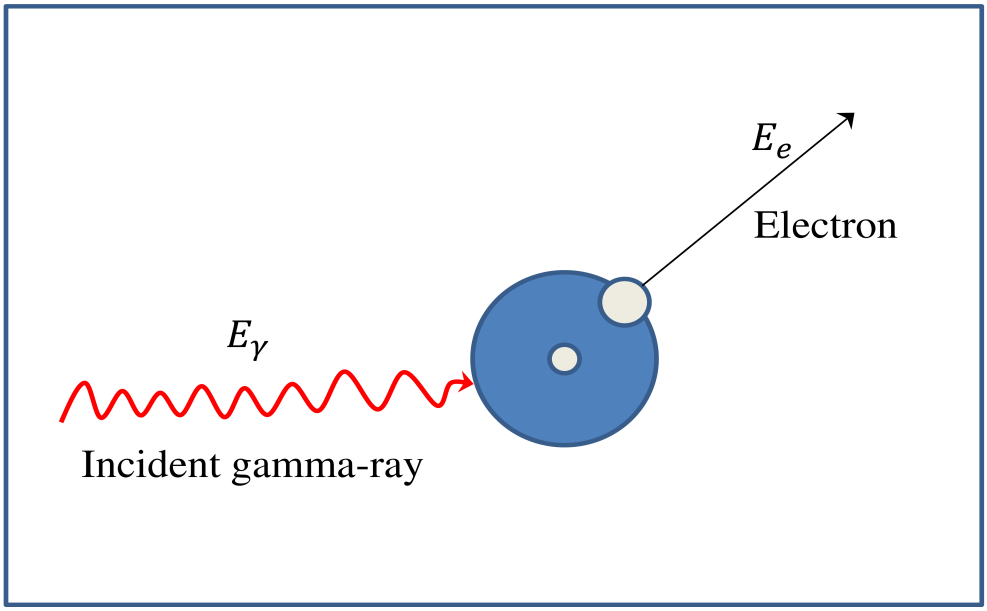

Figure 2.8: Schematic diagram of photoelectric absorption mechanism [Gil08].

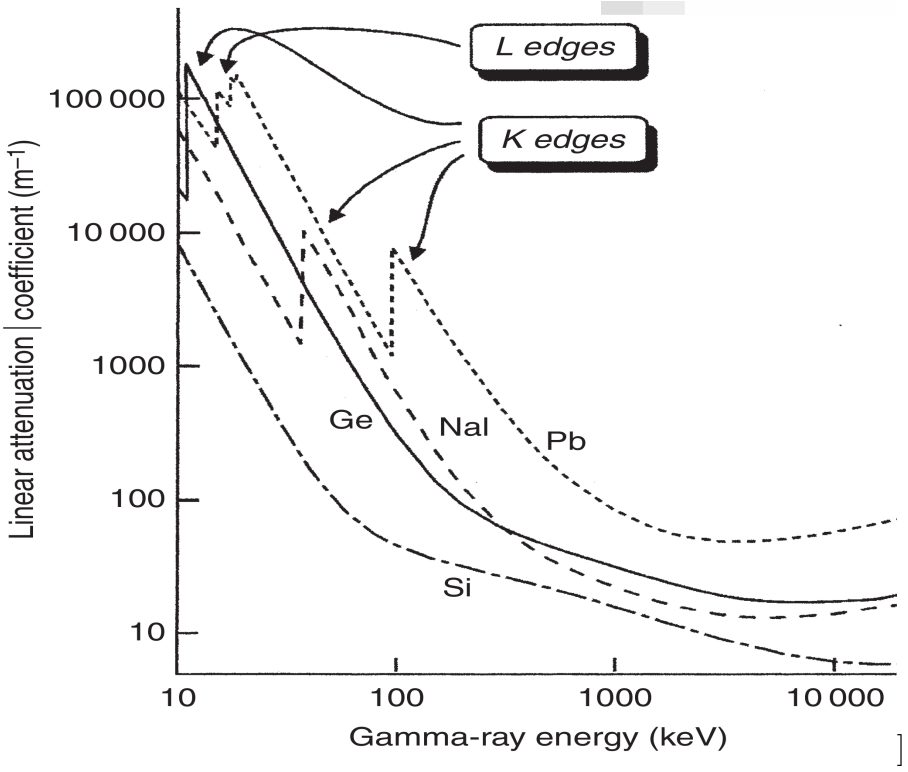

Figure 2.9: Linear attenuation coefficient of a materials relevant to gamma-ray spectrometry as a function of gamma-ray energy [Gil08].

The photoelectron is ejected from its shell with a kinetic energy, E_{e}, given by [Gil08];

$$E_e = E_\gamma - E_b \tag{2.33}$$

where E_b is the binding energy of the photoelectron in its original shell and E_γ is the energy of the gamma-ray.

The photoelectric process is the most favourable effect for gamma spectroscopy based on the fact that all of the photon energy is transferred to the electron in the detector material. There is no single analytical expression that is valid for probability of a photon to undergo photoelectric absorption per atom over all ranges of gamma-ray energy (E) and atomic atomic number (Z) [Kno99].

The dependence of photoelectric absorption probability on the atomic number of the absorber material is the major reason for the use of high-Z material in detectors and gamma-ray shielding (e.g lead). This can be expresses in terms of its differential cross-section σ

$$\sigma \propto \frac{Z^n}{E_\gamma^m} \tag{2.34}$$

where m and n range from 3 to 5, depending on the energy [Gil08].

2.6.2 Compton Scattering

Arthur Compton was the first person that introduced the theory of Compton scattering in 1922 [Bei81]. The scattering was of very low energy protons ($h\upsilon \ll m_o c^2$) by a free electron which is fairly described by non relativistic classical theory of J. J Thomson. This theory does not hold as $h\upsilon$ approaches $m_o c^2 =$ 0.511 MeV. Therefore it is very important to develop the relativistic theory of scattering. Figure 2.10 illustrates how the photon with energy (E_γ) interacts with an electron. After the interaction, the electron possesses some recoil energy (E_e) which leads to the reduction of Photon energy ($E_\gamma^{'}$). The recoil energy of the electron is given by the following equation:

$$E_e = E_\gamma - E_\gamma^{'}, \tag{2.35}$$

The fraction of the energy absorbed in any interaction is a function of incident gamma-ray energy (E_γ) and scattering angle θ.

$$E_\gamma^{'} = \left[\frac{E_\gamma}{1 + \frac{E_\gamma}{moc^2}(1 - \cos\theta)}\right]. \tag{2.36}$$

In a normal circumstances, all the scattering angles maybe seen in the detector.

The recoil electron energy can range from 0 for $\theta = 0^o$, the photon is directly scattering forward or not scattered at all and Eq.2.36 reduces to $E_\gamma = E_\gamma^{'}$. For the high energy that completely back scattered ($\theta = 180^o$), Eq.2.36 reduces to $E_\gamma \simeq mc^2/2$. The differential cross-section for Compton Scattering at an angle θ was one of the first to be calculated using Klein-Nishina formula [Leo87]:

$$\frac{d\sigma}{d\Omega} = {r_o}^2 \left[\frac{1}{1+\alpha(1-\cos\theta)}\right]^3 \left[\frac{1+\cos\theta}{2}\right] \left[\frac{1+\alpha^2(1-\cos\theta)^2}{(1+\cos^2\theta)[1+\alpha(1-\cos\theta)]}\right]. \quad (2.37)$$

Here $d\Omega$ is the solid angle increment in steradians, r_o is the classical electron radius ($r_o = e^2/4\pi\epsilon_o mc^2$) and ($\alpha = E_\gamma/mc^2$) is the photon energy in the unit of electron rest mass energy.

The result obtained from this interaction are the formation of ion-pair as in the case of photoelectric absorption. However, the photon energy continues to travel through matter until it dissipates all its kinetic energy by interacting with other electrons in a similar mechanism.

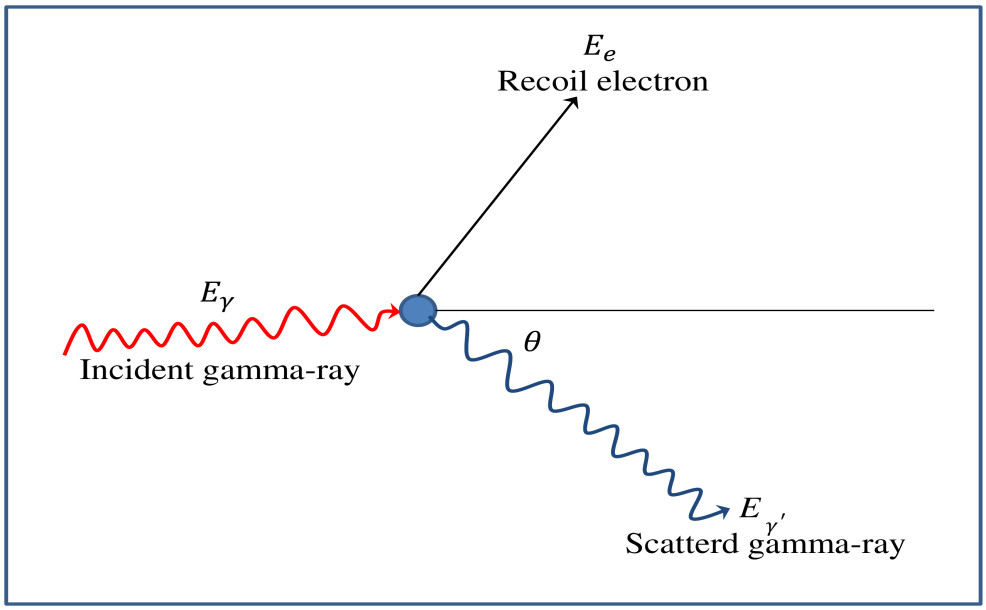

Figure 2.10: Schematic diagram of Compton scattering mechanism [Kno99].

2.6.3 Pair Production

Unlike photoelectric absorption and Compton scattering, pair production results from the interaction of the gamma-ray with the atom as a whole. Pair production occurs within the coulomb field of the nucleus resulting in the conversion of gamma-rays into an electron-positron pair. This process is energetically possible at gamma-ray energy larger than 1022 keV (twice the rest mass of an electron, 511 keV (see Fig. 2.11). These γ-rays can either be absorbed by or escape the detector crystal. Annihilation photon is seen as two processes in environmental samples. ^{22}Na parent nucleus undergoes β^+ decay, the positron emitted may only travel a few millimetre (depending on the material) before losing its kinetic energy and encountering an electron. The annihilation of an electron-positron pair generally does not occur until the energy of the positron is reduced to near the thermal energies, releasing the two 511 keV annihilation photons. This gives rise

to the escape peaks in the gamma spectrum [Kno99, Gil08]. Pair production can also occur under the influence of electron field, but the probability is too low and the threshold is twice greater 2044 keV. The incident γ-ray energy can be satisfied by the equation [Gil08]:

$$E_e = E_\gamma - 2m_o c^2 \tag{2.38}$$

No simple expression exists for pair production cross-section probability per nucleus, σ, but its magnitude varies approximately as the square of the absorber atomic number.

$$\sigma \approx Z^2 f(E_\gamma, Z). \tag{2.39}$$

The variation of σ with atomic size is dominated by Z^2, $f(E_\gamma, Z)$ is slightly dependent on Z and increases with energy from the threshold (1022 keV) [Gil08]. Therefore, for energies greater than 10 MeV, pair production is a dominant mechanism of interaction.

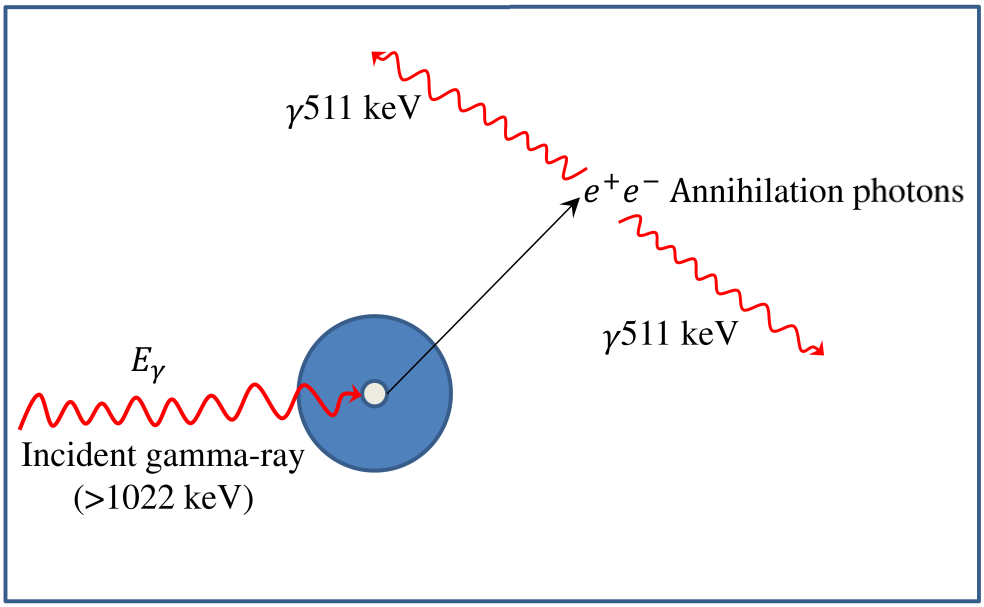

Figure 2.11: Schematic diagram of pair production mechanism and annihilation [Gil08]).

The three interaction processes discussed above mainly depends on the gamma-ray energy. Figure 2.12 gives the photon energy (hυ) *versus* atomic number (Z) of the material in which the border lines show where the probability of any of the two adjacent interaction process overlap.

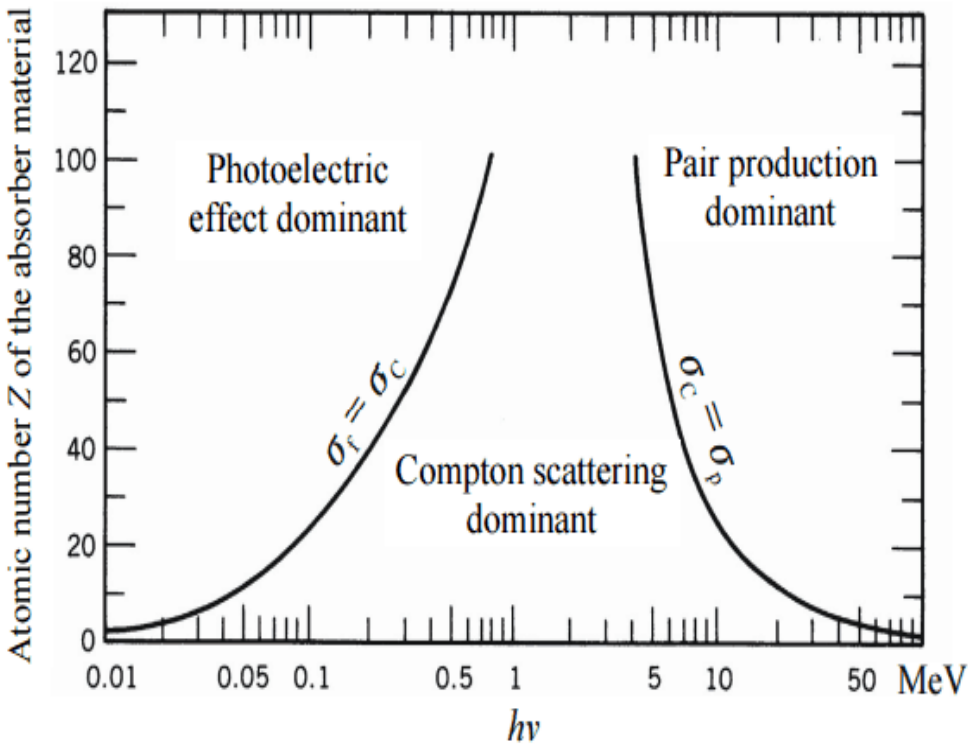

Figure 2.12: The three important γ-ray interaction processes [Kra88].

2.6.4 Gamma-rays Attenuation

A gamma-ray of any given energy that passes through any material will have a certain probability of being attenuated. Simply, for a number of gamma-rays incident on material, only a percentage of photons will fully pass through it. This is dependent on the gamma-ray energy, density and composition of the target material [Lan13]. The three interaction of gamma-ray discussed above, the photons can either absorbed or scattered. The total attenuation coefficient is defined as the

total probabilities per unit length (μ) for removal of a photon and is determined by the sum of probabilities given by [Kno99]:

$$\mu = \tau_{\text{photoelectric absorption}} + \sigma_{\text{compton scattering}} + K_{\text{pair production}}. \tag{2.40}$$

This equation governs the loss in intensity when passing any thickness (dx) of the material, and is formally constructed by using the equation:

$$dI/I = -\mu dx. \tag{2.41}$$

Attenuation formula of photons was given by "$BEERS\ LAW$" [Kno99], if

- "I" is the intensity of the gamma-rays through the material
- "I_o" is the intensity of the gamma-rays incident on the material
- "x" is the linear thickness of the material
- "μ" is the linear attenuation coefficient of the material at the energy of gamma-ray photon. This can be formally constructed as:

$$I = I_o \times e^{-\mu x}. \tag{2.42}$$

If the medium area thickness is given in g/cm^2 or mg/cm^2, then the mass attenuation coefficient of this interaction is given by μ_m, which depends on the incoming gamma-ray photon energy and not on the physical state of a given absorber. Therefore, it can be determined from the expression [Cem08]:

$$\mu_m = \frac{\mu_I}{\rho}. \tag{2.43}$$

The relationship between μ_I and μ_m is given by:

$$\mu_I(cm^{-1}) = \mu_m \left[\frac{cm^2}{g}\right] \times \rho \left[\frac{g}{cm^3}\right] \tag{2.44}$$

Furthermore, the mass attenuation can be re-written in this form;

$$I = I_o \times e^{-\mu_m \rho x} \tag{2.45}$$

where ρx is the mass thickness of the absorber in units of g/cm^2. For the measurement of radiation, the mass attenuation coefficient is often used more than the linear attenuation coefficient.

2.6.5 Attenuation Correction

The value of μ is not known for most environmental analysis and it should be estimated by measurements or by using an assumed sample density and composition. The distribution of the path lengths via the sample of the photon contributing to the peak count rate depends on sample geometry and slightly on the detector dimensions and photon-energy. In order to get a realistic evaluation of self attenuation corrections, a weighted average of transmission factor should be computed [Rob09]. In this case, a Monte Carlo simulation tool-kits is used, which takes into account distribution of the path lenghts. For example, self-attenuation correction factors ($C_{self}^{attenuation}$) for a cylindrical samples of x and a linear attenuation coefficient μ with a reference sample ($\mu \approx 0$) can be computed with the following equation:

$$C_{self}^{attenuation} = \frac{\mu x}{1 - exp(-\mu x)}. \tag{2.46}$$

Equation 2.46 was proposed for a measured cylindrical samples with an appropriate value of thickness, which can be computed from the dimension of sample holder [Sim92] [Sim97] [Sim01]. In order for the Eq. 2.46 to be useful, self-absorption component must be determined according to relative standard sample

(index c and index s) [Jod06]

$$C_s = \frac{C^a_{s,s}}{C^a_{s,c}} = \left[\frac{1 - exp(-\mu_c x).\mu_s}{1 - exp(-\mu_s x).\mu_c}\right] \tag{2.47}$$

The transmission method that links the transmission measurement of attenuation factor with the self-absorption in Eq. 2.46 for reference sample is expressed as [Cut83]:

$$C_s = \frac{ln(I_c/I_s)}{1 - (I_s/I_c)} \tag{2.48}$$

Where I_c I_s are the transmission experiment results for actual standard sample.

2.7 Gamma-ray Detection

Gamma-ray detection is one of the most important tools in nuclear physics. The detection of gamma-ray yields information on various properties of nuclei, such as decay energies, angular moments, excitation energy and so on. The process by which energy is detected is ionisation, where it gives all its energy or part to an electron. The charge is collected directly (in a semiconductor detector) or indirectly (in a scintillation detector), in order to determine the gamma-ray energy. There are various types of detector used to observe gamma-rays and their energies, either scintillator type or semiconductor (silicon and germanium) type. The energy resolution of the semiconductor detectors are better than the scintillator detectors. For the gamma-ray detection, germanium is more preferred compared to silicon because of its high atomic number and small binding energy. The detector material should also have as many electron-hole pairs as possible per unit energy.

Silicon and germanium detectors must be cooled to reduce the natural, thermally generated electrical noise levels in the crystal. However, the disadvantage of such detectors: the detector package must include capacity for cooling, this is usually the Dewar containing liquid coolant. The liquid nitrogen (LN_2) is one of the most popular gas use to cool the detector [Has19]. In a non-destructive assay it is very important not to measure the amount of radiations emanating from the samples only but also its energy spectrum. Therefore, most of the detectors use in a non-destructive assay application are those whose output signals are proportional to energy deposited by gamma-ray in the detector sensitive volume [Cro70, Kno99].

2.8 Coincidence Summing Process

For a radionuclides that emit two or more γ-rays within the resolving time of the gamma detector, a phenomenon known as coincidence summing occurs [Gil08]. In essence, the two photons arrive in the detector material at the same time, yielding an artificial photon at higher energy and decreasing the intensity of the original gamma-rays. Depending on the efficiency of the germanium detector and the geometrical composition of the sample, coincidence summing can severely underestimate the intensity of the original photons. For example, origin of summing was simplified from ^{152}Eu decay scheme shown in Fig. 2.13. There are two possible decay modes for this nuclide; (i) ^{152}Eu can either emit β^- particle and become ^{152}Gd (ii) or more likely (72.08 % of event) undergo electron capture process to form ^{152}Sm [Fir96]. For these decay modes, the daughter nuclei de-excites by emitting a number of gamma-rays until a stable nucleus is formed. The lifetime of the individual nuclear levels are more shorter than the resolving time of gamma-ray spectrometer system. Furthermore, each disintegration of an

^{152}Eu nuclei in the source releases a number of gamma-rays and possibly X-rays simultaneously [Gil08].

For the detector, there is high probability that the detector will detect more than one of these gamma-rays within the resolving time of the detector. In that case, the recorded pulse represents the sum of the energies of the two individual photons. This is known as coincidence summing-out, which reduces the intensity of the photon energy as recorded by the detector. It is also possible for multiple photons to sum to equivalent energy of photon of interest, thereby increasing the efficiency of the detector and this effect is referred to as the coincidence summing-in [Gil08].

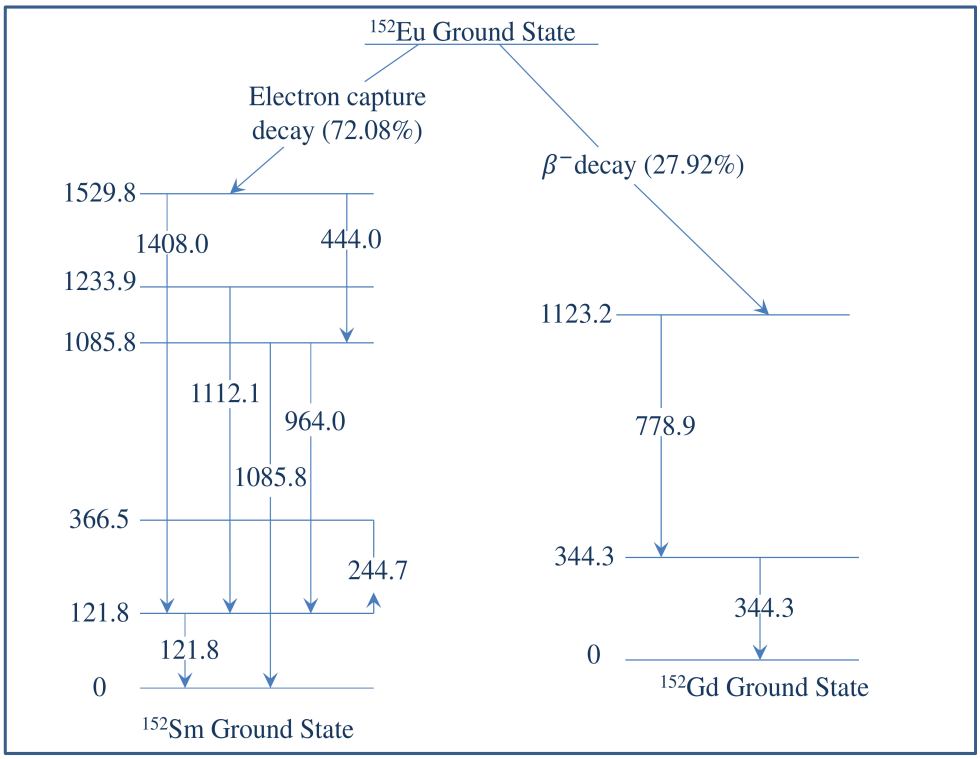

Figure 2.13: Schematic diagram of decay scheme for ^{152}Eu [Fir96].

Since there are two possible cases that generates deviations on the efficiency value, the correction factors must be greater or smaller than one, and can be obtained from the following equation [Ven15]:

$$K_{cs} = \frac{n_o}{n_o^{'}} \tag{2.49}$$

where K_{cs} is the coincidence summing, n_o is the count rate in the full-energy-peak and $n_o^{'}$ is the net peak area by summing with the i^{th} gamma-ray. n_o is expressed in Eq. 2.50 and $n_o^{'}$ has three possibilities according to Fig. 2.14 which represent the net peak area for γ_a in Eq. 2.51 (summing-out event), the net peak area for γ_b represent another summing-out event in Eq. 2.52 or the net peak area for γ_c (summing-in event) in Eq. 2.53 [Ven15]:

$$n_o = Ap_o\varepsilon_o \tag{2.50}$$

$$n_o^{'} = Ap_1\varepsilon_a - Ap_1\varepsilon_a\varepsilon_{t2} \tag{2.51}$$

$$n_o^{'} = Ap_2\varepsilon_b - Ap_1\varepsilon_b\varepsilon_{t1} \tag{2.52}$$

$$n_o^{'} = Ap_3\varepsilon_c - Ap_3\varepsilon_a\varepsilon_b \tag{2.53}$$

Here:

- Subscript "o" is the gamma-ray of interest (a,b or c)
- "A" is the number of atoms decaying
- "p_i" represent the probability emission of i^{th} gamma and the gamma-ray of interest
- "ε_{ti}" is the total efficiency of i^{th} gamma-ray
- "ε_i" is the probability of γ_i being detected and appearing in the full-energy-peak.

The total efficiency from Eqs. (2.51, 2.52 and 2.53) can be used for True-Coincidence-Summing [Ven15, Aga11, Gil08].

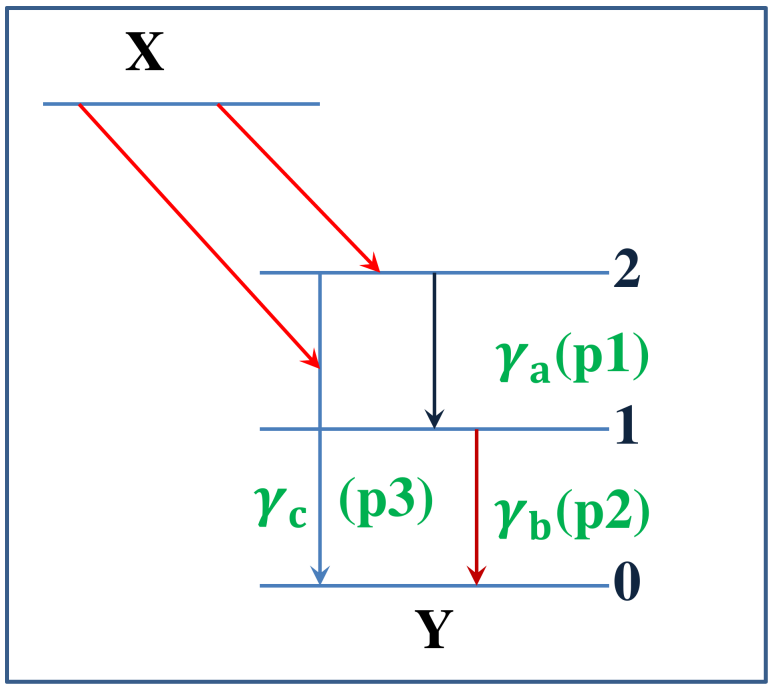

Figure 2.14: Schematic Decay scheme of a nuclide decaying from X to Y [Ven15].

Furthermore, the coincidence summing is not count rate dependent but geometry dependent, therefore, it is advisable to estimate the correction factors numerically or by the use of Monte Carlo Simulation tool-kits. [Kor93].

Chapter 3

Monte Carlo Methods

In order to appreciate the full potential of Monte Carlo (MC) simulations for modern physics applications, it is very important to understand the processes of the method. In this chapter, basic principles of the methods and two Monte Carlo codes (GEANT4 and FLUKA) out of the many that are available, will be discussed.

3.1 Introduction

Monte Carlo methods originated from Los Alamos National Laboratory after World War 2 in 1945 [Met56]. Many years later, Ulam (1987) suggested the use of random processes to simulate the flight paths of neutrons, based on the proposal written and developed in 1947 by Von [Ula87]. This project led to small-scale simulations whose results were indispensable in completing the project. The name Monte Carlo comes from a city in Monaco, which is famous for its casinos [Mey56]. Years later, Monte-Carlo methods are now used in various fields, from a complex physical simulation, such as radiation transport in the earth's

atmosphere and to simulate complex subnuclear processes in high-energy physics, astrophysics, physical chemistry, medicine and related applied fields [Ago03].

Boson et al. (2008) used Monte-Carlo to improve the estimation of gamma-ray detector efficiency as a function of energy and obtained 10-20% higher than what was found in the experimental work [Bos08]; similar discrepancy was previously reported by Korun et al. [Kor93]. A possible explanation for the discrepancy in efficiency estimations was due to uncertainties associated with the crystal dimensions as provided by the manufacturer [Bos08]. In order to correct for the efficiency of the detector using Monte Carlo simulations, benchmark tests are required to estimate the correction factor between the experimental and simulation data.

Furthermore, coincidence summing method has already been reported by various studies which offers higher accuracy and is still growing in popularity of Monte-Carlo simulations of the interaction of gamma rays with the detector [Arn04, Vid05].

3.2 Monte Carlo Method for Radiation Transport

Current applied nuclear physics research used extensively the simulation of instrument response in their planning and operation phases [Fer05]. This can also be used to solve deterministic problems by drawing random samples from probability distribution. The most common feature for these computational algorithms

is that it can run many iterations with the use of large numbers and some other properties to obtain a statistical uncertainty of interest [Ula87].

By using *random number*, a computer can create history of each particle related to random walk analysis. That is, the history of primary particle (assuming a photon) consists of its emission at the source, interaction with the detector and the surrounding materials. Production as well as transport of secondary particles are tracked until the photon escapes or undergoes photoelectric absorption in the system, depositing all its energy. A set of random numbers have no pattern and are sampled uniformly between zero and one. These are used to determine the interaction process that occurs, and predict the energy loss, including the new direction of the particle in the scattering event. In photon transport for example, a photon is emitted from a source placed at a position (x, y, z) in a specific direction (Ω), this will interact with surroundings in three different ways by photoelectric absorption, Compton scattering and pair production as discussed in Section 2.6.1, 2.6.2 and 2.6.3, respectively. The events that occur from the beginning of the particles are tabulated and become the history of that particle. Therefore, the history number needs to be assessed to accurately describe the previous events.

In Fig. 3.1, a typical flow chart of the process discussed above is shown. It is very crucial that the user provides the accurate geometrical input defining the problem to be simulated, while the Monte Carlo codes with buit-in physics model and cross-section data handles the resulting process that follows. Some of the information to be included by the user is the starting position of particle (or photon)(γ), the energy (E) and the initial direction (Ω) of the particle. Monte Carlo simulation is a

very useful application in gamma ray interaction with the matter, and in deriving interaction parameters analogous to experiment at various photon energies. The standard modelling technique implemented in the present work for estimation of photon interaction parameters can be utilised for various types of samples or complex materials. Some of the popular multi-purpose particle interaction and transport Monte Carlo codes are GEANT4 [Ago03], FLUKA [Fer05] and MCNPX [Pel08]. For the purpose of this study GEANT4 and FLUKA were used for the detector optimisation and the overview are provided in the sections that follows.

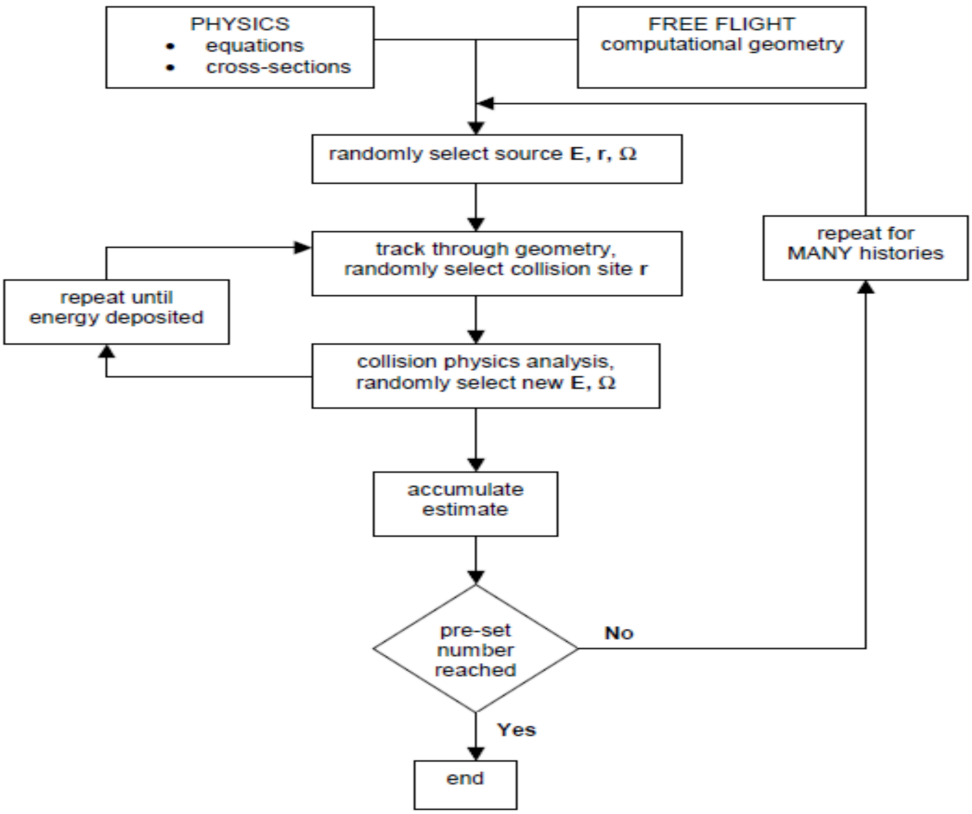

Figure 3.1: A schematic diagram showing workflow of radiation transport applied in Monte Carlo simulations [Hen02].

3.3 Monte Carlo Code: GEANT4

GEANT4 is a Monte-Carlo toolkit for the simulation of passage of particles through matter [Ago03]. Its application areas include high energy, accelerator and nuclear Physics, as well as studies in space and medical science [Ago03, Col12]. GEANT4 simulation software was developed and maintained by CERN, and it is scripted in C++ programming language that provides solutions to particle interaction with matter, including visual analysis of geometry [Ago03]. The code comes with various standard examples for a user to modify, and additional data libraries for various physics processes. This allows user to derive classes to describe the geometry of a detector, primary particle generator, user interface and physics processes with electromagnetic, hadronic and decay physics based on theory, experimental data or parameterisations as shown in Fig. 3.2. GEANT4 installation does not come with any User Interface (UI), but command line driven. User interfaces are available for the GEANT4 toolkit; however, this is particularly general as part of a framework that acts as an interface between GEANT4 and the user.

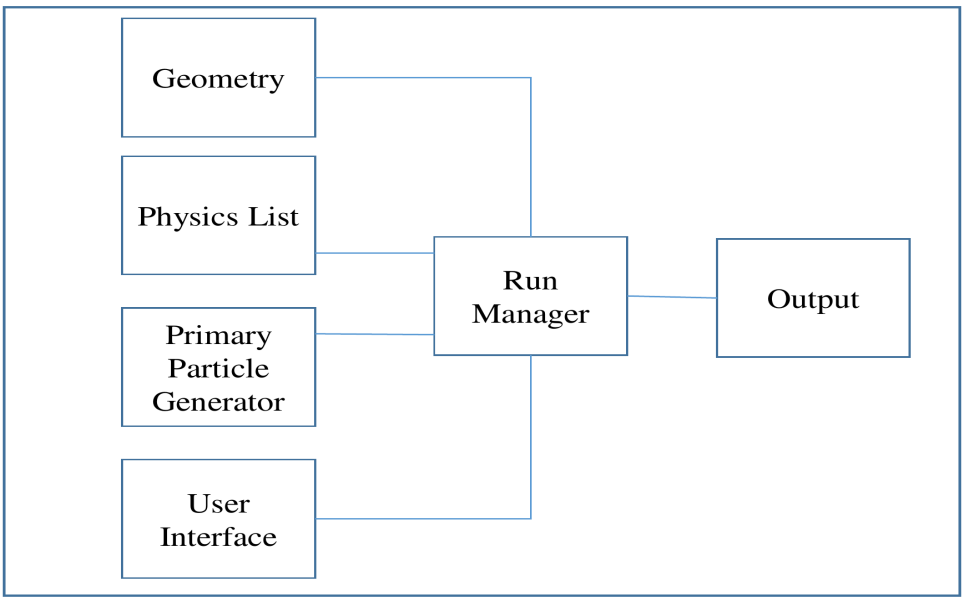

Figure 3.2: Simplified flow chat of GEANT4 simulation

Successfully installed GEANT4 with all the prerequisite can be used to simulate a number of source files, which are contained within the project directory. This creates an executable that can run in batch mode, and the user can specify the command for macro files. General Particle Source (GPS) can be modified in order to achieve the desired simulation results between the runs or by using a scripting language like BASH [Bas19] on Ubuntu (linux operating) system which can generate macro files, edit source files, recompile again and run the simulations until a reasonable result are achieved, as illustrated in Fig. 3.3.

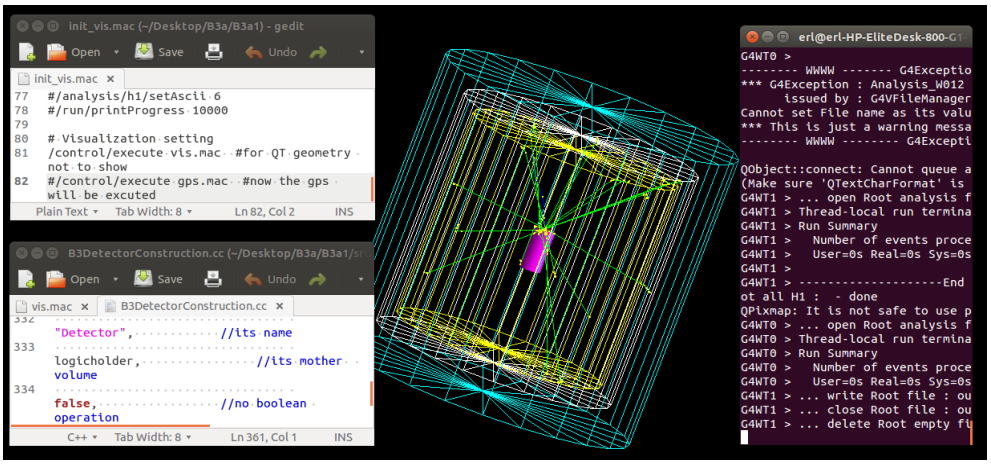

Figure 3.3: A screenshot of GEANT4 display ran on Ubuntu-16 operating system; RIGHT: The terminal; MIDDLE: Modified Geometry and; LEFT: Macro files with some GEANT4 commands.

GEANT4 offers the user with the requirement to interface the simulation in a few essential user classes. Three of the compulsory ones are the DetectorConstruction.cc (.hh) , the PhysicsList.cc(.hh) and the PrimaryGeneratorAction.cc(.hh) (see Section 3.3.1 and 3.3.2) [Col12]. To construct the geometry, the user has access to special classes that assist in the construction of various geometry shapes and volumes, and others that create and assign materials with user specified properties.

GEANT4 is embedded with materials that are made of elements, which in turn consist of isotopes. At any level of this hierarchy, the user is allowed to create own materials, elements, isotopes or select the suitable ones from the GEANT4 database material. By specifying the material inside DetectorConstruction class, the property of atoms such as atomic number, atomic mass, number of nucleons, and as well as quantity of cross-section per atom can be specified. Also, the user can specify the macroscopic parameters of matter like state, density, pressure,

temperature, mean free path, radiation length, and so on [Col12]. Example of how the materials are defined is shown in Fig. 3.4.

```
//....oooUUUUUooo........oooUUUUUooo........oooUUUUUooo........oooUUUUUooo...

 void B3DetectorConstruction::DefineMaterials()
{
  G4NistManager* man = G4NistManager::Instance();
  // define a material
  //Lead
  G4double a;  // mass of a mole;
  G4double z;  // z=mean number of protons;
  G4double density;
  new G4Material("G4_Pb", z=82., a= 207.2*g/mole, density= 11.35*g/cm3);

  //Air
  G4Material* Air = new G4Material("G4_AIR", 1.29*mg/cm3, 2);
  Air->AddElement(N, 70*perCent);
  Air->AddElement(O, 30*perCent);

  //Copper
  new G4Material("G4_Cu", z=29., a= 63.546*g/mole, density= 8.96*g/cm3);
 //Germanium
  new G4Material("G4_Ge", z=32., a= 72.64*g/mole, density= 5.323*g/cm3);
 // Aluminium
  new G4Material("G4_Al", z=13., a= 26.98*g/mole, density= 2.699*g/cm3);
```

(a) (b) (c) (d)

Figure 3.4: A screenshot of material definitions during GEANT4 simulation: (a) DetectorConstruction class specification; (b) Lead material used for detector shielding; (c) air material defined inside the lead castle; and (d) copper linning, the detector and aluminium materials.

Molecules are implemented by specifying the number of each atom type or by giving the fractional mass of each component. The primary particles can be radioactive source, proton beam, gamma spectrum, etc.; all this must be defined and physics behind the simulation must be added. GEANT4 can then simulate the passage of the primary particles through the detector, and transport each particle through a series of steps.

3.3.1 Physics List

GEANT4 PhysicsList define electromagnetic processes with effective energy from 250 eV and extend to TeV [Ago03]. Photon interactions used are Photoelectric effect, Compton scattering and Pair production, while the electrons interactions are consist of Bremsstrahlung and multiple scatterings as ionisation with illustration in Fig. 3.5. Atomic effects after photoelectric effect, such as Auger effect and X-ray emission are included. Therefore, it is possible to have point of interaction from photoelectric effect [Ama05]. Figure 3.6 shows how G4Boson, G4Lepton, G4Meson, G4Boson, G4Baryon and Ion Constructor are also included [Col12]. In GEANT4 some electromagnetic processes require a threshold below which no secondary particles are generated, because of this requirement the threshold used in this study were set to zero in order to acquire from lowest to highest energy possible. The PhysicsList allows the user to switch certain processes on or off, and to select different sub-lists from the photon interactions. In order for the user to be able to modify the parameters and select different type of physics sub-lists, a messenger class must be implemented, which allows changes to be made without compiling the simulation again.

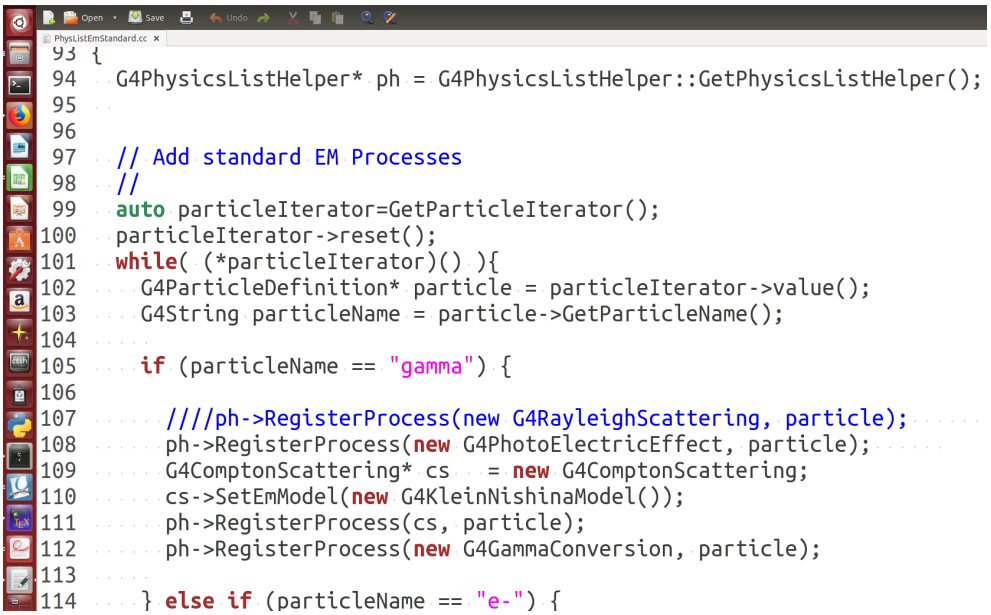

```
PhysListEmStandard.cc
 93 {
 94   G4PhysicsListHelper* ph = G4PhysicsListHelper::GetPhysicsListHelper();
 95
 96
 97   // Add standard EM Processes
 98   //
 99   auto particleIterator=GetParticleIterator();
100   particleIterator->reset();
101   while( (*particleIterator)() ){
102     G4ParticleDefinition* particle = particleIterator->value();
103     G4String particleName = particle->GetParticleName();
104
105     if (particleName == "gamma") {
106
107       ////ph->RegisterProcess(new G4RayleighScattering, particle);
108       ph->RegisterProcess(new G4PhotoElectricEffect, particle);
109       G4ComptonScattering* cs     = new G4ComptonScattering;
110       cs->SetEmModel(new G4KleinNishinaModel());
111       ph->RegisterProcess(cs, particle);
112       ph->RegisterProcess(new G4GammaConversion, particle);
113
114     } else if (particleName == "e-") {
```

Figure 3.5: A screenshot of how the photon interactions are defined.

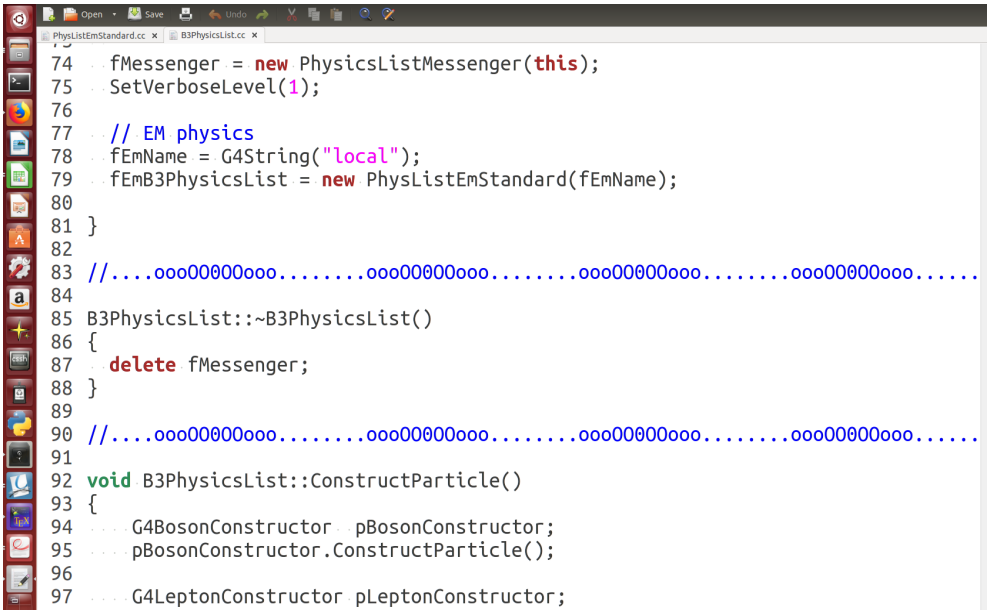

```
PhysListEmStandard.cc | B3PhysicsList.cc
 74   fMessenger = new PhysicsListMessenger(this);
 75   SetVerboseLevel(1);
 76
 77   // EM physics
 78   fEmName = G4String("local");
 79   fEmB3PhysicsList = new PhysListEmStandard(fEmName);
 80
 81 }
 82
 83 //....oooOOOOOooo........oooOOOOOooo........oooOOOOOooo........oooOOOOOooo......
 84
 85 B3PhysicsList::~B3PhysicsList()
 86 {
 87   delete fMessenger;
 88 }
 89
 90 //....oooOOOOOooo........oooOOOOOooo........oooOOOOOooo........oooOOOOOooo......
 91
 92 void B3PhysicsList::ConstructParticle()
 93 {
 94     G4BosonConstructor  pBosonConstructor;
 95     pBosonConstructor.ConstructParticle();
 96
 97     G4LeptonConstructor pLeptonConstructor;
```

Figure 3.6: A screenshot of Boson-Lepton particles constructor definitions.

3.3.2 Primary Particle Component

There are various ways of using primary particles generation in the primary Generatoraction.cc class, but the most commonly used are GeneralParticleSource (GPS) and G4ParticleGun module [Fer00]. The G4ParticleGun is for modelling a simple radiation field while GPS takes care of the complex ones. The GPS module is part of the GEANT4 simulation tool-kit that allows the user to specify the type of incident primary source particles as well as selecting their spatial, spectra, angular distribution, etc., while a multiple source particle can also be specified as depicted in Fig. 3.7. All the specifications are usually in the macro files but can also be modified through the command line. The source type can be point, plane, beam, surface and volume, (and the source shape type can be circle, square, rectangle, annulus, ellipsoid, cylinder, parallelepiped). In addition, the energy distribution needs to be selected by the user (mono-energetic, power-law, linear, exponential, bremsstrahlung, black-body, cosmic diffuse gamma-ray or Gaussian) [Col12].

However, the radioactive decay module includes the decay of coincidence, where excited nucleus may emit multiple gamma-rays before it reaches the ground state, and the emission of multiple decay products, such as beta and gamma-radiation. In this method, the selected isotope decays to stability and therefore, if the nuclide is part of a decay chain, multiple isotopes will be sequentially decayed within the same event until stability is reached (see Section 2.2). This is often not the intended effect, and decay chains can be limited by specifying where the chain should end within the macro file that is used to run the simulation (when including the radioactive decay process within the physics lists, the messenger.cc class required to do this will be automatically loaded).

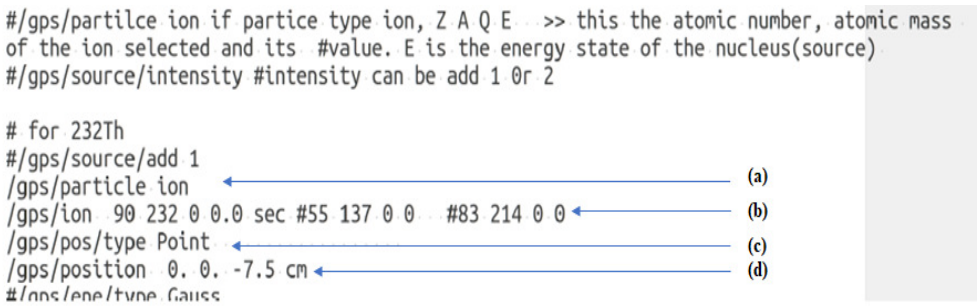

Figure 3.7: This illustrates how the General Particles Source (GPS) is defined: (a) particle ion (represent particles, such as electron, proton and gamma) specification; (b) atomic number and atomic mass of the source; (c) Source type (point source); (d) Source position.

3.3.3 Environmental Radioactivity Laboratory Detector System Setup

The geometry simulation needs to be a close approximation of the actual physical design to correctly model particle interactions in the detector regions. In order to have the correct absorption and production of secondary particles, the geometry simulation should include as much of the surrounding materials as possible. In the present work, simulation input for the HPGe detector set-up used includes the shield material (lead), copper lining, aluminium cryostat, aluminium holder and the detector crystal (Ge) (refer also to Figs. 4.5 and 4.6 for the system picture and sketch). The geometric characteristics such as the composition and thickness of the detector have been modelled, as depicted in Fig. 3.8, according to technical specifications given in Table 3.1 as provided by the manufacturer [Ger].

Table 3.1: HPGe detector modelled specifications using GEANT4 [Ger]

Component	**Dimension (cm)**
Lead shielding thickness	10
Copper lining thickness	2 mm
Aluminium cryostat length	7.100
Aluminium cryostat radius	3.503
Aluminium holder length	6.530
Aluminium holder radius	3.251
Germanium detector length	5.950
Germanium detector radius	3.125

GEANT4 offers various debugging tools, in order for the user to avoid introduction of bugs, and also to verify the correct experimental modelling set-up. The experimental set-up is modelled specifically by using the case incrementally from the small geometrical components to a large complex one. The users must test the geometry one after the other at each development cycle. The procedure for testing should include the following:

- visualisation of the experimental set-up to give an impression of the geometry being modelled
- by using a checkOverlaps() method at the level of Physical volume geometry, this is to verify the geometrical volume overlaps during the initialisation phase of the simulation as illustrated in Fig. 3.9.
- if geometry overlap occurs, use debugging tool to show the overlapping region from the experimental set-up

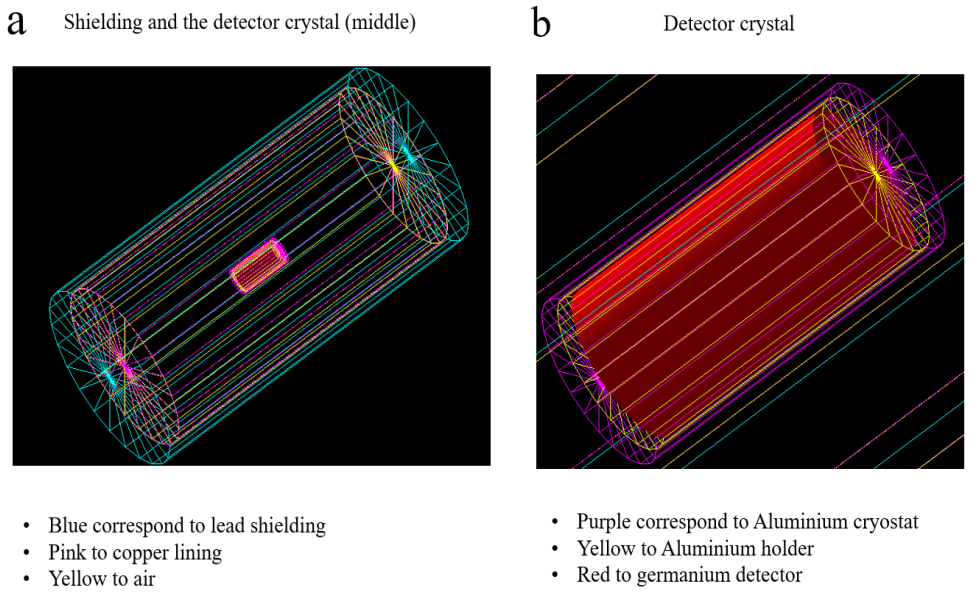

Figure 3.8: Acquired image of HPGe dectector constructed with GEANT4: (a) correspond to the shielding and the detector crystal; (b) illustrates the zoomed detector crystal.

```
190   G4double PbshieldRadius = 50.*cm;
191   G4Tubs*
192   solidPbshield = new G4Tubs("Pbshield", 0.,  //its name
193                   PbshieldRadius,0.5*Pbshieldlength, 0.,twopi);//its size
194
195   G4LogicalVolume*
196   logicPbshield = new G4LogicalVolume(solidPbshield,        //its solid
197                                       LeadMaterial,         //its material
198                                       "Pbshield");          //its name
199   G4VPhysicalVolume*
200   physiPbshield = new G4PVPlacement(0,                      //no rotation
201                                     G4ThreeVector(),        //at (0,0,0)
202                                     logicPbshield,          //its logical
      volume
203                                     "Pbshield",             //its name
204                                     logicWorld,             //its mother
      volume
205                                     false,                  //no boolean
      operation
206                                     0,                    //copy number
207                                     fCheckOverlaps);      // checking overlaps
208   //
```

Figure 3.9: A screenshot diagram showing how the geometry was constructed

In general, GEANT4 *geometry* is referred to as the volumes built in the simulation, whether they are sensitive components registering hits or merely pieces of material that traverse the particles. The part of the system that generates the pri-

mary particles is not included in the *geometry* definition but in the *primaryevent* definition.

3.3.4 Reproduction of Source

The reproduction of a source matrix can be defined as the source size, position and material, and also creating the object within the geometry simulation. The geometry source information is given by an external library file, which then allows access to this information for particle generation. The decay source can be generated as a random coordinate within the geometry source, and further supplemented by source holder/point as necessary. Summing effects in terms of the source activities are controlled by calculating the probability of the detector viewed from the distance of 0 cm to X cm within the detector characteristic decay time. Moreover, it uses the probability to generate extra decays in a corresponding number of events. Error in the uniformity of the source may cause unwanted effects and the thickness of attenuation within the detector are often only approximately known. To minimise these errors, secondary measurements are made of all components to verify their dimensions. Example of how the source is defined are shown in Fig. 3.7.

3.4 Monte Carlo Code: FLUKA

FLUKA is a multi-purpose transport code for simulating particle transport and interaction with matter [Fer05]. The code is currently managed by CERN and Italian National Institute for Nuclear Physics (INFN), and is written in Fortran. FLUKA also covers an extended range of applications spanning from calorimetry,

activation, detector design, dosimetry, proton and electron accelerator shielding and target design, radiotherapy and neutrino physics. FLUKA can transport 60 different type of elementary particles and heavy-ion, it can perform hadron-hadron, electromagnetic, neutrino, hadron-nucleus and μ-interactions from 1 keV up to thousands of TeV for charged particles [Fer05]. The simulation code can also handle a complex geometry using an improved combinatorial geometry package (CGP). The example of the geometry and the specifications used in this study are given in Figs. 3.10 and 3.11. Although FLUKA is a powerful tool for particle simulation problems, the Default Package(DP) offers a limited number of auxiliary programs and tools for building the input and post processing the output of the code [Fer05].

The FLUKA Advanced Interface (FLAIR) objective was developed to investigate and overcome problems with logical errors and input syntax. The use of FLAIR is by addressing the above problems and to provide an Integrated Development Environment for all the stages starting from building input file and processing the result [Vla09]. Furthermore, it consists of a fully included editor for editing an input files in a readable way with syntax and highlighting the errors, without hiding the FLUKA inner functionality for the users. FLAIR also offers the users to build an executable file, debugging geometry, running the code, monitoring the status of the runs, checking the output files, post processing of the binary files and an interface for plotting utilities like gnuplot for high-quality plot [Wil98]. FLAIR is an open source file with an Application Programming Interface (API) for manipulating FLUKA input files.

The material used for the study in FLUKA are implemented by ASSIGNMA card, which differentiate the region from each other (see Fig. 3.12). Also, the physics list used in this study for FLUKA are RADDECAY and EMF cards for preparing the atmosphere for measurement of radioactive decay. The The RADDECAY card requires the simulation of radioactive decay with biasing while EMF card is an electromagnetic FLUKA card that allows transport of electrons, positrons and photons [Fer05].

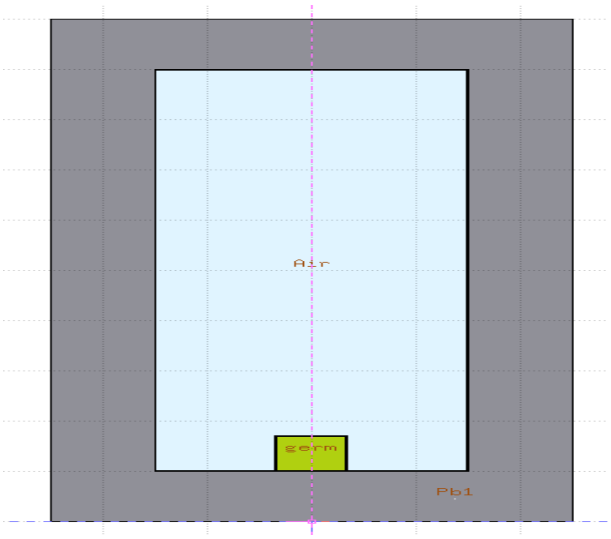

Figure 3.10: HPGe detector geometry surrounded with Lead shielding constructed using FLUKA code.

Figure 3.11: Example of geometry specifications used in FLUKA.

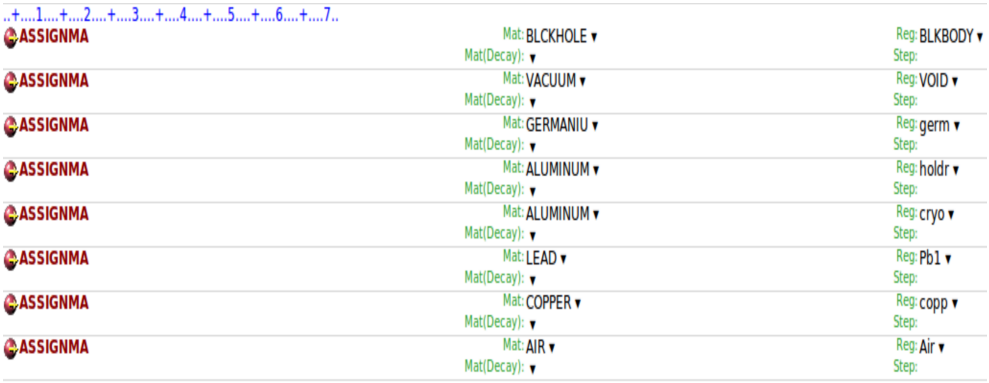

Figure 3.12: Screen shot assigning materials to various regions in FLUKA.

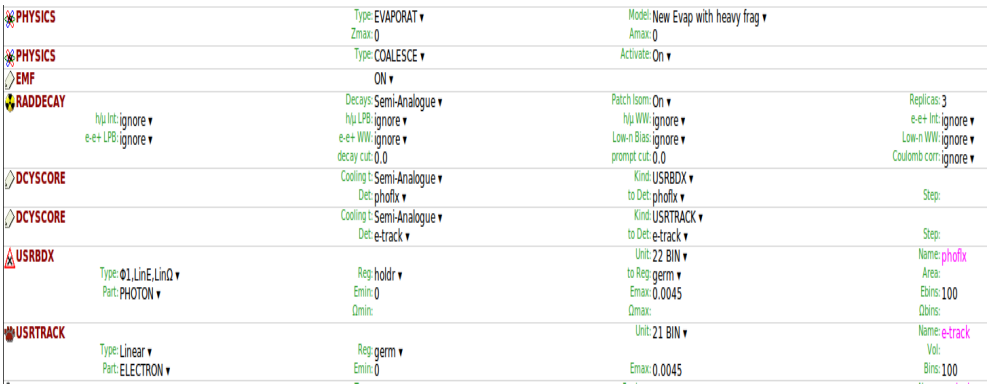

Figure 3.13: Screen shot illustrating the Physics list used in FLUKA.

3.4.1 Extracting Information from FLUKA

The FLUKA code allows the user to choose their own Scoring mesh from the available built-in cards. This is done by defining the size, position and resolution over the geometry which accumulates the required quantities over the simulation, for instance surface flux, energy deposited, the number of counts recorded, and so on. The values can be written to file for processing since the sensitive regions in the geometry have been set to read out the energy deposited within each event. Scoring cards need to be explained in more details. Each scoring card is designed to provide a specific quantity. The two cards used in this study are USRBDX and USRTRACK (both listed in Fig. 3.13). The USRBDX defines a detector for a boundary crossing fluence estimator. It is used to score the differential fluence of the source and secondary particles in a shield. The second scoring card, USRTRACK, is used to score detector track-length fluence estimator. FLUKA uses a special user routine code to read from the source file and to generate particles in the amount and of the energy specified in the source file. When these particles are incident on a scoring detector, the output of the detector card is always time independent.

Chapter 4

Experimental Setup

High-resolution gamma-ray spectroscopy method is one of the most widely used procedures for identifying and quantifying both known and unknown gamma-ray emitting radionuclides. To achieve accuracy in these measurements using gamma-ray detectors, several calibrations are required before any measurement could be done. In addition, complementary technique with Inductively Coupled Plasma-Mass Spectrometry (ICP-MS) was applied for quantifying isotopic concentrations in the investigated samples.

4.1 Sample Collection and Preparation

4.1.1 Study Area and Sample Collection

Twenty soil samples were collected from Yapala, located in Mayo-Dallah in Southern area of Chad, about 40 km from the city of Pala. Pala is a town of around 60,000 inhabitants, 46,600 of whom live in urban areas and 80% of whom live mainly from agro-pastoral activities. Exposure to ionizing radiation of the pop-

ulation of the study area varies slightly from sector to sector, but the average radiation dose from all natural sources is approximately 1.51 millisievert (mSv) per year [Pen18]. By comparison, on a global scale, the total average dose from natural radiation is approximately 2.4 mSv per year [Uns00]. It has an area spanning seventy-three thousand five hundred and twenty (73,520) hectares [Ins19]. Each composite sample consisted of a mixture of five samples taken from an area of three(3) square metre separated from each other. The spacing between the composite samples was randomised to cover the study site and to observe a significant local spatial variation in terrestrial radioactivity as illustrated schematically in Fig. 4.1. Four samples were collected at the edges of the sampling points and one in the centre to form a composite sample. Samples labelled S1 to S16 were from the former large open mining plains where mining is no longer undertaken at these locations, whereas samples S17 to S20 were taken from new large open mining plains where mining activities are underway. Sampling must be done in a systematic way to ensure accurate representation of the distribution of NORMs in the environment. Figure 4.2 illustrate the map of sample collection location. After the collection procedures, samples were posted to Environmental Radioactivity Laboratory (ERL) at iThemba LABS, Cape Town for further preparation and measurement procedures.

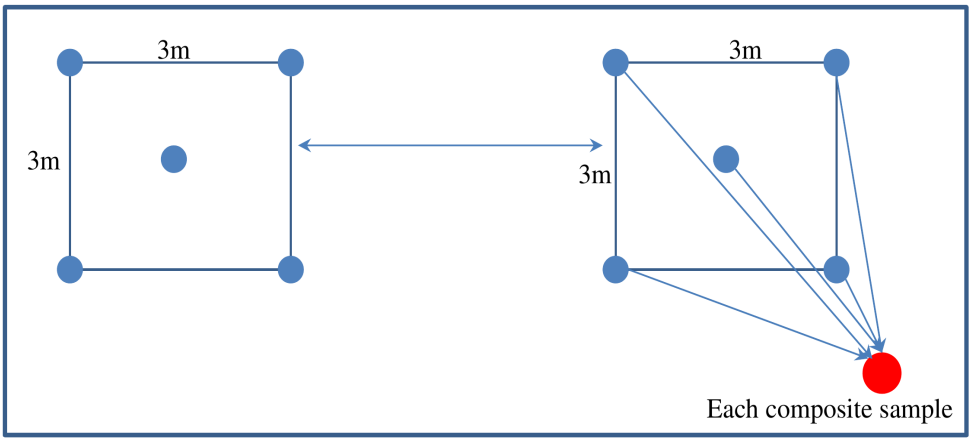

Figure 4.1: Schematic diagram illustrating the spacing between the composite sampling points.

Figure 4.2: Map of sample collection location. (Extracted from Google Map).

4.1.2 Sample Preparation

Sample preparation requires various steps before measurements using Hyper Pure Germanium (HPGe) detector. The samples were stored at the Environmental Radioactivity Laboratory, after arrival from Chad. Samples were crushed with mortar and pestle, and sieved through a mesh to remove organic material and to obtain an homogeneous sample. The bigger sized portion of the sieved particles

from the samples were crushed again and the remaining portion which failed to crush were totally removed. Each sample was poured onto a heating tray to be ready for heating in the oven. The oven was pre-set at a temperature of 105^{o}C in order to remove any excess moisture in the samples, following which, the prepared samples were dried in the oven for 24 hours. After drying, the samples were weighed on the scale and transferred with a spoon into 100 ml bottles, labelled and air-tight to minimise any gaseous progenies from escaping from the sample holder. The sample preparation process are shown in Fig. 4.3.

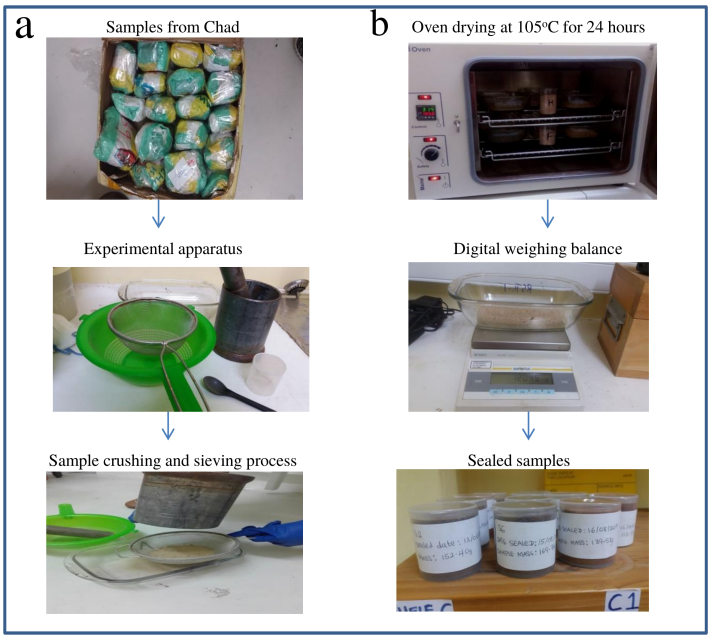

Figure 4.3: Sample preparation process used for this study.

4.2 HPGe Gamma-ray Detector System

The measuring system used for this study consist of Hyper-Pure Germanium (HPGe) detector, lead (Pb) shielding, sample holder, digital weighing balance and standards, electronics data acquisition system and computer with a processing

software to generate, store and display final gamma-ray spectrum obtained. The ERL Canberra HPGe detector has 2.2 keV Full Width Half Maximum (FWHM) at 1332 keV energy and a relative efficiency of 45% to the NAI (3x3 inch) at 1332 keV. The HPGe crystal is housed in a rigid cryostat with liquid nitrogen dewar to inhibit thermal conductivity between the crystal and the surrounding air. The mass of the liquid nitrogen in the detector is about 20 kg which allowed for weekly filling, so as to keep the detector operating at liquid nitrogen temperatures. The detector characteristics are listed in Table 4.1. Also, the detector setup is in low background condition, the detector crystal is enclosed inside a 10cm thick lead castle, since lead is more efficient as a material for shielding due to its high density and large atomic number. The aim of the shielding is to reduce the effects of background from the environmental conditions and other materials in the surroundings that would have effects on the sample (see Subsection 4.3.3). Copper helps in absorbing the characteristic of K X-rays created in the lead that are excited by the background or source radioactivity, and also prevents them from getting to the detector.

The HPGe is coupled with voltage bias supply along with a pre-amplifier, amplifier, multi-channel analyser (MCA) and a computer with Atomki Palmtop software to collect, store and process the detector signal, schematically illustrated in Fig. 4.4. Figures 4.5 and 4.6 illustrate the main HPGe detector with a built-in pre-amplifiers, lead castle of approximately 10 cm thick with a 2 mm copper lining. Bias supply is required in order for the detector system to function properly, therefore, the bias supply provides the voltage needed in order to collect all the charges that are in the detector. The operating bias voltage is 3500 Volt and

the pulse shaping that is produced due to the ionisation is converted into an electronic pulse by a semiconductor germanium crystal. The electronics pulse shaping is very weak and thus separated from the detector crystal by pre-amplifier. The pre-amplifier is used to collect and convert pulses to a voltage pulse, which will then be sent to amplifier in the electronic set-up. The pre-amplifier is normally located close to the detector to minimise the signal noise and thus improve the energy resolution. The pulses serve as input to the amplifier (which can be used to adjust the peak shape) are later sent to MCA. The MCA is based on shaping analog pulse which is converted to digital form by an analog-to-digital converter (ADC) [Kno99]. The pulses are collected and sorted according to pulse height in analog-to-digital converter and a spectrum file containing channel and counts are stored.

Table 4.1: Technical specifications of HPGe detector system used in this study

Detector Model	GC4520
Geometry	P-type (Co-axial two open end facing window)
Diameter	6.25 cm
Length	5.95 cm
Distance from the window	0.1 cm
Bias high Voltage/Model	3500 V/SILENA MILANO 7716
Preamplifier Model	2002CSL
Amplifier Model	ORTEC 572
Coarse gain	20
Shaping Time	6 μs
MCA Model	Palmtop Atomki

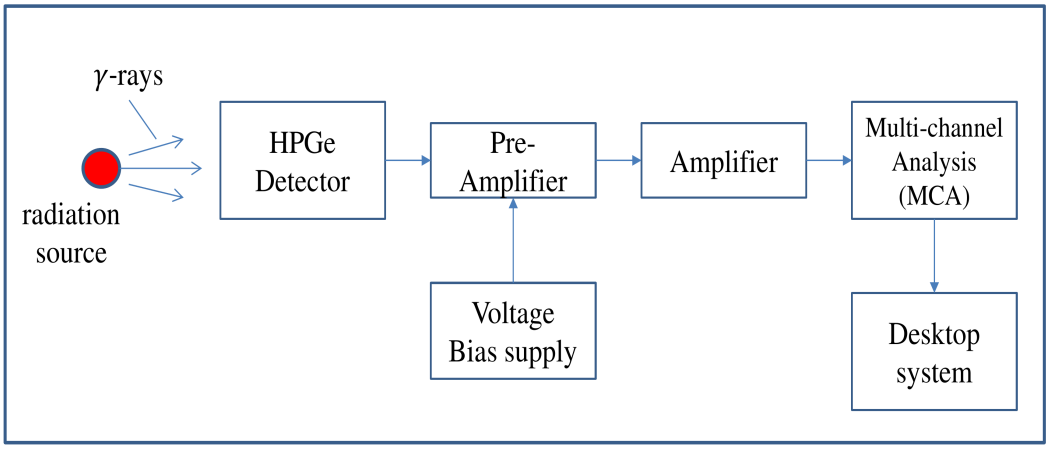

Figure 4.4: Schematic diagram of Hyper-Pure Germanium detector setup, showing the electronics accessories.

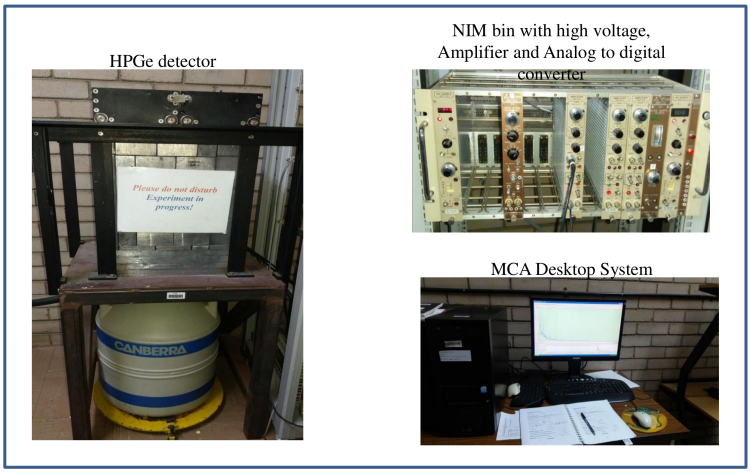

Figure 4.5: Experimental set-up for Environmental radioactivity laboratory HPGe detector system.

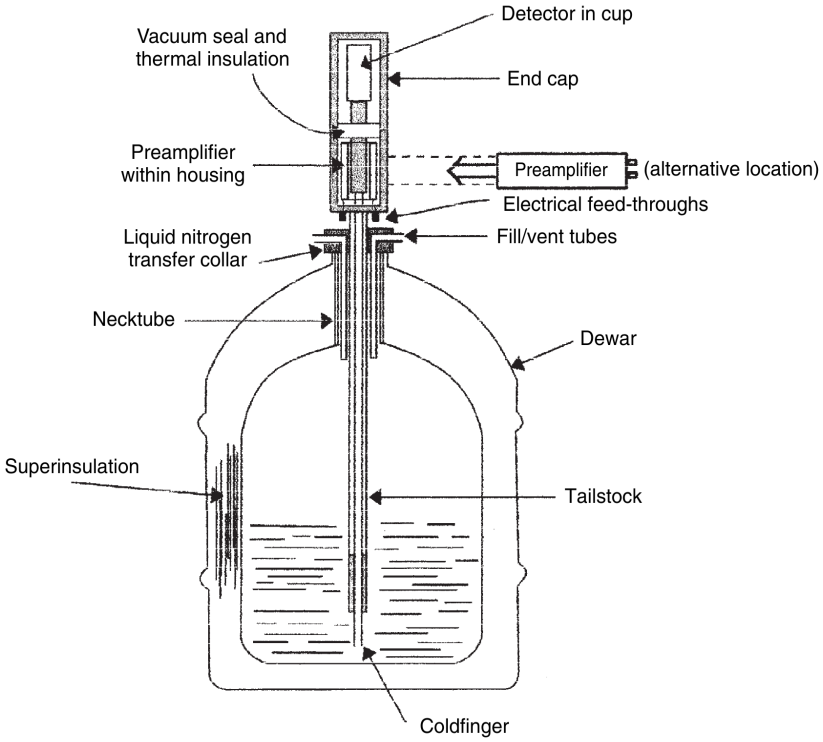

Figure 4.6: HPGe detector with liquid nitrogen cross-section diagram [Gil08].

4.3 Gamma Spectroscopy Data Analysis

This section presents the processes used to identify and quantify radionuclides present in collected samples.

4.3.1 Energy Calibration

The aim of this calibration is to determine the relationship between the peak position in channel numbers to the corresponding gamma-ray energies in keV [Gil08]. An IAEA/RGTh-1 standard source (^{232}Th ore) and KCL (13910 Bq for ^{40}K) were used for energy calibration due to the wide range of gamma-ray energies which covers low to high energies. The ^{232}Th and ^{40}K samples were prepared in

one litre Marinelli beakers and placed at the top of the detector, and the energy spectrum was collected for 3600 seconds (i.e. one hour). Region of interest (ROI) are manually set on the collected spectrum and the in-built algorithm calculates the net counts and its uncertainty. The calibration must be done before measuring any samples, and then this is performed every week in order to check any drift in the gain of the detector, thus giving the measurement a good quality. Figure 4.7 shows the linearity of energy response for the Hyper-Pure Germanium detector used, as measured, using the ^{232}Th source. Table 4.2 shows the selected gamma lines and the channel number. Although two or three gamma lines can be used to get a fit but it would not take into account the nonlinearity of a few channels over a thousand range. In order to account for the nonlinearity, it is important to use more gamma lines for calibration at various points along the energy range [Gil08].

Table 4.2: List of gamma-energies and channel numbers obtained for ^{232}Th and ^{40}K standard sources.

Nuclide	Energy (keV)	Channel Number
^{232}Th	129.07	248.18
	209.25	400.40
	338.32	646.46
	583.19	1113.07
	911.21	1739.73
	2614.53	4988.79
^{40}K	1460.83	2787.23

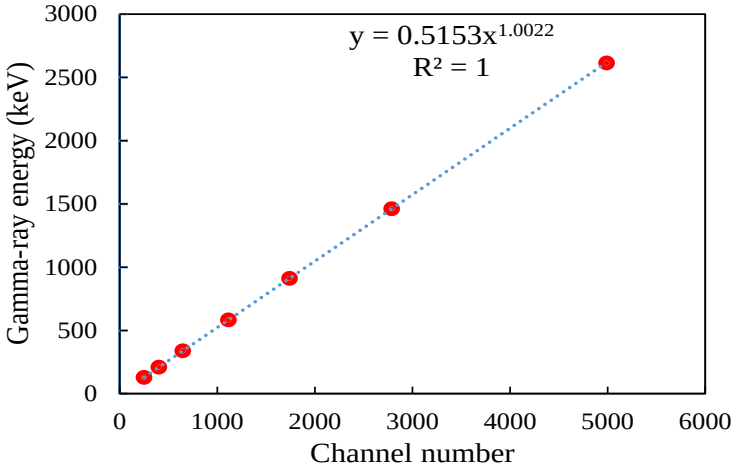

Figure 4.7: Energy versus channel relationship for energy calibration using ^{232}Th standard source.

4.3.2 Determining the Full Energy Efficiency

The efficiency of a detector relates the number of pulses counted to the number incident on the detector. The gamma-ray energy that is absorbed by the detector results in a peak that appears on the spectrum and is usually referred to as full-energy-peak efficiency. Full-Energy-Peak Efficiency (FEPE) is the ratio of the number of counts detected to the number of gamma-ray photons of that specific energy emitted by a source. Therefore, the efficiency used in the analysis was calculated with the following equation;

$$\varepsilon_f = \frac{C_{true}}{P_\gamma \times A \times m \times t}, \tag{4.1}$$

where C_{true} is the corrected full-energy peak counts, P_γ is the gamma-ray decay probability, A is the source strength, m is the mass of the sample and t is the Elapsed time. Efficiency was evaluated using sources which consist of ^{238}U, ^{232}Th

and ^{40}K as illustrated in Table 4.3 and Fig. 4.8, ^{40}K was added to both ^{238}U and ^{232}Th due to its availability in environmental samples. Also, geometry for the standard source and the soil sample are the same, therefore, the counting of the standard source were acquired for 7200 seconds while the soil samples were acquired for 86400 seconds and the net counts for each gamma line were recorded. A set of discrete gamma-ray energies ranging from lower energy to 2614 keV were covered using the standard reference sources. However, when measuring a low level radioactivity at close geometry, much care needs to be dedicated to an efficiency calibration of the detector used. Full-energy peak efficiency for a specific detector is a complicated function, that depends on various parameters such as gamma-ray energy, detector dimensions, source dimensions, the density of the sample, the arrangement of the detector geometry and the source [Sha97].

The response of the efficiency curve gives the relative importance of the major interaction processes of gamma-ray across the detector crystal. Photoelectric absorption dominant mechanism is observed in the range 0-200 keV [Deb88]. During the process, the incident gamma-ray photons transport all their energy to an electrons and get absorbed completely, therefore, the photons contribute to the overall full-energy-peak efficiency (FEPE) of the detector. However, the efficiency increment is due to the number of incident gamma-rays that is absorbed or deposited in the detector material as the energy increases to maximum in that range. From the range of 100 keV and 1 MeV, the dominant Compton effect cause the photon to scatter within the detector. Also, the gamma-ray photons escape from the detector instead of contributing to FEPE and thus decrease in the efficiency at this energy.

Table 4.3: Gamma-ray transitions and the corresponding full energy efficiency for ^{238}U, ^{232}Th and ^{40}K [Fir96, New08]

Nuclide	Energy (keV)	Decay Probability	Efficiency
^{238}U	186.10	0.062	0.090
	295.21	0.184	0.065
	351.92	0.358	0.058
	1238.11	0.059	0.025
	1377.67	0.039	0.023
	2204.21	0.049	0.017
^{232}Th	129.07	0.024	0.093
	209.25	0.039	0.073
	338.32	0.113	0.058
	583.19	0.304	0.044
	911.21	0.266	0.036
	2614.53	0.357	0.021
^{40}K	1460.83	0.107	0.022

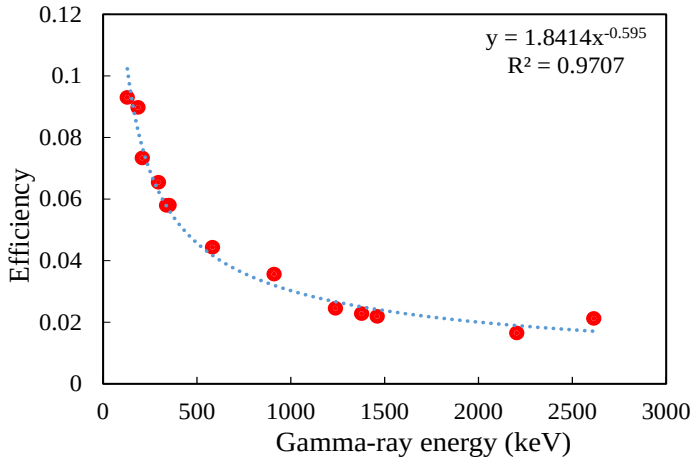

Figure 4.8: Full energy peak efficiency curve from ^{238}U, ^{232}Th and ^{40}K reference source.

4.3.3 Background Counting

Measurements of background is used to determine the minimum level of activity, most importantly when a low level counting of environmental samples are involved. The background radiation in the environment is mainly from the detector material, shielding material, building materials and reactions from outer space cosmic. However, the environmental gamma emitters at Environmental Radioactivity Laboratory (ERL) were investigated using an empty closed lead castle, counting for relatively longer period than the samples. The measured background spectrum was collected for three days. Most of the gamma energy peaks originated from primordial radionuclides can be seen in Fig. 4.9, where the top panel represents the full background spectrum while the other panels represent the peaks from lower energy to higher energy. Similarly, the ^{235}U and ^{40}K were also present

in the background data, as well as 511 keV (Annihilation). Moreover, the background radiation cannot be zero because the terrestrial nuclear radiations (^{238,235}U and ^{232}Th decay chain and ^{40}K) has been created since the formation of the earth, which are present in rock, soil, air, etc. These also depend on the content of mineral present in rock materials and the incident cosmic rays, which later depend on the altitude and latitude. Furthermore, the counting system must have a background as low as reasonable, therefore using a lead shielding is very important to reduced the gamma ray background radiation in the environment.

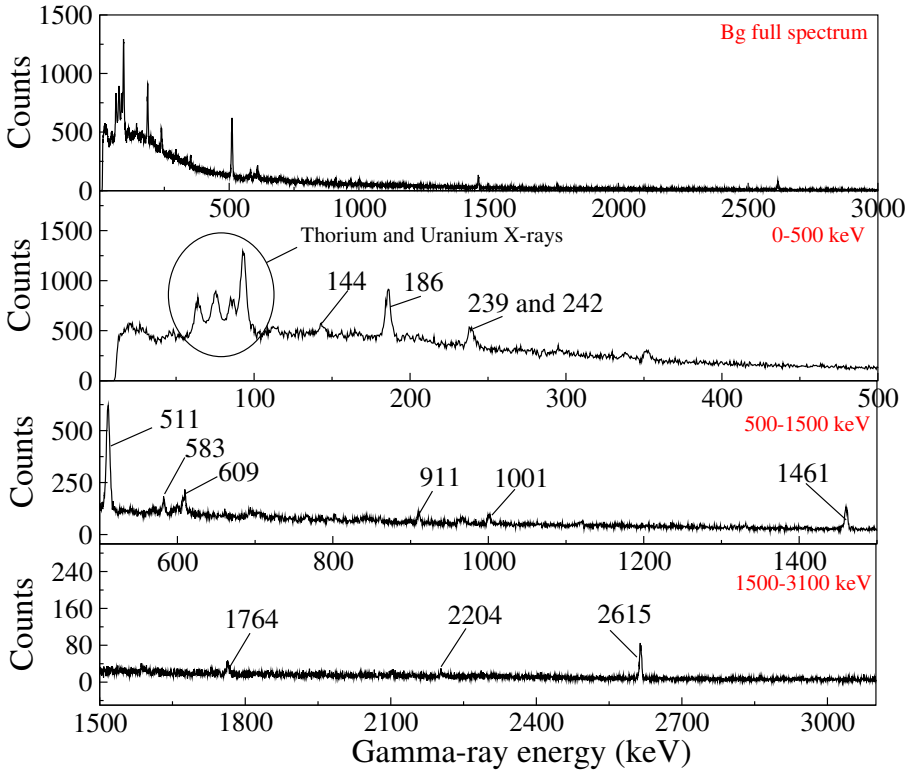

Figure 4.9: A background spectrum measured with empty lead castle (closed) for 3 days.

4.3.4 Activity Concentration Calculation

The activity concentration was calculated by measuring the net counts area after correcting the background, efficiency of energy of interest, counting time, mass of the sample and decay intensity (statistical chance that a gamma-ray is emitted per decaying nucleus). To get an accurate activity concentration of radionuclide, the photopeak efficiency for a given sample geometry is needed which is discussed in Subsection 4.3.2. Photon energies used for the activity concentration calculation are shown in Appendix A.1. Activity concentration of the sample A (Bq/kg) is given by the following expression:

$$A(\text{Bq/kg}) = \frac{C_{true_{sam}}}{P_\gamma \times \varepsilon_f \times \text{t} \times m}, \tag{4.2}$$

Where $C_{true_{sam}}$ is the corrected full-energy peak counts(net counts from ATOMKI software). The corrections consider contribution from the background spectrum, is estimated as follows;

$$C_{true_{sam}} = C_{net_{sam}} - \left[C_{net_{bg}} \times \frac{t_{sam}}{t_{bg}}\right], \tag{4.3}$$

Where $C_{net_{sam}}$ is the net peak area in the sample spectrum, $C_{net_{bg}}$ is the corresponding net peak area in the background spectrum, t_{sam} and t_{bg} are the elapsed time of sample and background, P_γ is the gamma-ray decay probability, t is the elapsed time for the spectrum collected in seconds, ε_f is the full-energy peak efficiency and m is the mass of the sample in kg. The analysis applied in the present study involves the statistical fluctuations, such as full energy peak efficiency and activity concentration are calculated from the measured data. To determine the measurements "n" of one quantity and the uncertainties, the average and the variance are given:

$$A_{x_i} = \frac{1}{n}\sum_{x=1}^{n} A_x \text{and} \tag{4.4}$$

$$\sigma_A^2 = \frac{1}{n-1}\sum_{x=1}^{n}(A_x - A_{x_i}). \tag{4.5}$$

The best way to estimate the data with unequal uncertainties is to introduce the weighted average and the variance, which is given by the following equation:

$$A_w = \sum_{x=1}^{n} \frac{A_x}{\sigma_{A_x}^2}/\sigma_{A_w}, \tag{4.6}$$

where

$$\sigma_{A_w}^2 = \left[\sum_{x=1}^{n} \frac{1}{\sigma_{A_x}^2}\right]^{-1}. \tag{4.7}$$

where $\sigma_{A_w}^2$ is the standard deviation [Deb88]. The data can be checked by using χ_R^2 (reduce chi-square), is given by:

$$\chi_R^2 = \frac{1}{\text{DoF}}\sum_{x=1}^{n} \frac{(A_x - A_w)^2}{\sigma_{A_x}^2} \tag{4.8}$$

where DoF is the number of degree of freedom, χ_R^2 provides information about the inappropriate peak shapes that lead to poor fitting. If the value of χ_R^2 is much larger than 1.0, then the uncertainties need to be reconsidered. But if the fit is accepted then it is advisable to quote the larger of the variances, internal or external [Deb88].

4.4 Estimation of Radiation Protection Quantities

Radiation protection quantities can be estimated using various equations. The equation used to calculate the ionising radiation received by human being are Gamma Dose Rate, Radium Equivalent, External Hazard Index, Internal Hazard Index, Annual Effective Dose Equivalent (AEDE) and Excess Lifetime Cancer Risk (ELCR). All these are calculated in order to determine the potential health risk factors that human beings are exposed to.

4.4.1 Gamma Dose Rate

Human beings are exposed to gamma radiation from different environmental sources. The radiological risks from the absorbed dose at 1 m above the ground was estimated using the following equation [Pen18]:

$$D_{out}(nGy/h) = 0.043A_{Ra} + 0.666A_{Th} + 0.047A_K \tag{4.9}$$

where D_{out} is the absorbed dose rate in the air and A values are the measured activity of ^{226}Ra, ^{232}Th and ^{40}K in Bq/kg, respectively. According to [Uns00], indoor absorbed dose rate were calculated based on the worldwide average gamma dose rate indoors of 1.4 times higher than outdoors:

$$D_{in}(nGy/h) = 1.4D_{out} \tag{4.10}$$

where D_{in} is the indoor absorbed dose rate.

4.4.2 Activity Concentration of $\mathbf{Ra_{equivalent}}$ ($\mathbf{Ra}_{equ}$)

One of the most important parameter on radiological risk assessment is the radium equivalent activity. This quantity is calculated by:

$$Ra_{equivalent} = A_{Ra} + 1.43A_{Th} + 0.077A_K \tag{4.11}$$

where A_{Ra}, A_{Th} and A_K are the activity concentration of ^{226}Ra, ^{232}Th and ^{40}K in Bq/kg, respectively. The maximum value allowed for activity concentration of radium equivalent is 370 Bq/kg, which corresponds to the effective dose limit of 1 mSv for the general public [Uns00, Aja09].

4.4.3 External Hazard Index

The external radiological risks index of the present soil samples are assessed by calculating the external exposure hazards to ^{226}Ra using the following equation [Kri81]:

$$H_{external} = (A_{Ra}/370) + (A_{Th}/259) + (A_K/4810) \leq 1... \tag{4.12}$$

where A_{Ra}, A_{Th} and A_K are the same for the activity equivalent of radium.

4.4.4 Internal Hazard Index

The hazards from the internal exposure of NORMs and TENORMs are expressed by the formula below [Kri81]:

$$H_{internal} = (A_{Ra}/185) + (A_{Th}/259) + (A_K/4810) \leq 1... \tag{4.13}$$

If the highest activity concentration of ^{226}Ra is half of the acceptable limit, therefore, the $H_{internal}$ will be lower than the unit.

4.4.5 Annual Effective Dose Equivalent (AEDE)

Annual effective dose equivalent can be calculated by using the following equation [Pen18]:

$$AEDE(nSv/yr) = ((D_{out} \times OF_{out}) + (D_{in} \times OF_{in})) \times T \times CF \tag{4.14}$$

Where AEDE (nSv/yr) is the annual effective dose equivalent, D_{out}(nGy/h) and D_{in}(nGy/h) is the outdoor and indoor absorbed dose mean, OF_{out} and OF_{in} are the occupancy factors of outdoor and indoor (0.2 and 0.8, respectively), T (h) is the conversion from year to hours (8760h) and CF is the conversion factor (0.7×10^{-6} (Sv/Gy)) given by UNSCEAR [Uns00] to convert absorbed dose in air to effective dose equivalent in human being.

4.4.6 Excess Lifetime Cancer Risk (ELCR)

In order to calculate excess lifetime cancer risk, certain processes need to be considerd such as absorbed gamma dose rate and annual effective dose equivalent. The annual effective dose equivalent(AEDE) was estimated by applying gamma dose rate conversion factor of 0.7 Sv/Gy and the calculated factors from outdoor and indoor of 0.2 and 0.8 respectively. After all the prerequisites, the ELCR can be calculated to determine the probability on how the worker can develope cancer due to exposure of radiation, and is calculated using the following equation:

$$ELCR = AEDE(mSvy^{-1}) \times ADOL(70y) \times RF(0.05 \times 10^{-3} mSv^{-1}) \quad (4.15)$$

where AEDE is the annual effective dose equivalent, ADOL is the average duration of lifetime and RF is the the risk factor. Due to low background radiation dose which is assumed to cause stochastic effects, ICRP Publication 106 used RF value for any public [ICRP91]. The recommended value of ELCR is 0.29×10^{-3}

4.5 Inductively Coupled Plasma Mass Spectrometry Overview

Inductively Coupled Plasma-Mass Spectrometry (ICP-MS) is a technique of choice for the determination of elemental analysis of metals and non metals at ultra-trace concentrations in environmental samples, owing to its low detection limits, multi-element capabilities, high sample throughput and low sample consumption [Dam95]. The efficiency of ICP-MS in producing singly-charged positive ions for most elements makes it an effective ionization source for mass spectroscopy. ICP-MS can discriminate between the mass of various isotopes of an element

where more than one isotope occurs. Isotope dilution in which a change in the isotope-ratio of two selected isotopes of an element of interest is measured in a solution. After the addition of a known quantity of a spike of the enrichment of one of the isotopes permits calculation of the concentration of the elements [Tra20].

Figure 4.10 illustrates a schematic diagram of ICP-MS. There are six fundamental components of ICP-MS single quadrupole: (1) the sample introduction system (2) inductively coupled plasma (ICP) (3) interface (4) ion optics (5) mass analyser and (6) detector. Liquid samples prepared are first nebulised in the sample introduction system, creating a fine aerosol that is subsequently transferred to the argon plasma. Plasma atomises and ionises the sample, generating ions which are then extracted through the interface region and into a set of electrostatic lenses called the ion optics. Ion optics focuses and guides the ion beam into the quadrupole mass analyser. Then, mass analyser separates ions according to their mass charge ratio (m/z), and these ions are measured at the detector [Kos03, Dam95]. In the final process, an ion detector converts the ions into an electrical signal. This signal is expressed as counts using Masshunter software for calculating results. The Limit of Detection (LOD) for every elements that was identified in the samples was also provided as shown in Appendix B, Tables B.1 and B.2.

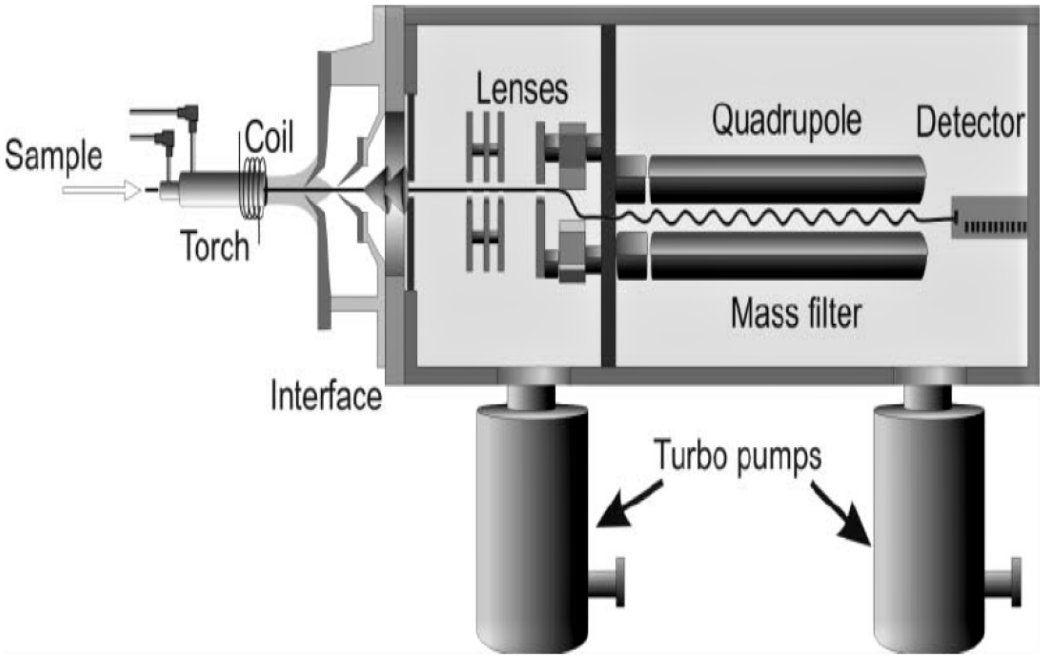

Figure 4.10: Schematic diagram of ICP-MS [Kos03].

4.6 ICP-MS Sample Preparation

Ten out of twenty samples collected from Chad were purposively selected for further elemental analysis at the Central Analytical Facilities (CAF), Stellenbosch University. ICP-MS Agilent 7900x model with Octupole reaction system, available at CAF was used for this analysis. A small quantity of 0.1 g dried homogenous sample was weighed directly into microwave digester Teflon vessels. Digestion was done in order to detect the heavy elements that were present in the selected samples. Subsequently, the 0.1 g dried homogenous samples were mixed with 6 ml of HNO_3 and 2 ml of Supra HCl in a MARS microwave digestion vessel. After this, the mixture was then diluted to a final volume of 50 ml.

4.7 Benchmark Tests

Benchmark tests between Monte Carlo simulations and experimental data were done for HPGe detector with the specification discussed in Section 3.3.3. However, the simulations presented in this study focused only on three aspects of gamma-ray spectrometry;

- To correct the coincidence summing that usually occurs in the experiments with GEANT4, and
- Also, to check the validity of efficiency calibration by two well known codes GEANT4 and FLUKA.
- To calculate the coincidence summing correction factors for HPGe detector with ^{238}U and ^{232}Th samples.

Results for these benchmark tests will be presented in Chapter 5. The following certified reference point sources ^{60}Co, ^{22}Na, ^{152}Eu, ^{40}K and ^{137}Cs were available for these tests. Details on coincidence summing is illustrated in Section 2.8 and correction factors can be estimated numerically or using Monte Carlo methods to determined appropriate correction factors. This method can also allow additional complexity in the source matrix which may be difficult in numerical approach. Therefore, using GEANT4 for the coincidence summing correction factors on the source and geometry gives more rigorous test of simulations validity. Furthermore, the accuracy obtain from a gamma-ray spectrometry depends on the efficiency calibration of the detector. For this reason, it is important to compare the accuracy of the experiments with the simulation codes. The full-energy peak efficiency (ε) for the simulation codes were calculated using the following equation:

$$\varepsilon = \frac{N_{FEP}}{N} \tag{4.16}$$

where N_{FEP} is the net count in the full energy peak and N is the number of photons emitted by the source of energy. The experimental detector efficiency was calculated with the Eq. 4.1 in Subsection 4.3.2. Details on efficiency simulations and experimental comparisons are presented in Chapter 5. Natural decay series such as ^{238}U and ^{232}Th contain many radionuclides, but they are not all measurable by gamma spectrometry, either because their gamma emissions are too weak, or they are emitted at a very low energy. Among all the nuclides that can be measured, several have complicated decay patterns and True Coincidence Summing problems [Ven15]. To calculate the sum of the true coincidences for the natural decay series (^{238}U and ^{232}Th), a general method based on the EFFTRAN software was used 2.8. The code is written in Fortran 77 and is based on deterministic calculus. It has the ability to perform coincidence summation corrections as long as a peak-total calibration is performed. Coincidence correction factors can be calculated after defining the sample geometry and detector related parameters [Mil18]. The software calculates the true coincidence correction factor for the gamma ray of interest using the equations in Section 2.8.

Chapter 5

Results and Discussion

In this chapter firstly, it involve testing of EFFTRAN program to calculate the coincidence summing and also to create the Monte Carlo codes that could be used to validate against gamma-ray detector efficiency. Also, radionuclides identification and quantification in the twenty soil samples collected from chad are presented in Section 5.2, the main purpose of gamma-ray spectrometry with Hyper Pure Germanium (HPGe) detector is the ability to determine the activity concentration of each gamma emitting radionuclide that are present in the samples. The results from Section 5.2 were published in the Journal of Radiation Protection and Environment. However, ten samples were selected for further analysis using ICP-MS to determine the elemental concentration that are present in the sample. The trace elements found in the samples were compared with Maximum Allowable Limit (MAL). Also the uranium and potassium found with HPGe and ICP-MS result were then compared with each other as shown in Section 5.4.

5.1 Monte Carlo and Experimental Results: Benchmark Exercise

This Section presents the results obtained from experiments using standard reference point source and the simulation codes (GEANT4 and FLUKA). Meanwhile, the methods used in getting the results are discussed in Section 3.3 and 3.4. The goodness of results obtained from gamma ray spectrometry depends on the efficiency calibration of the detector system. For this reason, to obtain an accurate activity measurement, good knowledge of the detector and the efficiency response is required. Thus, the standard reference sources often contain some radionuclides that exhibit coincidence summing when measured in close proximity to the detector. As a result of this, GEANT4 and EFFTRAN were used to calculate the coincidence summing.

5.1.1 Coincidence Summing corrections (GEANT4)

Coincidence summing process has been discussed in Section 2.8. These are usually controlled by a complex electronics with high accuracy of the timing system. Monte Carlo simulations can duplicate coincidence by recording the energy deposition in the detector within the same event. To investigate and confirm coincidence summing with the simulation, ^{60}Co and ^{22}Na sources were used, due to the fact that both have the simplest summing pattern at a much wider energy range than it would usually covered. The sources were placed at 0 cm on the surface of the detector. An artificial photon peak was noticed at 2505 keV and 1786 keV for ^{60}Co and ^{22}Na as illustrated in Figs. 5.1 and 5.2. The artificial peak is the summing energy within the detector resulting from the coincidence of gamma-rays

from ^{60}Co and ^{22}Na source. Meanwhile, the simulation corrected the coincidence summing by placing the source at an X cm distance from the surface of the detector as illustrated in Figs. 5.3 and 5.4, respectively.

In addition, the energy-resolution model could successfully reproduce the observed response of the detector for the whole energy region of the measured spectrum. It should be noted that the simulation spectrum for ^{60}Co and ^{22}Na gave a good agreement with the measured spectrum. Consequently, the energy spectrum of any isotopes can be successfully reproduced by using GEANT4 simulation toolkit. Additionally, a complex source like ^{152}Eu was also investigated with the simulation code. The sources were placed at 0 cm on top of the detector. Furthermore, simulated spectrum has been generated to the number of events determined by the strength of the source and the duration of the run time using low energy electromagnetic (EM) model (see Fig. 5.5).

However, EFFTRAN software described in Section 4.7 was used to calculate the coincidence summing factors for Environmental Radioactivity Laboratory system with set of energies under this study as shown in Table 5.1. It can be confirmed that there are very good agreements between the results obtained from both experiments and GEANT4 simulations of the detector responses as illustrated with the correction factors for the set of gamma-ray energies shown in Table 5.1. Therefore, overall confidence limit of approximately 99% was achieved for the detector, which confirms its reliability and high standards for experimental results achieved at the ERL laboratory of iThemba LABS.

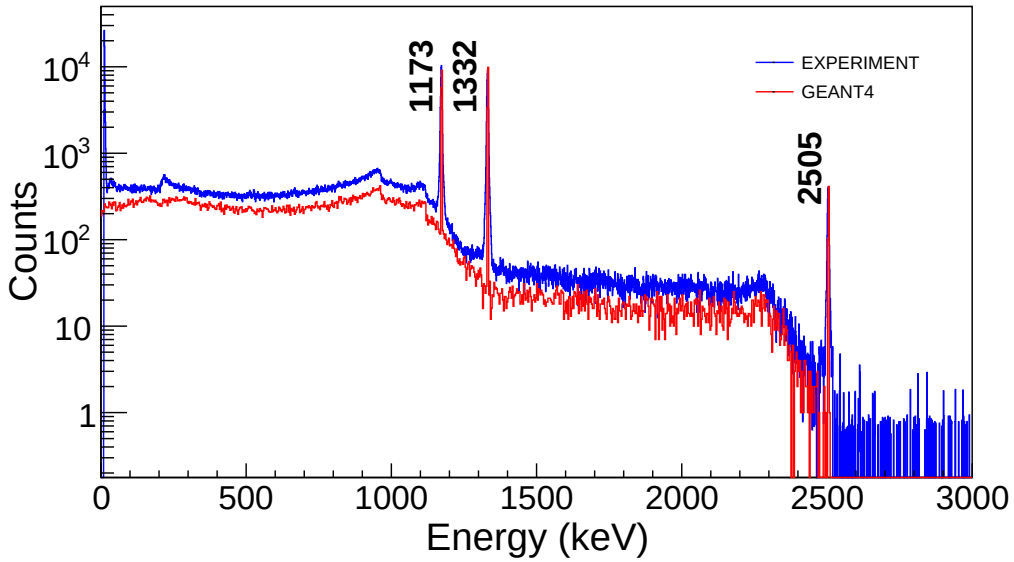

Figure 5.1: Measured and simulated spectra with coincidence summing using ^{60}Co point source placed at a surface of the detector.

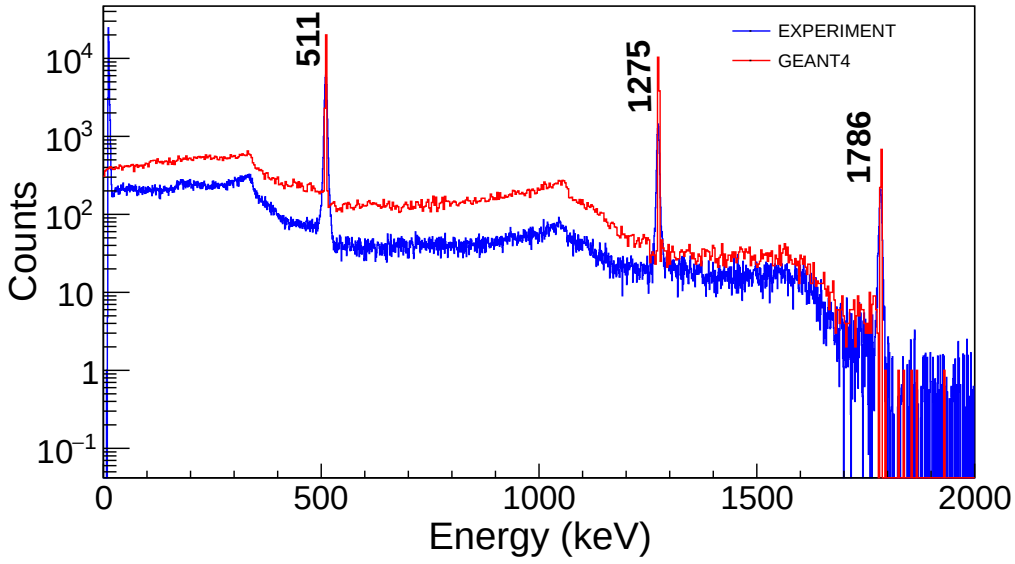

Figure 5.2: Measured and simulated spectra with coincidence summing using ^{22}Na point source placed at a surface of the detector.

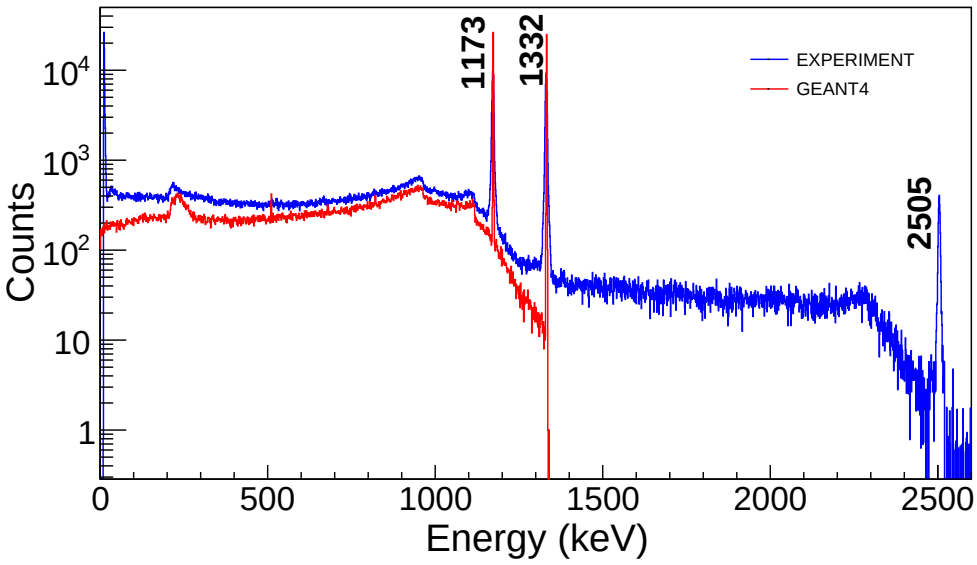

Figure 5.3: Corrected simulated spectra without coincidence summing, using ^{60}Co point source. The source was placed at -20.5 cm from the surface/front of the detector as to observe the effect of additional peak due to coincidence summing.

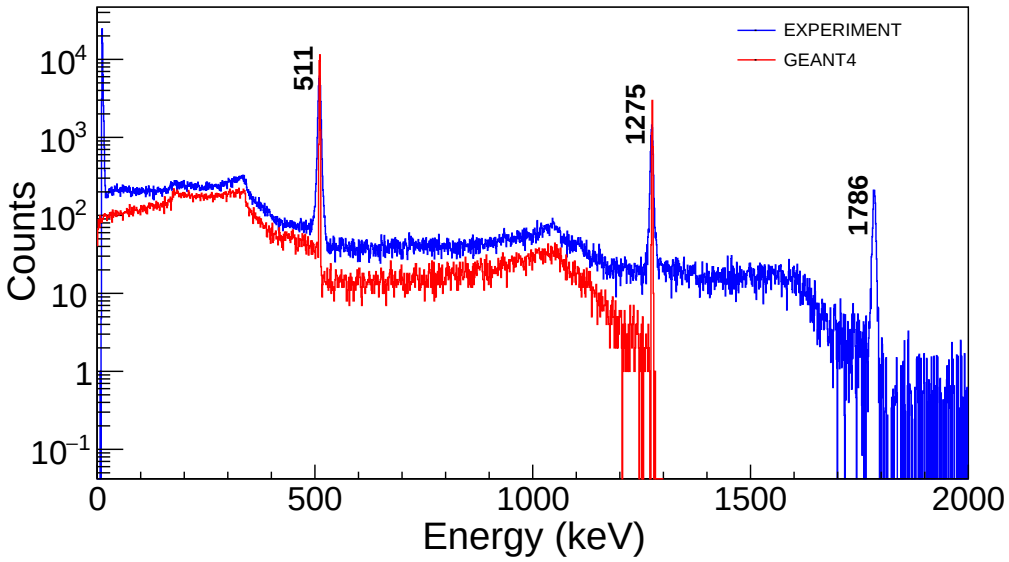

Figure 5.4: Corrected simulated spectra without coincidence summing, using ^{22}Na point source. The source was placed at -20.5 cm from the surface/front of the detector as to observe the effect of additional peak due to coincidence summing.

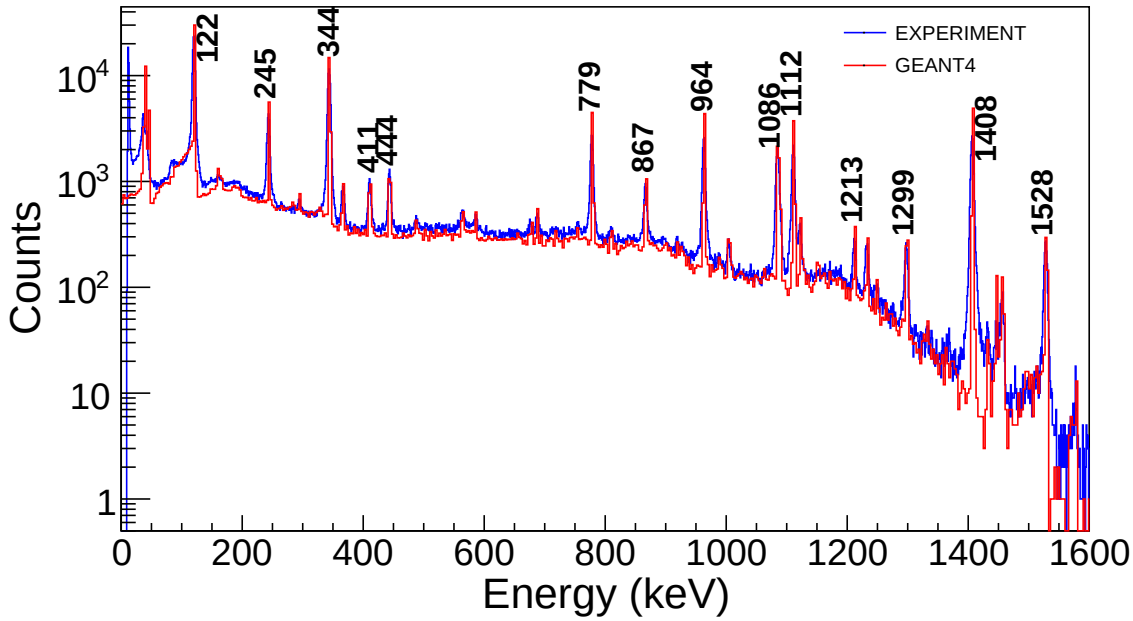

Figure 5.5: Simulated and measured spectra using ^{152}Eu point source placed at surface of the detector.

Table 5.1: Coincidence summing correction factor for gamma energy

Uranium series		
Nuclide	Energy (keV)	Correction factor
^{226}Ra	186.10	0.062
^{214}Pb	295.21	1.000
	351.92	1.001
^{214}Bi	609.31	1.088
	768.36	1.108
	934.06	1.100
	1120.29	1.096
	1238.11	1.091
	1377.67	0.097
	1729.60	0.867
	1764.49	0.998
	2204.21	1.091
Thorium series		
Nuclide	Energy (keV)	Correction factor
^{212}Bi	727.20	1.027
^{208}Tl	583.19	1.276
	860.56	1.035
	2614.53	1.127

5.1.2 Comparison of Experimental Data with GEANT4 and FLUKA

The resolution of the detector was taken into account using a Gaussian broadening feature. The broadness of the distribution was chosen according to actual detector resolution. Photons were Uniformly distributed and isotropically released in volume of source. Once the simulation was completed, the energy collected from the primary and secondary particles was recorded in the volume of the detector and sorted into a histogram using the ROOT toolkit (GEANT4)

and GNUPLOT (FLUKA)for data analysis.The relative errors for experimental measurements were 3% and simulated data were lower than 2%.

Figure 5.6 shows the example of simulated spectrum for ^{60}Co point source and the summation peak at 2500 keV resulting from the summation of 1173 and 1332 keV energies as reported in Section 5.1.1. The simulated full-energy-peak efficiency for FLUKA and GEANT4 were calculated using Eq. 4.16. The comparison between the experiment and the Monte Carlo codes were done by calculating the ratio between them which are illustrated in Table 5.2. The proportion shows strong agreement between experimental and simulated efficiency for the geometry. As pointed out earlier, the experimental and the simulated efficiency agree within 97% for all the source except ^{22}Na (see Fig. 5.7). The disagreement in this line could be attributed to the contribution of other gamma lines.

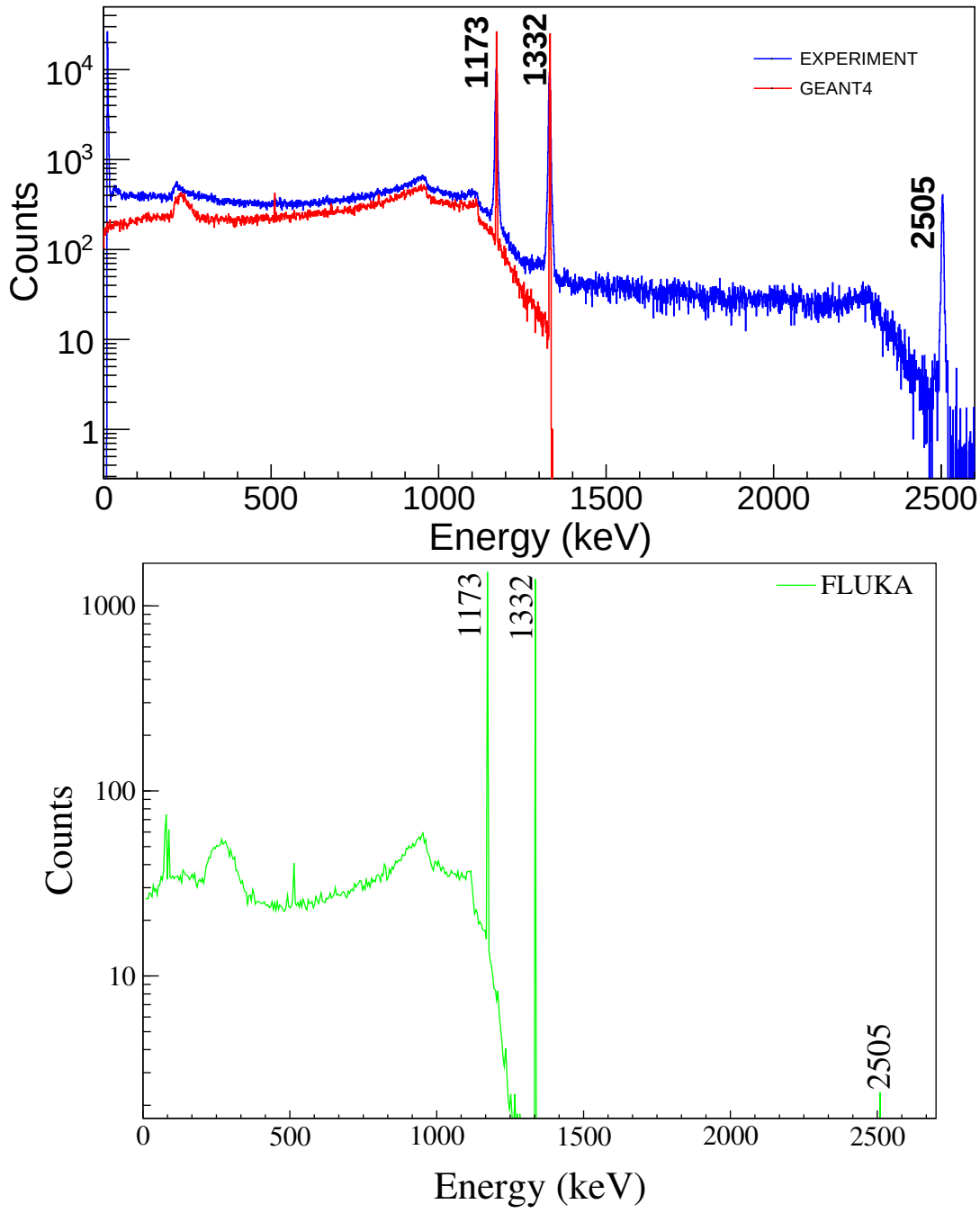

Figure 5.6: Top: shows the GEANT4 simulated and measured spectra for ^{60}Co point source; Bottom: shows the FLUKA simulated spectra for ^{60}Co point source.

Table 5.2: Comparison of measured and simulated peak efficiencies with the corresponding ratios for GEANT4 and FLUKA codes

Nuclide	Energy keV	Exp	GEANT4	Ratio (Exp /GEANT4)	FLUKA	Ratio (Exp /FLUKA)
^{152}Eu	122	0.0809	0.0810	0.9989	0.0833	0.9715
	867	0.0193	0.0185	1.0457	0.0184	1.0506
	1408	0.0157	0.0161	0.9761	0.0163	0.9615
	344	0.0495	0.0507	0.9767	0.5203	0.95226
^{60}Co	1173	0.0148	0.0152	0.9675	0.0154	0.9564
	1332	0.0153	0.0160	0.9610	0.0162	0.9482
^{137}Cs	661	0.0402	0.0410	0.9805	0.0408	0.9853
^{22}Na	1275	0.0183	0.0213	0.8591	0.0210	0.8707
^{40}K	1461	0.0154	0.0150	1.0257	0.0152	1.0141

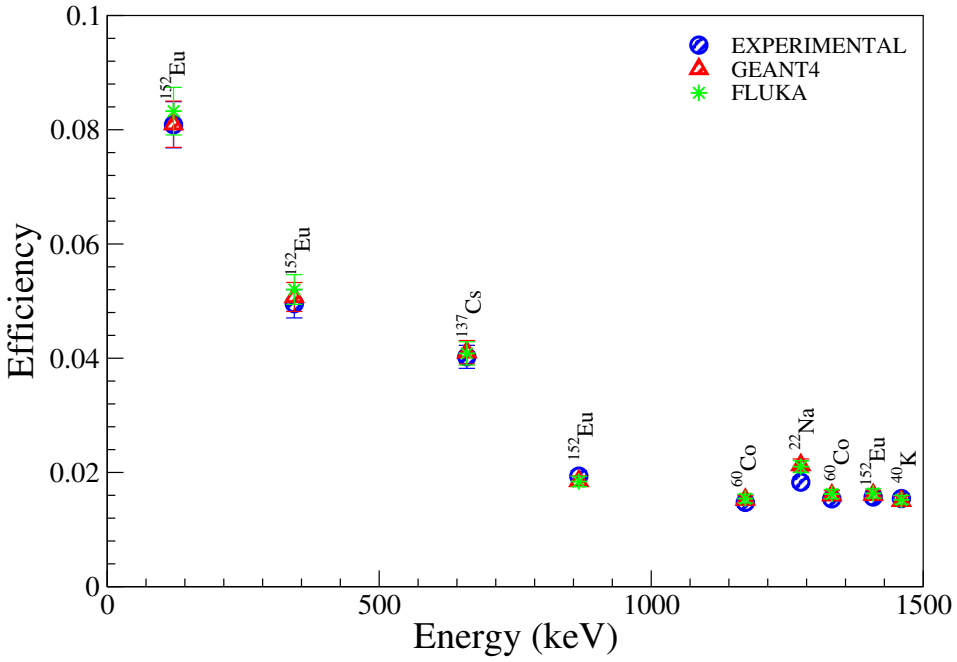

Figure 5.7: Experimental (blue), GEANT4 (red) and FLUKA (green) full energy peak efficiency as a function of gamma energy.

5.2 Radionuclide Identification and Quantification: HPGe

The Yapala soil samples used in this present work were analysed, taking into consideration the energy region of interest from ^{238}U, ^{232}Th decay progeny, and ^{235}U, ^{40}K and ^{137}Cs. After counting of the gamma-ray samples, a detailed peak centroid was done for each spectrum acquired. A general spectrum fitting and analysis software called gf3 Radware was used to determined net area of the peak of interest [Rad95]. Background corrections were done for all the measured samples and the results are shown in Appendix A, Table A.2 and A.3. Moreover, radionuclides identified during sample analysis include ^{238}U decay progenies

(^{226}Ra, ^{214}Pb, ^{214}Bi, ^{234m}Pa) , ^{232}Th decay progenies (^{228}Ac, ^{208}Tl, ^{212}Pb, ^{212}Bi), ^{235}U and ^{40}K. In addition, anthropogenic radionuclide peak at 662 keV which was traced to belong to ^{137}Cs was also observed, but yet to conclude its origin.

5.2.1 Activity Concentration

To calculate the activity concentrations of radionuclides accurately, various corrections are required which include half lives, coincidence summing and self-attenuation [IAEA20]. From the sample preparation in Section 4.1.2 , it shows that the samples were not stored for twenty one days to undergo a secular equilibrium, most expecially for ^{238}U. In addition, the samples were sealed in 100 ml bottle after drying and not filled to the top (i.e there is air space between the top level of the samples and the lid), therefore some air can still accumulate in the space and somehow escape out of the system (see Figs. 2.4 and 2.6). For radionuclides consisting of various gamma lines (e.g ^{238}U and ^{232}Th) weighted average method was used. This is done by using multiple gamma-ray lines from the same decay chains in order to reduce the systematic uncertainty in the activity concentration.

The error in the specific activity have been minimised by using standard reference sources for calibration, which have the same density and thus self-attenuation for measured samples. Moreso, activity concentrations for ^{40}K and ^{137}Cs (anthropogenic radionuclide) were also determined using their single gamma-ray energies, including ^{235}U using only the 143 keV gamma-ray energy. Thus, the straight line from the figures represent the weighted average of each data points, the formula and the error propagation used in the analysis were explained in Section 4.3.4

with Eqs. 4.6 and 4.7. Details about the datas are discussed below.

5.2.1.1 Activity Concentration of ^{238}U

Figures 5.8 to 5.27 illustrate the activity concentration obtained for terrestrial decay chains of ^{238}U (daughter nuclides) for sample S1 to S20. It can be observed that the activities of ^{234m}Pa (from ^{234}Th β-decay) at gamma line of 1001 keV and ^{226}Ra at an energy of 186 keV are higher than the activity concentrations of ^{214}Bi and ^{214}Pb. This can be explained from to the fact that ^{226}Ra and ^{234m}Pa from Fig. 2.4 are before ^{222}Rn (the only gas product in the chain), while ^{214}Bi and ^{214}Pb are after ^{222}Rn. This occurs as a result of samples not properly sealed, hence there was no secular equilibrium. This explains why the observed activities for ^{226}Ra and ^{234m}Pa are higher than that of ^{214}Bi and ^{214}Pb unexpectedly.

Table 5.3 gives activity concentrations based on the weighted average values of ^{214}Bi and ^{214}Pb for sample S1 to S20. There is a uniformity across the samples except for samples S17 to S20 with abnormally higher activity concentrations. The ^{238}U activity values obtained from sample S1 to S16 range from 2±0.1 to 35±0.7 Bq/kg while the values from S17 to S20 ranged from 131±2.2 to 239±3.9 Bq/kg, respectively. Furthermore, the Chi-square value per degree of freedom (χ^2_R) ranged from 12.0 to 37.4 for the twenty samples collected (more details in Section 4.3.4). The high concentration in ^{238}U indicates enrichment of heavy elements and a wider distributions of radionuclides.

Table 5.3: Activity concentrations (weighted average) for ^{238}U in all samples

Sample	Activity concentration (Bq/kg)	χ^2_R value
S1	5.1±0.2	29.7
S2	9.8±0.3	29.6
S3	6.3±0.2	37.4
S4	13.1±0.3	32.2
S5	3.1±0.1	25.3
S6	4.9±0.2	25.8
S7	6.6±0.2	27.7
S8	5.8±0.2	26.6
S9	5.2±0.2	26.3
S10	8.0±0.2	25.6
S11	6.8±0.2	27.5
S12	6.4±0.2	24.9
S13	5.8±0.2	25.6
S14	35.3±0.7	12.0
S15	5.7±0.2	25.1
S16	2.4±0.1	15.1
S17	217.2±3.4	19.3
S18	147.2±2.4	14.6
S19	130.9±2.2	16.1
S20	239.3±3.9	13.7

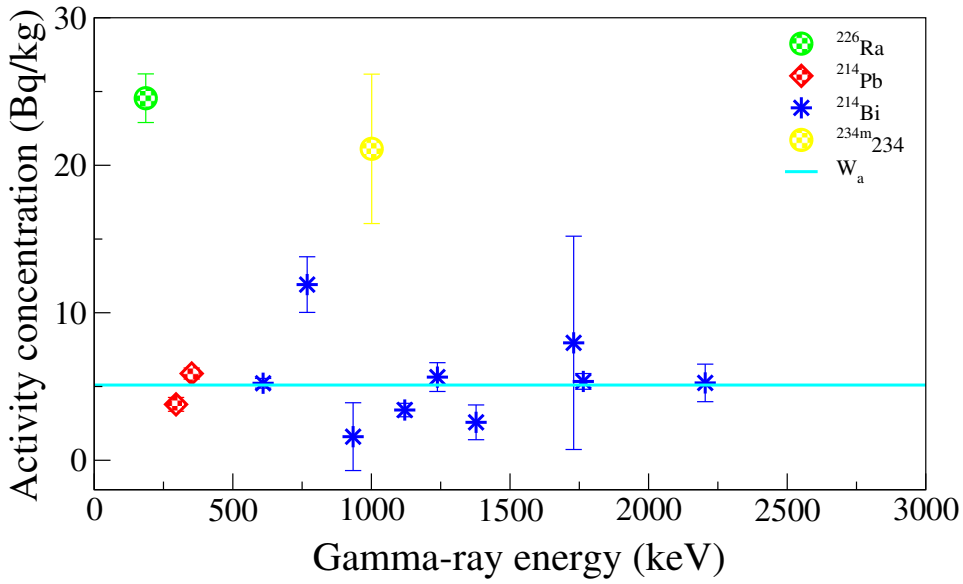

Figure 5.8: Sample S1: Activity concentrations as function of gamma-ray energy for various radionuclides (^{234m}Pa, ^{226}Ra, ^{214}Bi and ^{214}Pb) in the ^{238}U series.

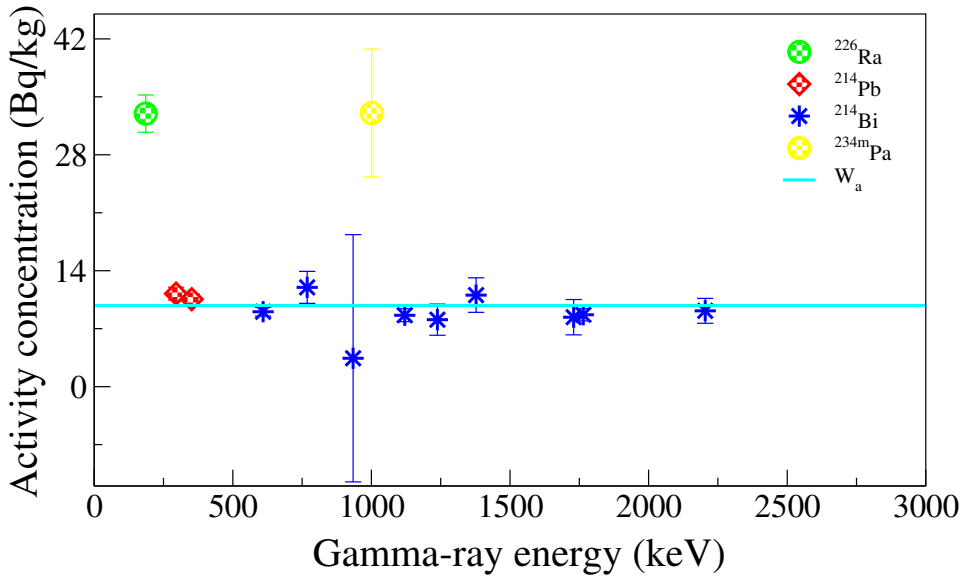

Figure 5.9: Sample S2: Activity concentrations as function of gamma-ray energy for various radionuclides (^{234m}Pa, ^{226}Ra, ^{214}Bi and ^{214}Pb) in the ^{238}U series.

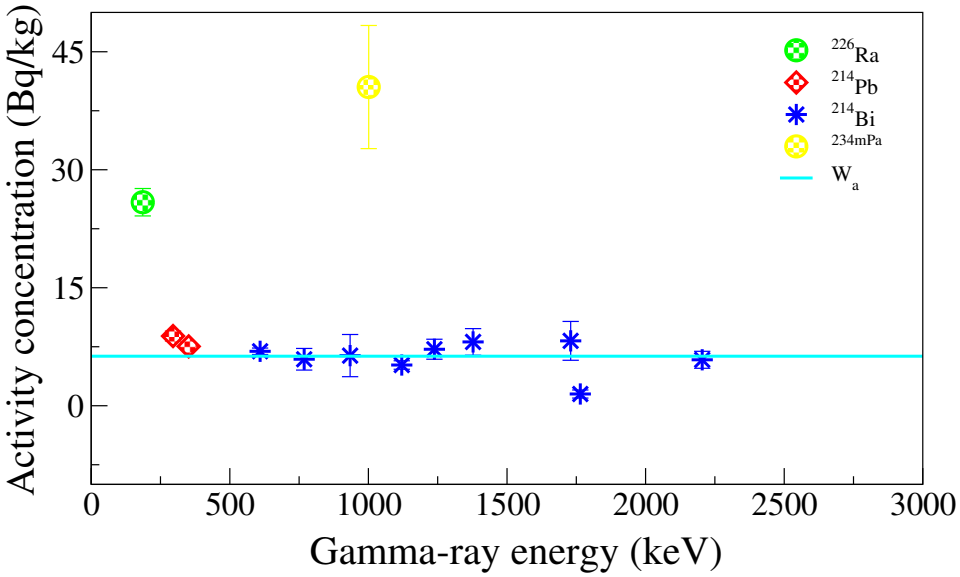

Figure 5.10: Sample S3: Activity concentrations as function of gamma-ray energy for various radionuclides (^{234m}Pa, ^{226}Ra, ^{214}Bi and ^{214}Pb) in the ^{238}U series.

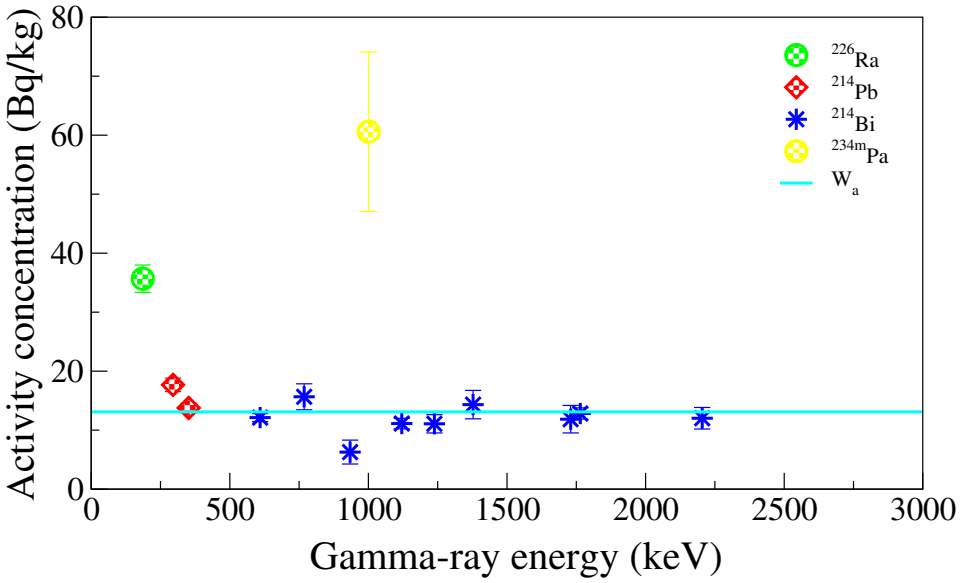

Figure 5.11: Sample S4: Activity concentrations as function of gamma-ray energy for various radionuclides (^{234m}Pa, ^{226}Ra, ^{214}Bi and ^{214}Pb) in the ^{238}U series.

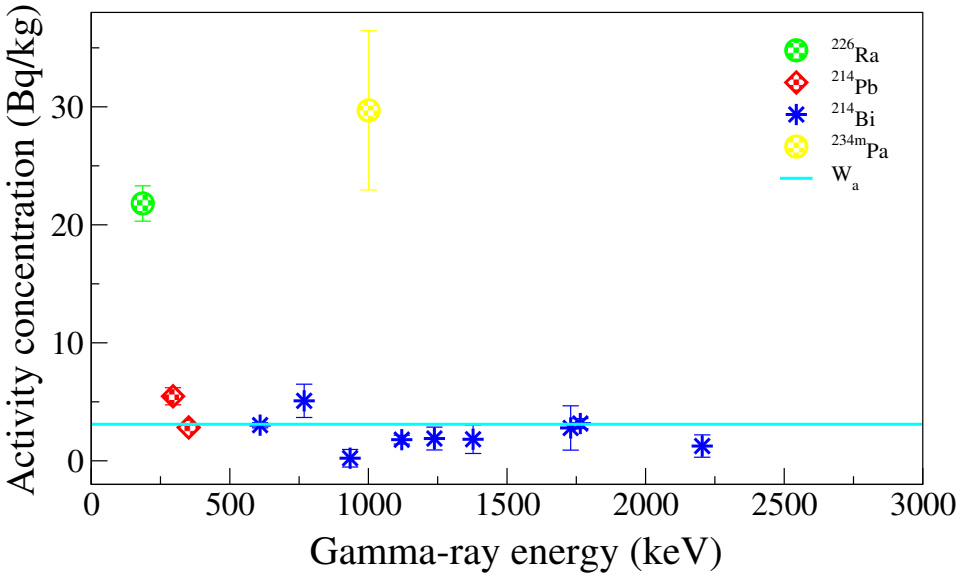

Figure 5.12: Sample S5: Activity concentrations as function of gamma-ray energy for various radionuclides (^{234m}Pa, ^{226}Ra, ^{214}Bi and ^{214}Pb) in the ^{238}U series.

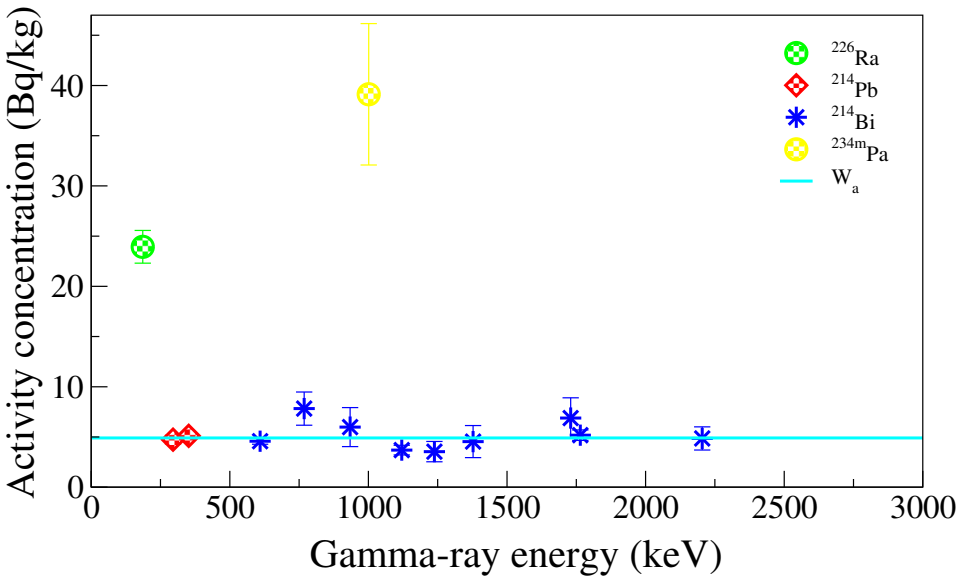

Figure 5.13: Sample S6: Activity concentrations as function of gamma-ray energy for various radionuclides (^{234m}Pa, ^{226}Ra, ^{214}Bi and ^{214}Pb) in the ^{238}U series.

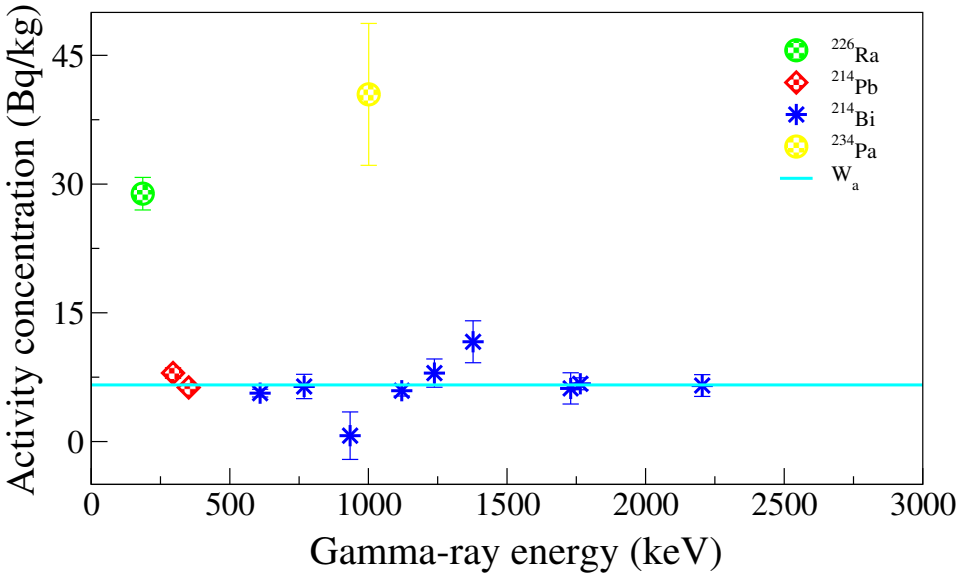

Figure 5.14: Sample S7: Activity concentrations as function of gamma-ray energy for various radionuclides (^{234m}Pa, ^{226}Ra, ^{214}Bi and ^{214}Pb) in the ^{238}U series.

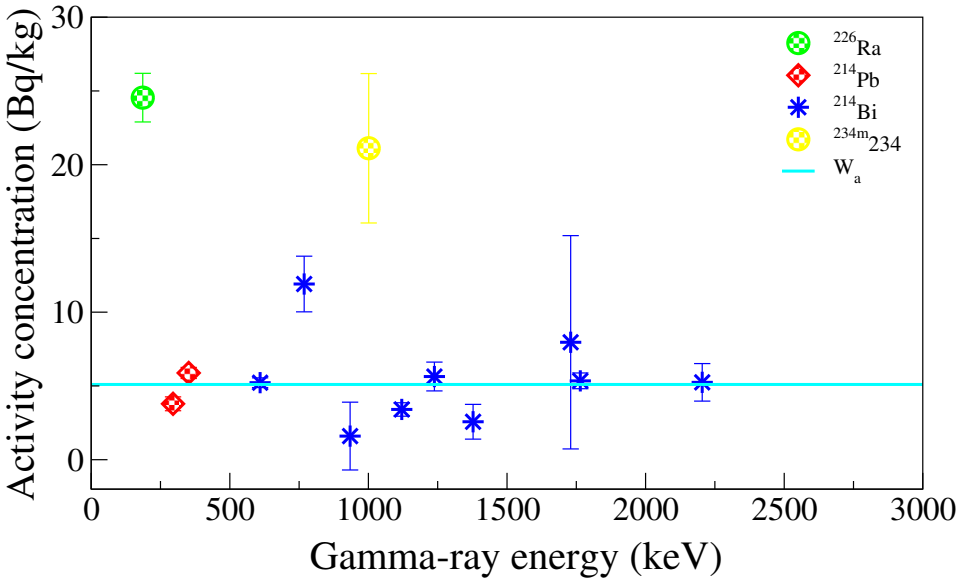

Figure 5.15: Sample S8: Activity concentrations as function of gamma-ray energy for various radionuclides (^{234m}Pa, ^{226}Ra, ^{214}Bi and ^{214}Pb) in the ^{238}U series.

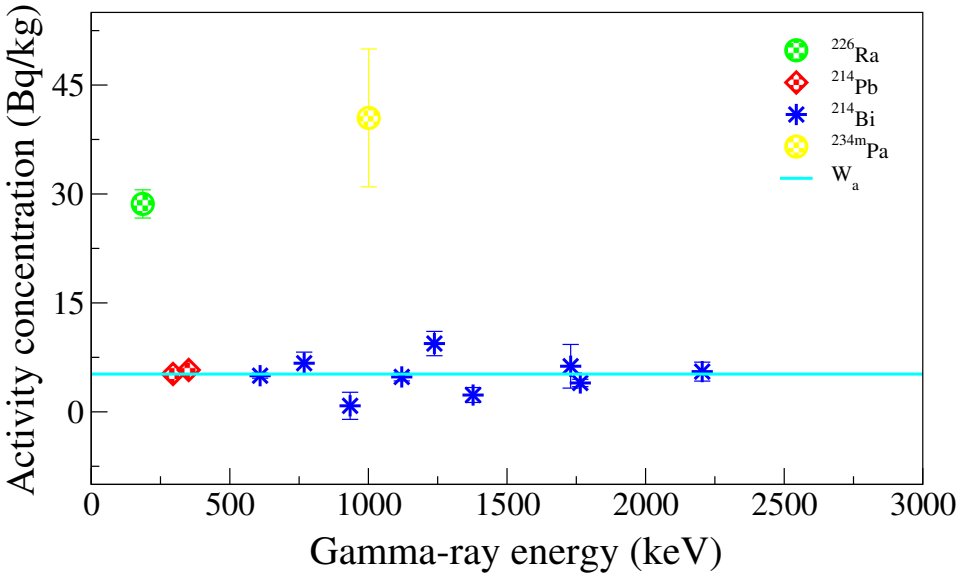

Figure 5.16: Sample S9: Activity concentrations as function of gamma-ray energy for various radionuclides (^{234m}Pa, ^{226}Ra, ^{214}Bi and ^{214}Pb) in the ^{238}U series

.

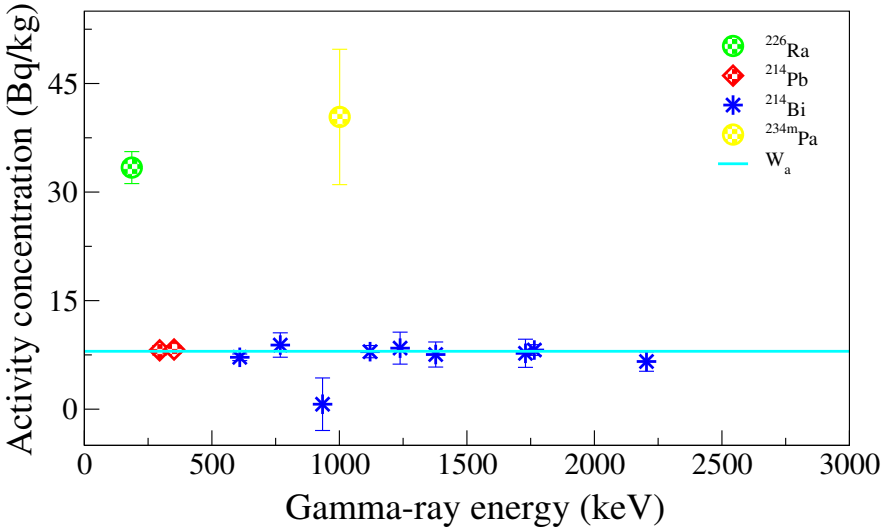

Figure 5.17: Sample S10: Activity concentrations as function of gamma-ray energy for various radionuclides (^{234m}Pa, ^{226}Ra, ^{214}Bi and ^{214}Pb) in the ^{238}U series.

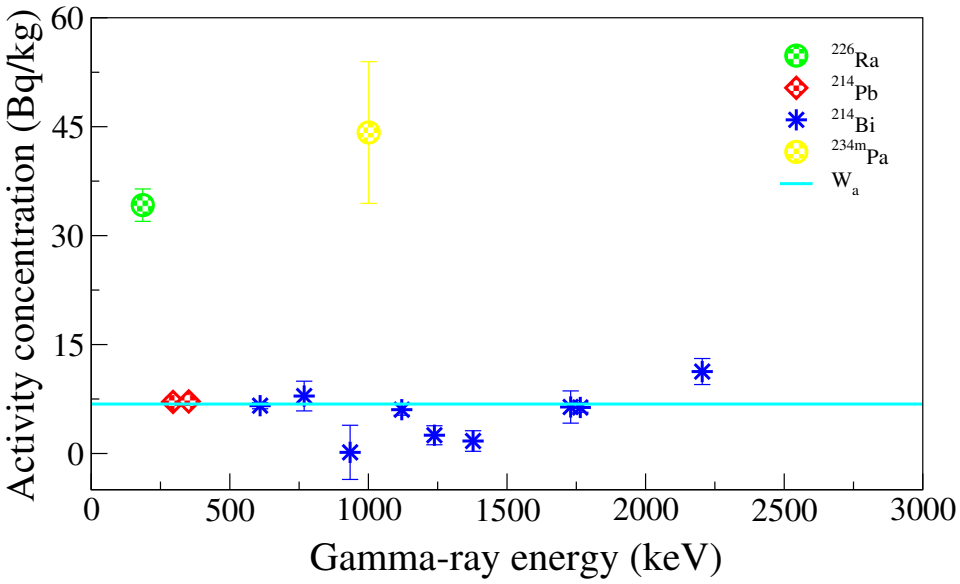

Figure 5.18: Sample S11: Activity concentrations as function of gamma-ray energy for various radionuclides (^{234m}Pa, ^{226}Ra, ^{214}Bi and ^{214}Pb) in the ^{238}U series.

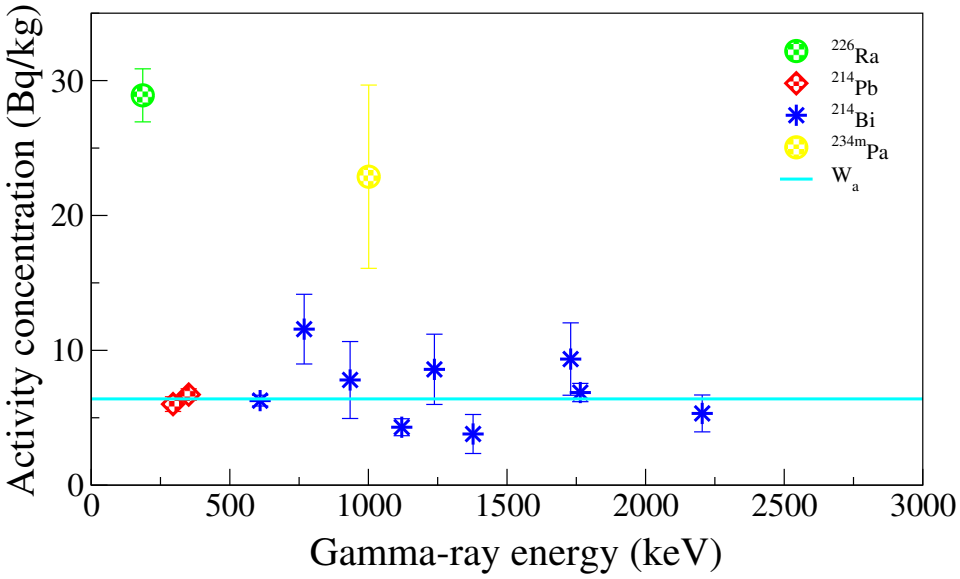

Figure 5.19: Sample S12: Activity concentrations as function of gamma-ray energy for various radionuclides (^{234m}Pa, ^{226}Ra, ^{214}Bi and ^{214}Pb) in the ^{238}U series.

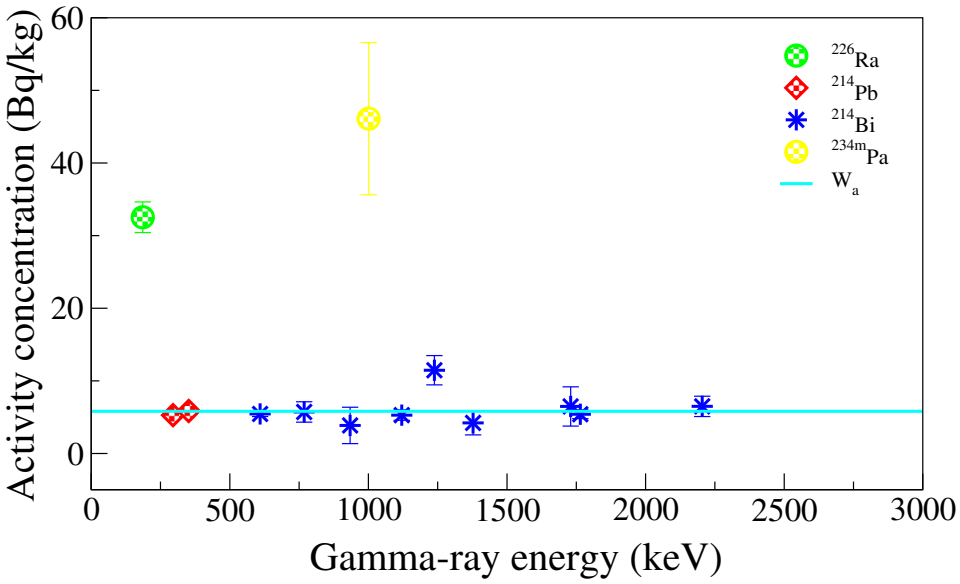

Figure 5.20: Sample S13: Activity concentrations as function of gamma-ray energy for various radionuclides (^{234m}Pa, ^{226}Ra, ^{214}Bi and ^{214}Pb) in the ^{238}U series.

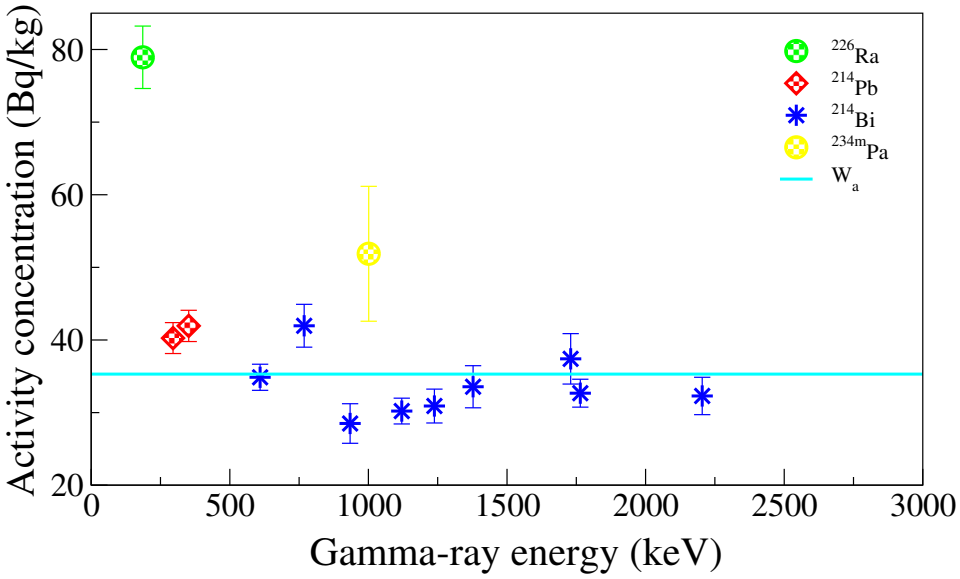

Figure 5.21: Sample S14: Activity concentrations as function of gamma-ray energy for various radionuclides (^{234m}Pa, ^{226}Ra, ^{214}Bi and ^{214}Pb) in the ^{238}U series.

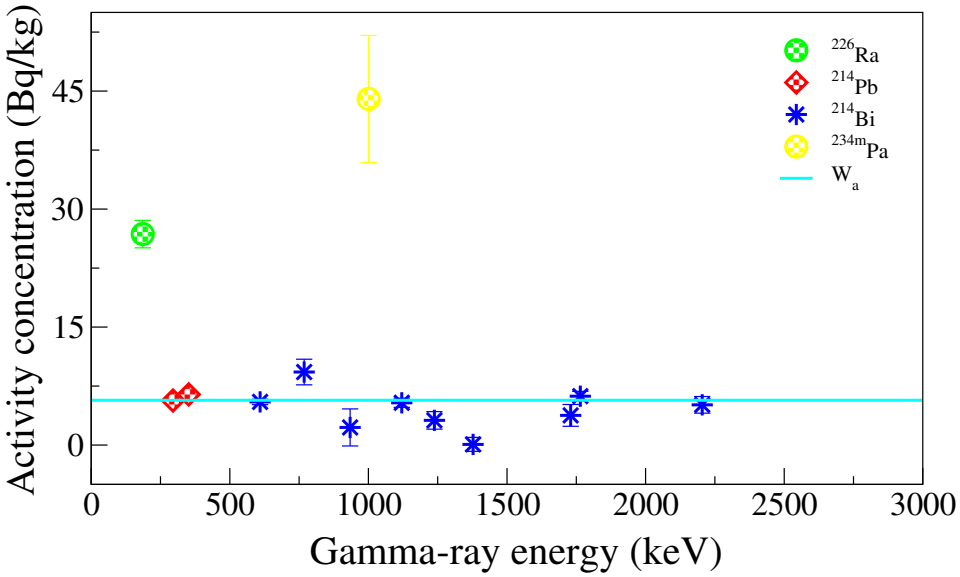

Figure 5.22: Sample S15: Activity concentrations as function of gamma-ray energy for various radionuclides (^{234m}Pa, ^{226}Ra, ^{214}Bi and ^{214}Pb) in the ^{238}U series.

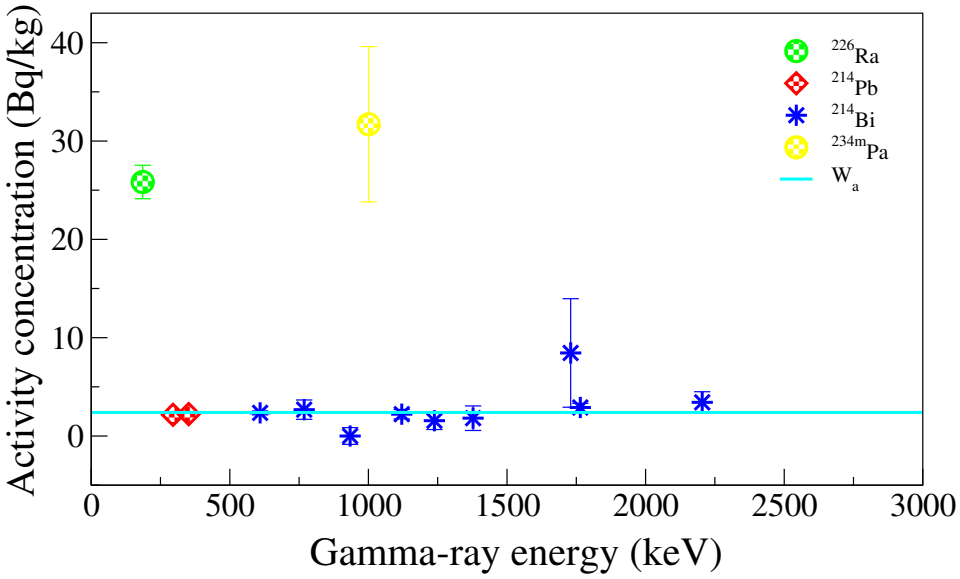

Figure 5.23: Sample S16: Activity concentrations as function of gamma-ray energy for various radionuclides (^{234m}Pa, ^{226}Ra, ^{214}Bi and ^{214}Pb) in the ^{238}U series.

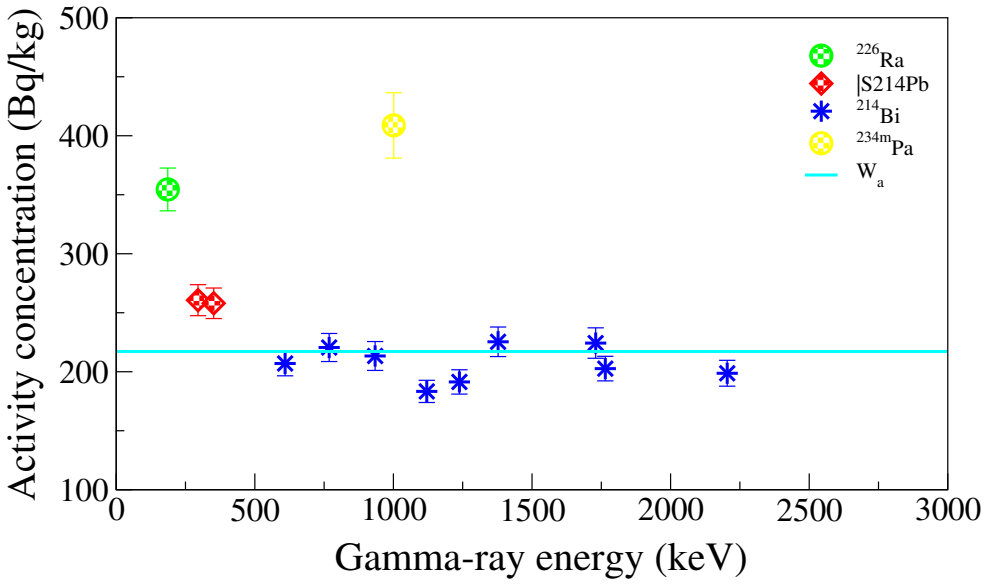

Figure 5.24: Sample S17: Activity concentrations as function of gamma-ray energy for various radionuclides (^{234m}Pa, ^{226}Ra, ^{214}Bi and ^{214}Pb) in the ^{238}U series.

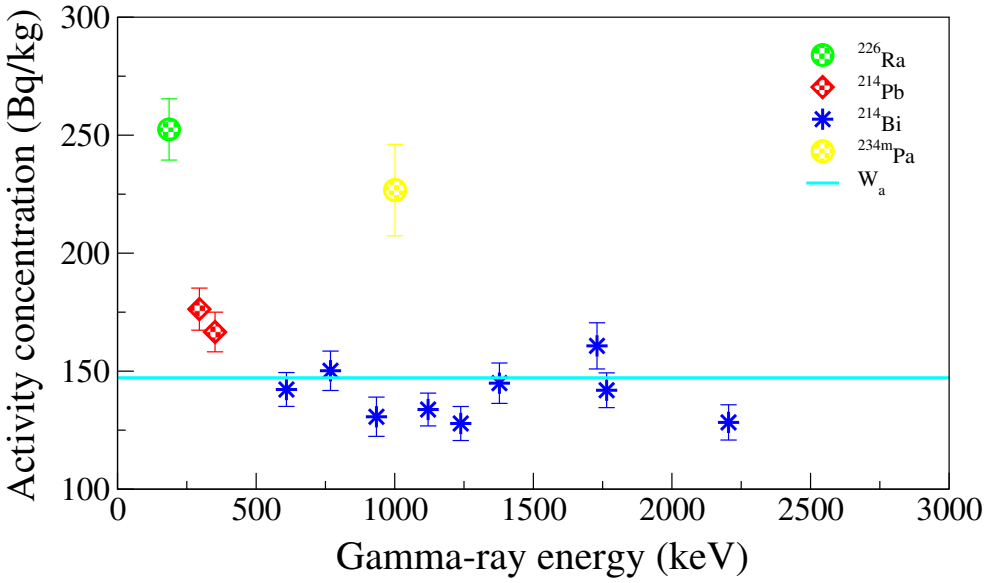

Figure 5.25: Sample S18: Activity concentrations as function of gamma-ray energy for various radionuclides (^{234m}Pa, ^{226}Ra, ^{214}Bi and ^{214}Pb) in the ^{238}U series.

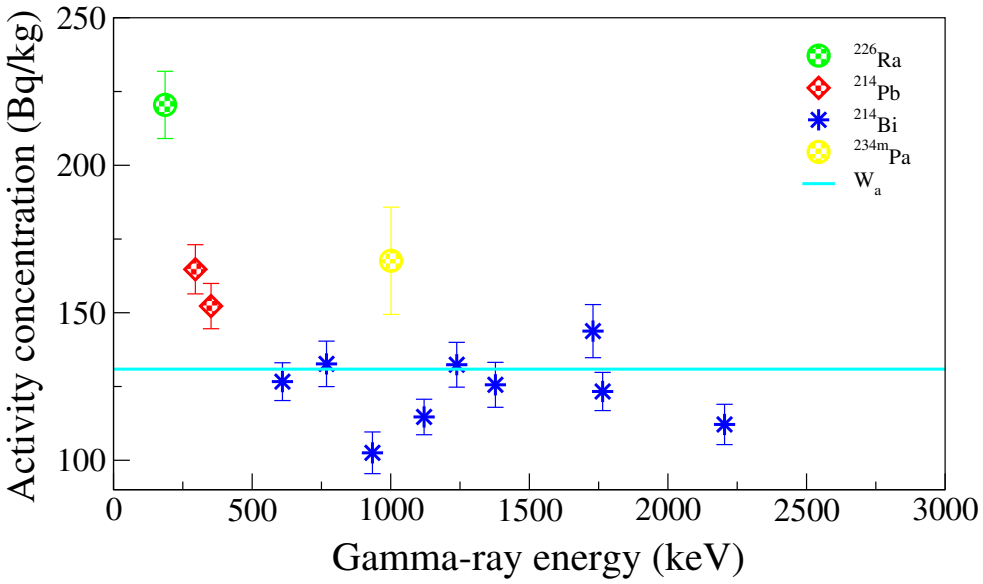

Figure 5.26: Sample S19: Activity concentrations as function of gamma-ray energy for various radionuclides (^{234m}Pa, ^{226}Ra, ^{214}Bi and ^{214}Pb) in the ^{238}U series.

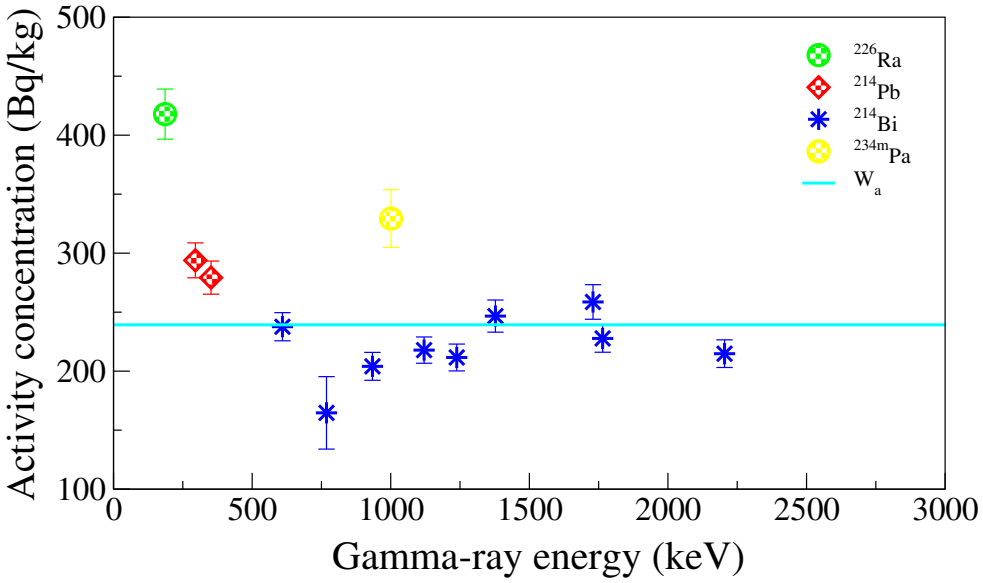

Figure 5.27: Sample S20: Activity concentrations as function of gamma-ray energy for various radionuclides (^{234m}Pa, ^{226}Ra, ^{214}Bi and ^{214}Pb) in the ^{238}U series.

5.2.1.2 Activity Concentration of ^{232}Th

The individual activity concentrations of the observed gamma-ray transitions from sample S1 to S20 are due to ^{228}Ac, ^{212}Bi and ^{208}Tl from ^{232}Th decay chain as shown in 5.28 to 5.47, respectively. There is consistency across the gamma energy except some gamma-ray lines which are relatively higher than the weighted average line. This could be due to their low gamma-ray decay probability. However, ^{232}Th is not a gamma emitters which leads to their deduced activities from the members of the decay chain (see Fig. 2.6), provided that the the system is closed, and secular equilibrium is achieved. Therefore, the reason some gamma energy are higher could also be due to the samples not sealed for twenty one days to obtain secular equilibrium.

Table 5.4 gives the weighted average for sample S1 to S20 which were obtained based on the collective activities from ^{228}Ac, ^{208}Tl and ^{212}Bi decay. There is a uniformity across the samples except for the unexpectedly higher activity values for samples S17 to S20. The ^{232}Th activity concentration values obtained from sample S1 to S16 range from 2.1±0.2 to 16.5±0.5 Bq/kg. Also, values from S17 to S20 ranged from 14.4±0.5 to 20.5±0.7 Bq/kg.

Furthermore, the Chi-square value per degree of freedom (χ^2_R) for ^{232}Th ranged from 1.0 to 10.0 for the twenty samples collected (more details in Section 4.3.4).

Table 5.4: Activity concentrations (weighted average) for ^{232}Th in all samples

Sample	Activity concentration (Bq/kg)	χ^2_R value
S1	6.1±0.3	9.3
S2	13.5±0.4	2.7
S3	7.7±0.3	4.0
S4	16.5±0.5	5.8
S5	2.2±0.2	5.4
S6	5.0±0.2	2.6
S7	7.4±0.3	3.5
S8	7.3±0.3	1.9
S9	6.5±0.3	3.3
S10	8.3±0.3	4.1
S11	7.2±0.3	1.0
S12	6.9±0.3	2.3
S13	6.8±0.3	2.5
S14	3.6±0.2	4.3
S15	4.2±0.2	3.5
S16	2.1±0.2	3.4
S17	39.8±0.1	7.2
S18	14.9±0.5	10.0
S19	14.4±0.5	4.3
S20	20.5±0.7	7.3

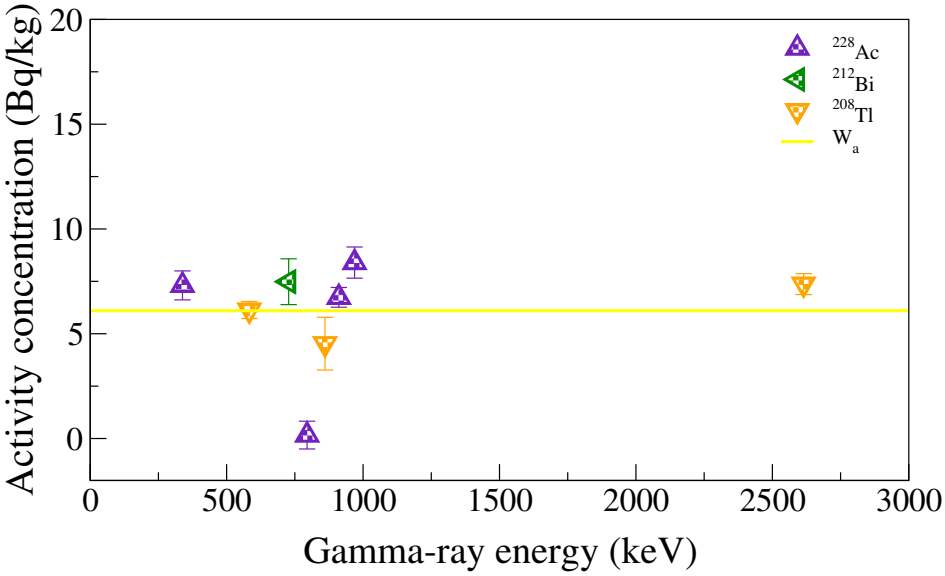

Figure 5.28: Sample S1: Activity concentrations as function of gamma-ray energy for various radionuclides (^{208}Tl, ^{212}Bi and ^{228}Ac) in the ^{232}Th series.

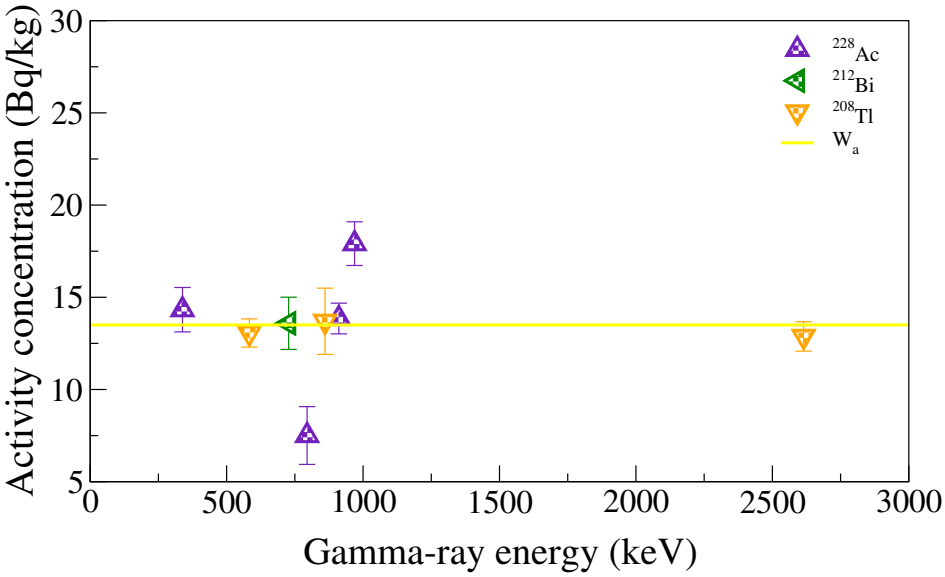

Figure 5.29: Sample S2: Activity concentrations as function of gamma-ray energy for various radionuclides (^{208}Tl, ^{212}Bi and ^{228}Ac) in the ^{232}Th series.

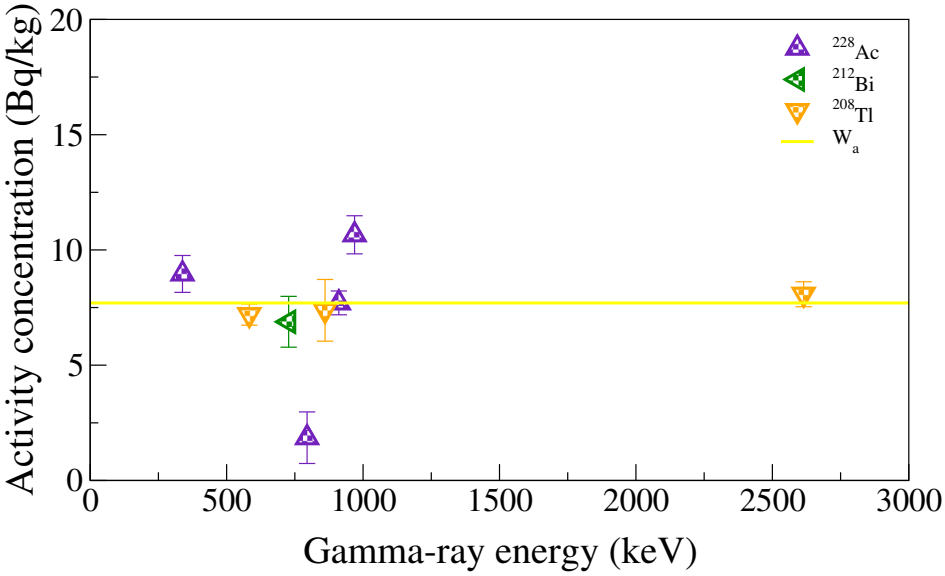

Figure 5.30: Sample S3: Activity concentrations as function of gamma-ray energy for various radionuclides (^{208}Tl, ^{212}Bi and ^{228}Ac) in the ^{232}Th series.

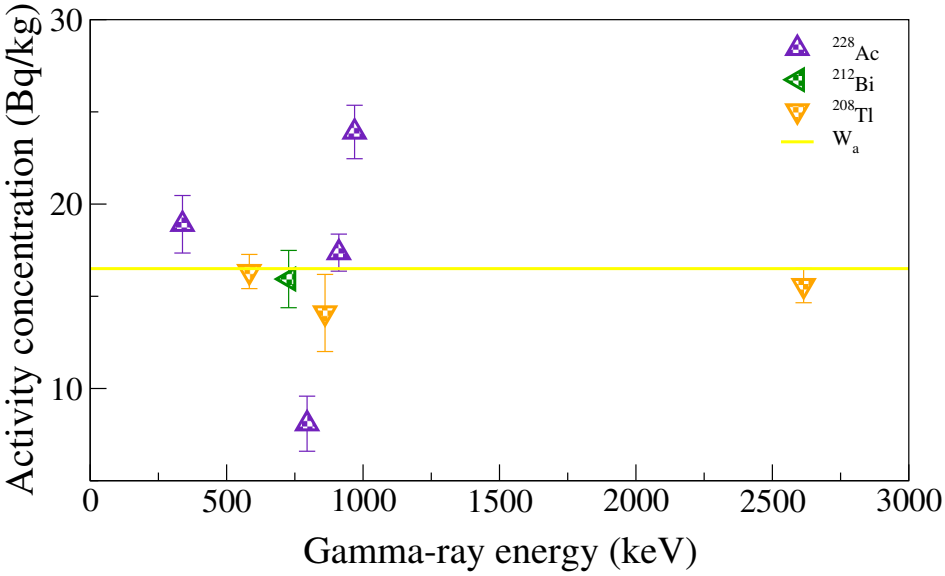

Figure 5.31: Sample S4: Activity concentrations as function of gamma-ray energy for various radionuclides (^{208}Tl, ^{212}Bi and ^{228}Ac) in the ^{232}Th series.

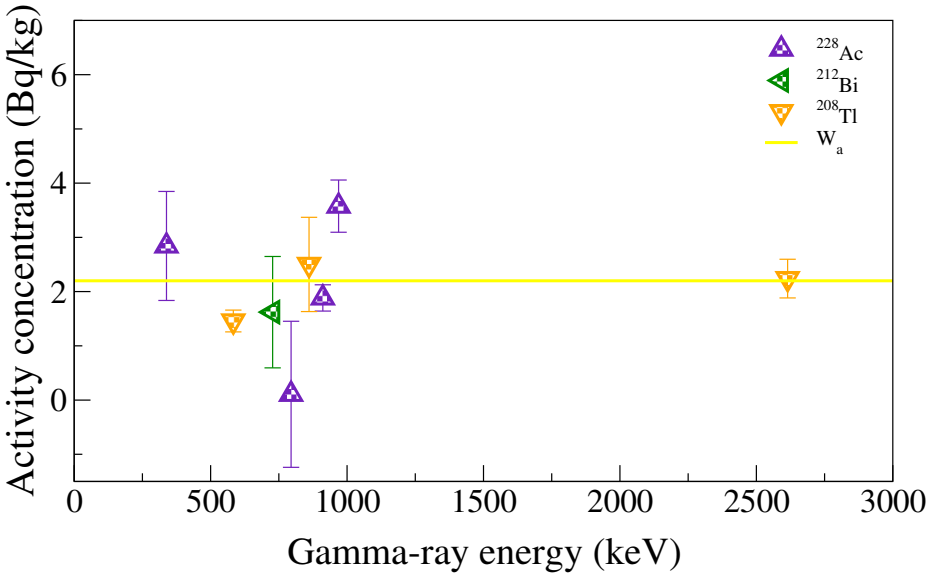

Figure 5.32: Sample S5: Activity concentrations as function of gamma-ray energy for various radionuclides (^{208}Tl, ^{212}Bi and ^{228}Ac) in the ^{232}Th series.

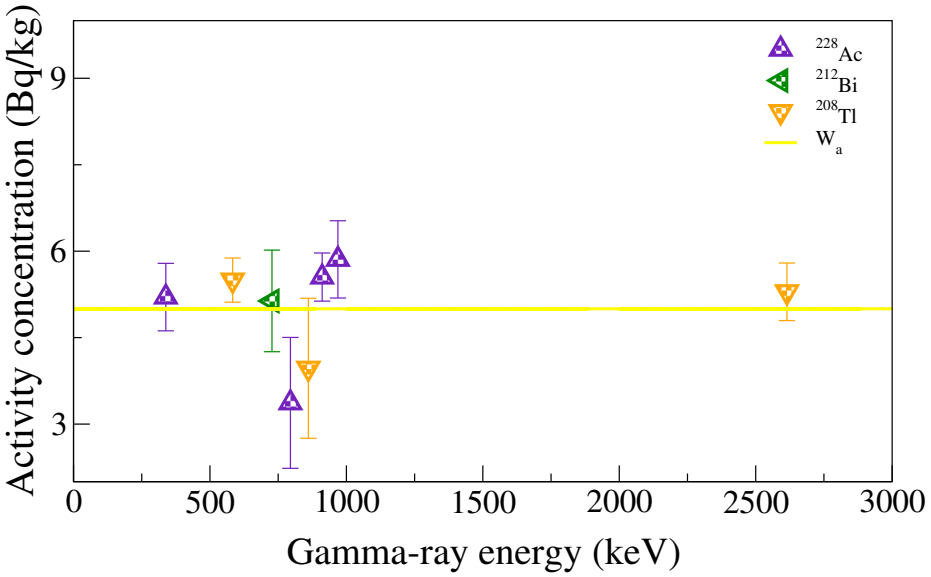

Figure 5.33: Sample S6: Activity concentrations as function of gamma-ray energy for various radionuclides (^{208}Tl, ^{212}Bi and ^{228}Ac) in the ^{232}Th series.

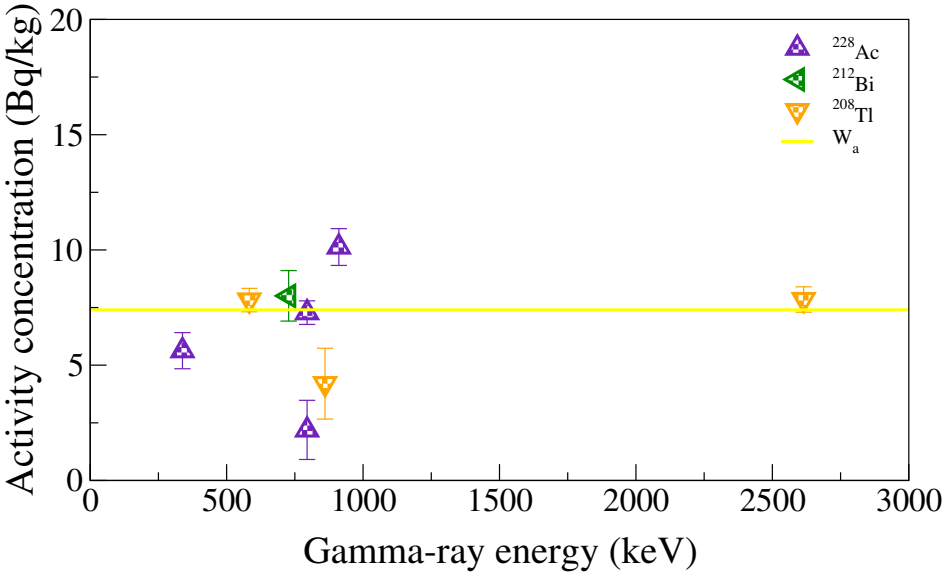

Figure 5.34: Sample S7: Activity concentrations as function of gamma-ray energy for various radionuclides (^{208}Tl, ^{212}Bi and ^{228}Ac) in the ^{232}Th series.

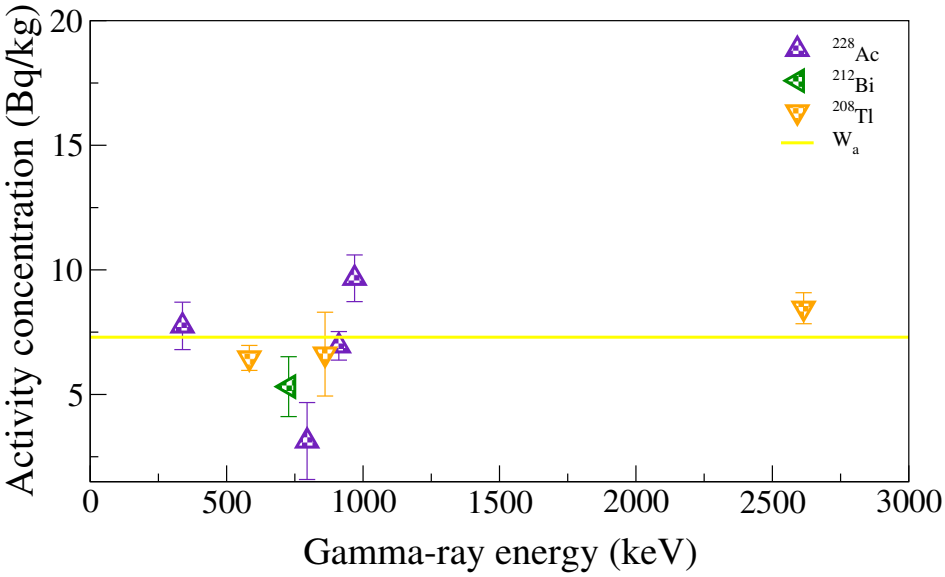

Figure 5.35: Sample S8: Activity concentrations as function of gamma-ray energy for various radionuclides (^{208}Tl, ^{212}Bi and ^{228}Ac) in the ^{232}Th series.

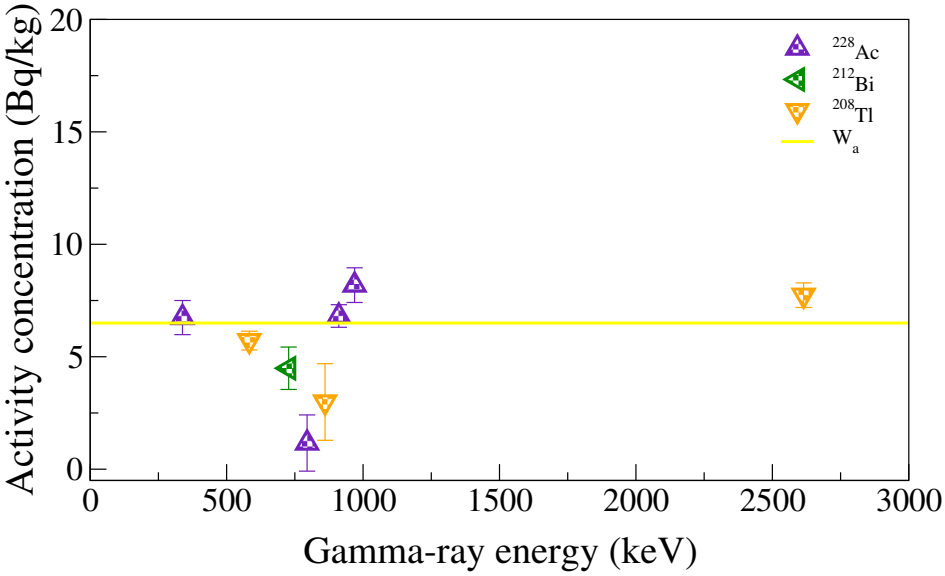

Figure 5.36: Sample S9: Activity concentrations as function of gamma-ray energy for various radionuclides (^{208}Tl, ^{212}Bi and ^{228}Ac) in the ^{232}Th series.

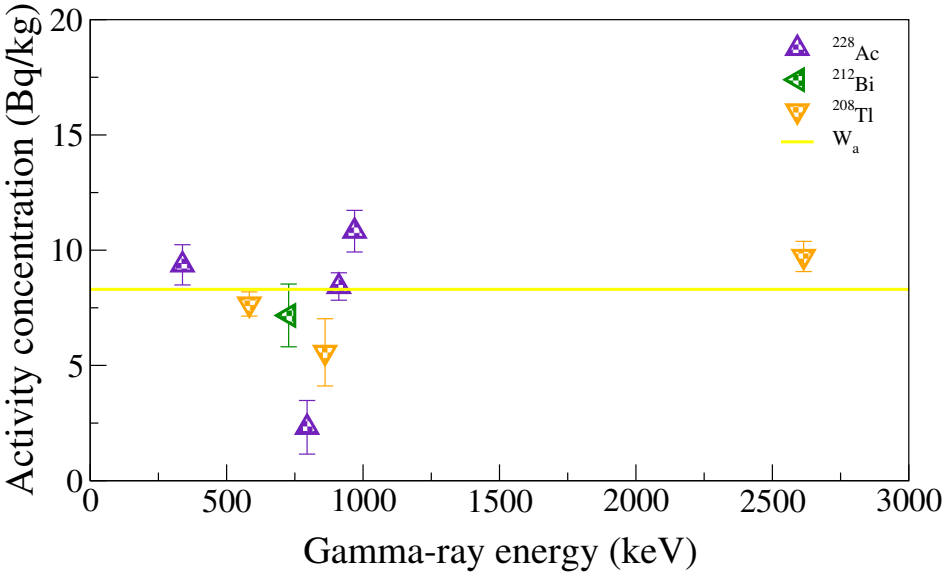

Figure 5.37: Sample S10: Activity concentrations as function of gamma-ray energy for various radionuclides (^{208}Tl, ^{212}Bi and ^{228}Ac) in the ^{232}Th series.

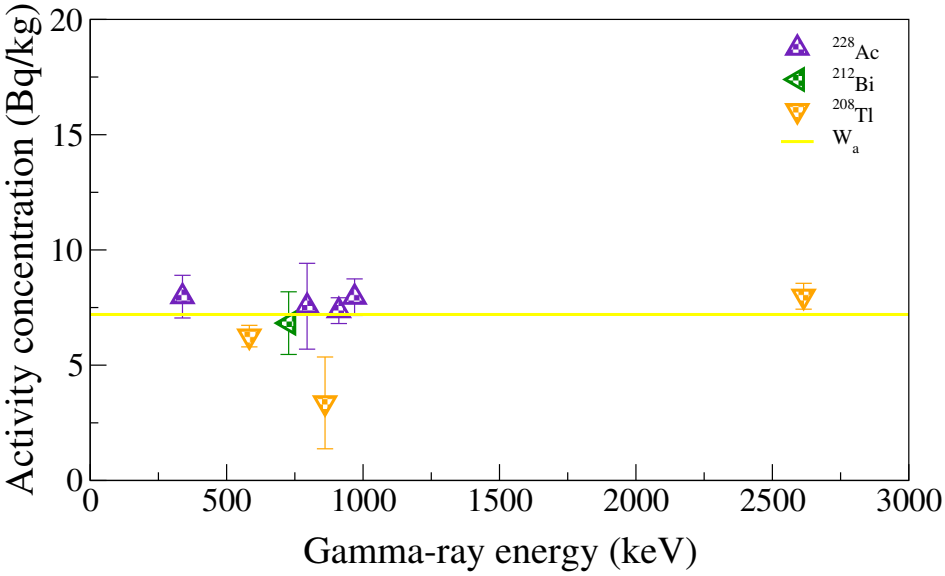

Figure 5.38: Sample S11: Activity concentrations as function of gamma-ray energy for various radionuclides (^{208}Tl, ^{212}Bi and ^{228}Ac) in the ^{232}Th series.

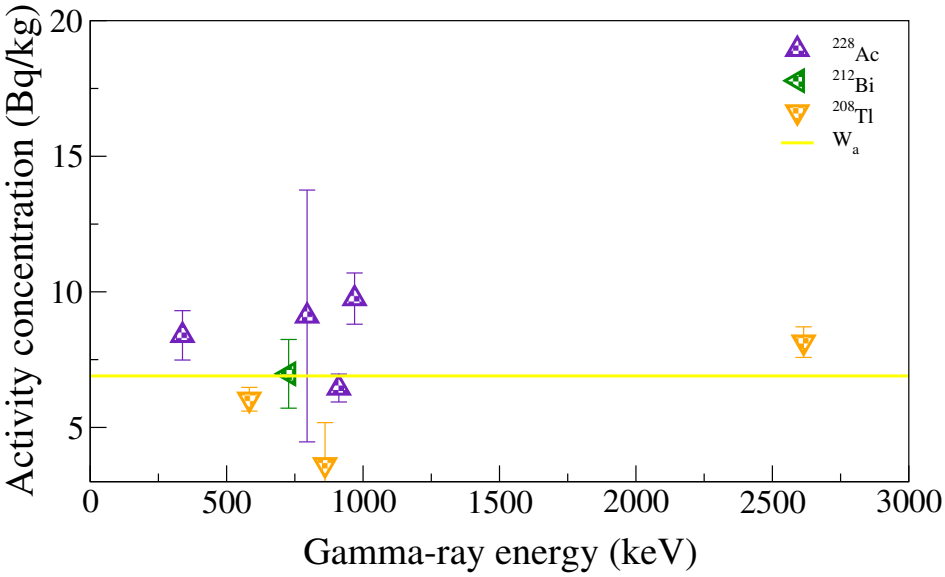

Figure 5.39: Sample S12: Activity concentrations as function of gamma-ray energy for various radionuclides (^{208}Tl, ^{212}Bi and ^{228}Ac) in the ^{232}Th series.

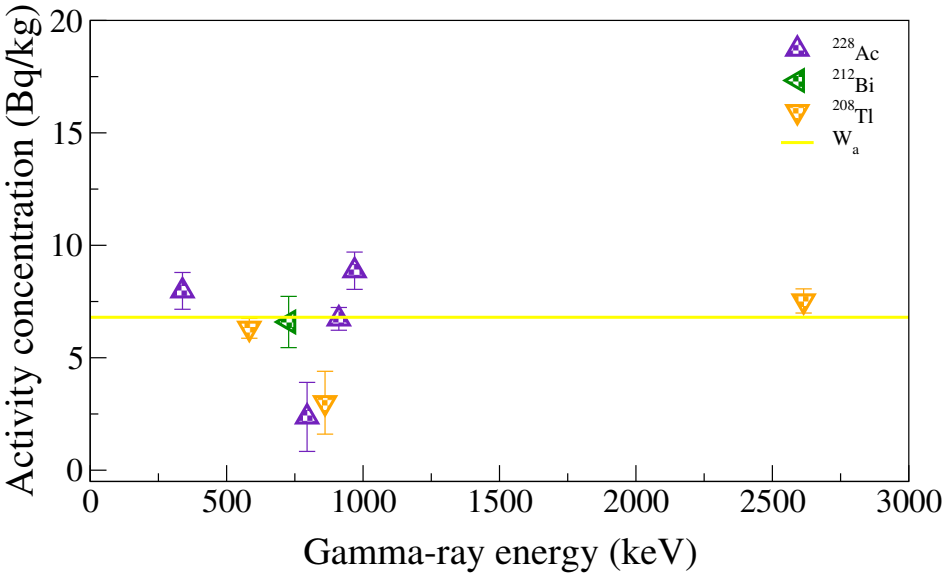

Figure 5.40: Sample S13: Activity concentrations as function of gamma-ray energy for various radionuclides (^{208}Tl, ^{212}Bi and ^{228}Ac) in the ^{232}Th series.

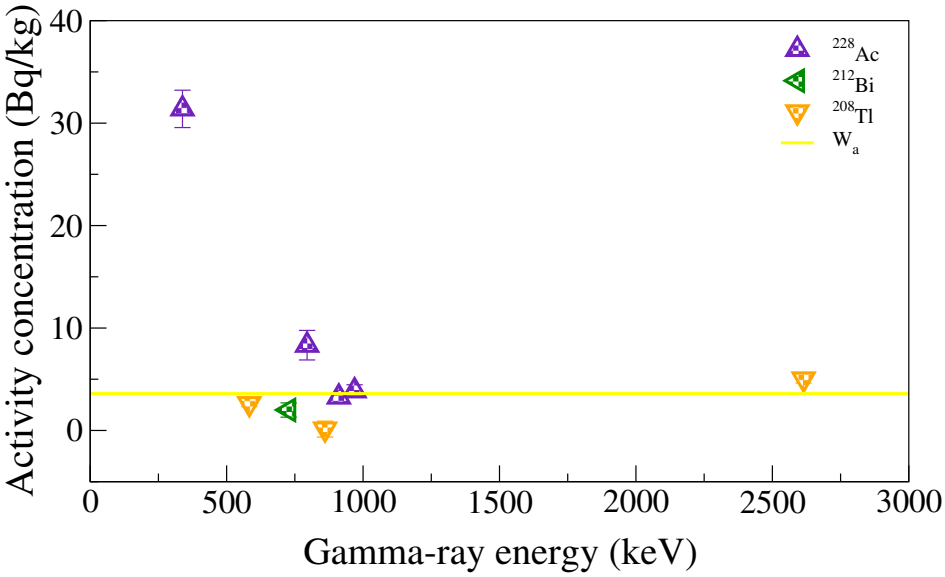

Figure 5.41: Sample S14: Activity concentrations as function of gamma-ray energy for various radionuclides (^{208}Tl, ^{212}Bi and ^{228}Ac) in the ^{232}Th series.

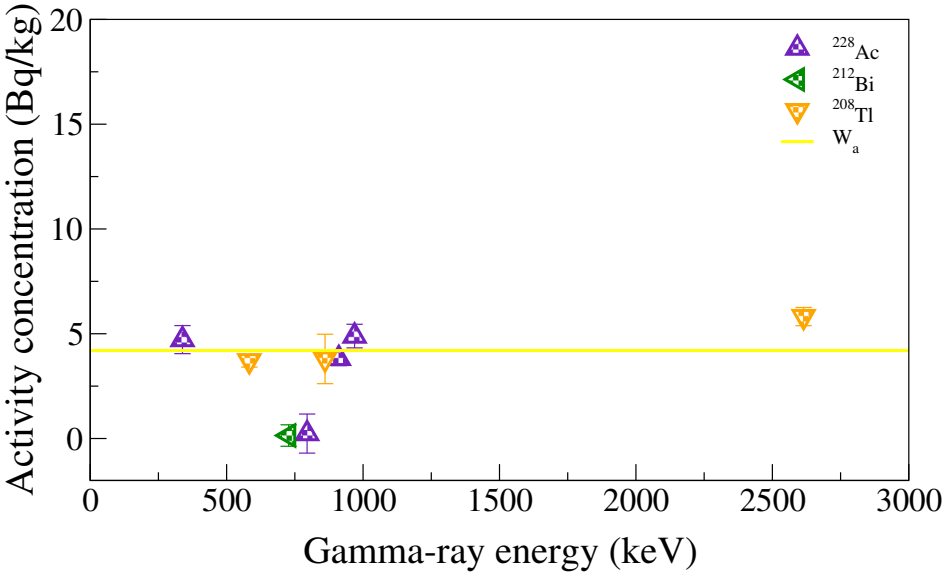

Figure 5.42: Sample S15: Activity concentrations as function of gamma-ray energy for various radionuclides (^{208}Tl, ^{212}Bi and ^{228}Ac) in the ^{232}Th series.

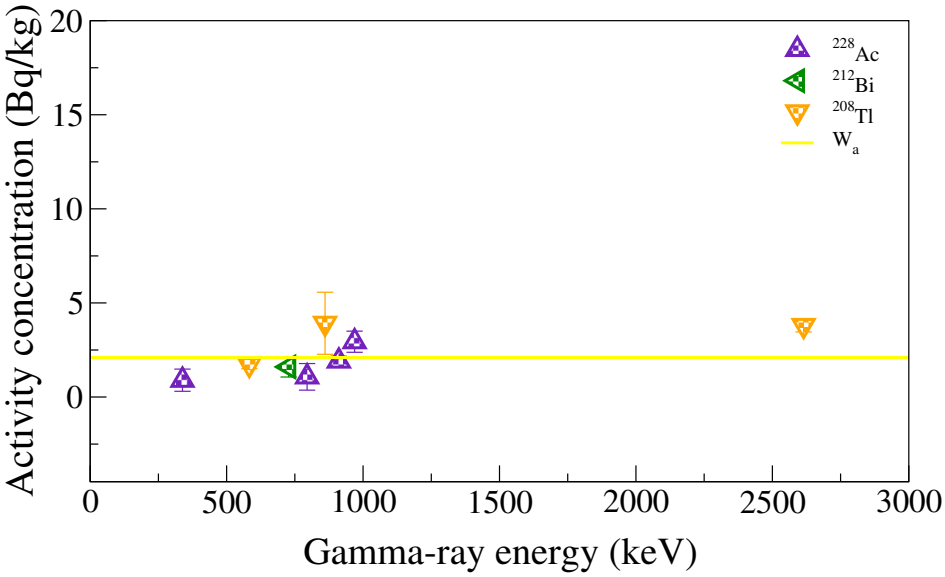

Figure 5.43: Sample S16: Activity concentrations as function of gamma-ray energy for various radionuclides (^{208}Tl, ^{212}Bi and ^{228}Ac) in the ^{232}Th series.

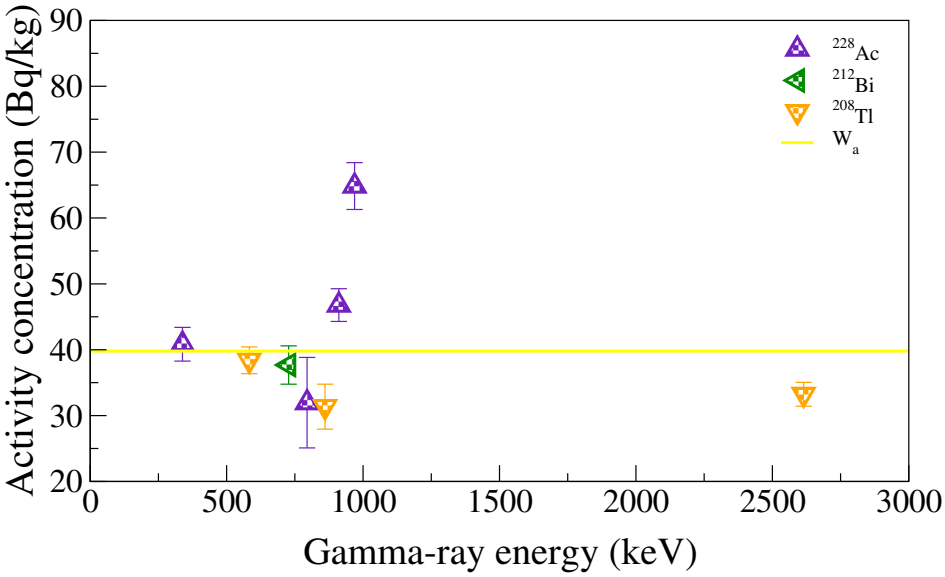

Figure 5.44: Sample S17: Activity concentrations as function of gamma-ray energy for various radionuclides (^{208}Tl, ^{212}Bi and ^{228}Ac) in the ^{232}Th series.

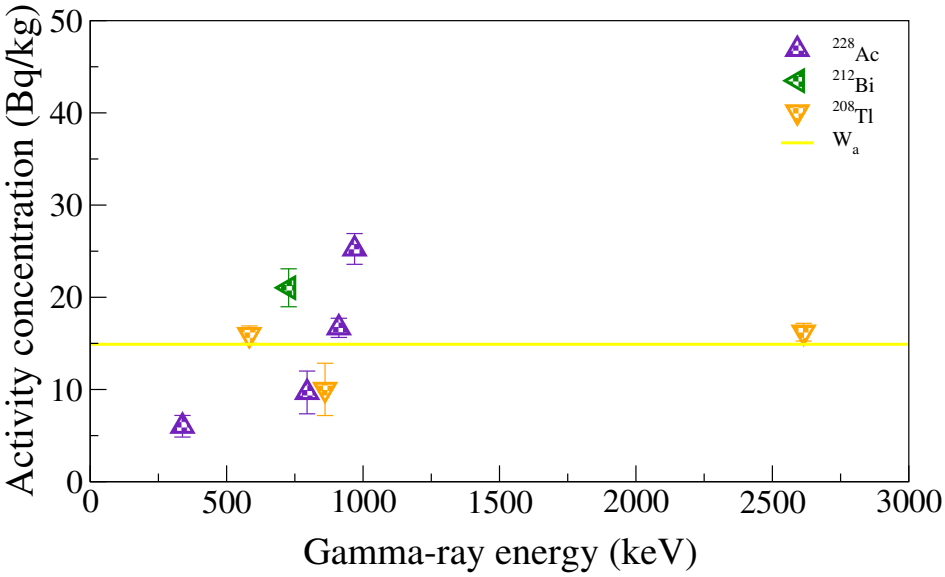

Figure 5.45: Sample S18: Activity concentrations as function of gamma-ray energy for various radionuclides (^{208}Tl, ^{212}Bi and ^{228}Ac) in the ^{232}Th series.

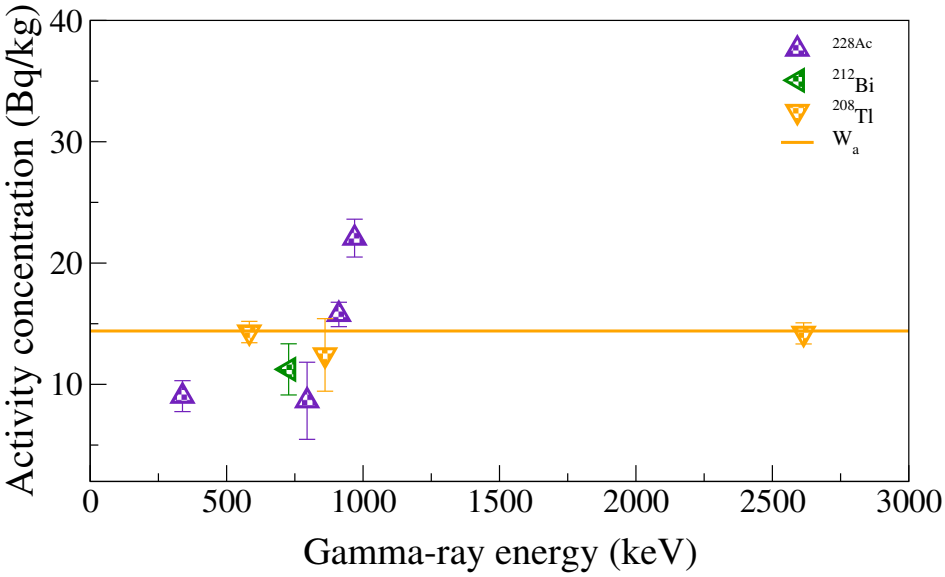

Figure 5.46: Sample S19: Activity concentrations as function of gamma-ray energy for various radionuclides (^{208}Tl, ^{212}Bi and ^{228}Ac) in the ^{232}Th series.

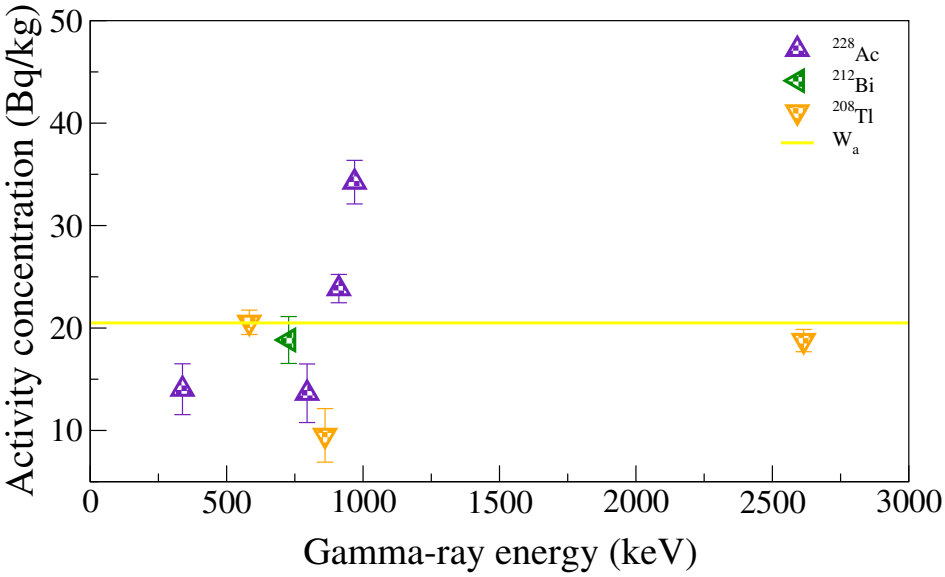

Figure 5.47: Sample S20: Activity concentrations as function of gamma-ray energy for various radionuclides (^{208}Tl, ^{212}Bi and ^{228}Ac) in the ^{232}Th series.

5.2.1.3 Activity Concentration of ^{235}U, ^{137}Cs and ^{40}K

Activity concentration of ^{235}U, ^{137}Cs and ^{40}K radionuclide were directly measured using a single gamma line as illustrated in Table 5.5. The individual activity concentrations of the observed gamma-ray transitions from sample S1 to S20 ranged from 0.8 to 21.7 Bq/kg for ^{235}U, 0.3 to 3.8 Bq/kg for ^{137}Cs and 20.6 to 454.8 Bq/kg ^{40}K. It can also be observed that the activity concentration are relatively higher for sample S17 to S20 (see Section 4.1.1 for more details). The activity concentration of ^{40}K were determined considering possible interference due to ^{232}Th contribution through ^{228}Ac at 1459.2 keV line with branching ratio of 0.83%. This contribution was considered low given the relatively low concentrations of ^{232}Th (Table 5.4) as compared to ^{40}K (Table 5.5) in majority of the samples. The relatively high concentration of ^{40}K could be related to the agricultural activities in the region whereby potassium rich fertilizers are used while the low concentration shows uniformity in the distribution of radionuclides. Also, the relatively high concentration of ^{137}Cs in sample S17 and S20 could be due to variations in many factors, such as surface topography or landscape of the area and factors that are related to soil, for instance, density and consequent soil movement, and chemical properties of the soil. For this study, the origin of ^{137}Cs identified in the samples is unknown. The results as presented, show that the activity concentration of ^{137}Cs in the samples collected, were above the minimum detectable activity of the HPGe system that was used. Moreover, complementary elemental analysis with ICP-MS has shown no traces of ^{137}Cs in the samples analysed, hence we assume this to be insignificant.

Table 5.5: Activity concentration of ^{235}U, ^{137}Cs and ^{40}K

sample	Activity concentration (Bq/kg)		
	^{235}U	^{137}Cs	^{40}K
S1	2.1±0.6	0.4±0.1	22.3±1.5
S2	2.1±0.7	0.8±0.1	87.3±4.7
S3	2.9±0.6	0.5±0.1	20.3±1.4
S4	2.5±0.6	0.4±0.1	22.7±1.6
S5	0.9±0.3	0.4±0.1	25.2±1.6
S6	2.5±0.5	0.6±0.2	20.6±1.4
S7	0.9±0.4	1.3±0.1	58.9±3.5
S8	1.4±0.4	1.7±0.1	49.3±3.0
S9	3.0±0.8	1.4±0.1	62.4±3.5
S10	3.0±0.7	0.5±0.2	178.8±9.5
S11	1.9±0.7	0.5±0.1	281.8±14.5
S12	0.8±0.3	0.4±0.1	268.6±13.8
S13	1.9±0.5	0.3±0.1	155.5±8.2
S14	3.5±0.6	0.5±0.1	42.6±2.5
S15	1.1±0.4	0.4±0.1	77.9±4.3
S16	1.8±0.6	0.3±0.1	43.3±2.5
S17	16.3±1.6	2.4±0.2	150.4 ±8.0
S18	12.6±1.4	1.6±0.2	199.8±10.4
S19	7.8±1.1	1.8±0.2	454.8±23.1
S20	21.7±1.9	3.8±0.2	215.7±11.2

5.2.1.4 Summary of Activity Concentration

According to Ref. [Uns00], the world mean value for these nuclides are: ^{238}U : 33 Bq/kg, ^{232}Th: 45 Bq/kg and ^{40}K: 420 Bq/kg, with range of 17-60, 11-64 and 140-850 Bq/kg [Aja20]. Due to these activities, sample S1 to S16 are still within the world range value but sample S17 to S20 of ^{238}U are relatively higher than world range values while ^{232}Th and ^{40}K are still within the world range values. The main reason behind the higher activity concentrations observed in sample S17 to S20 can be attributed to samples taken from large open mining plains where mining activities are underway (see Section 4.1 for more details). The summary of activity concentrations for all samples compared to other countries are illustrated in Table 5.6. The results obtained in [Pen18] show consistence with the present study since they are both from Chad, although different regions.

Table 5.6: Activity concentration values in all samples compared with some other countries across the world

Country	Activity concentration (Bq/kg)		
	^{238}U	**^{232}Th**	**^{40}K**
USA [Uns00]	35	35	370
France [Lab92]	38	38	599
Spain [Uns00]	n.a	33	470
Iran [Uns00]	28	22	640
Iran Golestan [Lot17]	23	31	453
Malaysian Peninsula [Alm12]	45	83	455
Kuwait [Baj15]	13	11	300
Nigeria [Muh10]	8	34	641
Northwest Libya [Elk08]	8	4	28
Egypt [Uns00]	17	18	320
Chad [Pen18]	3.29	3	158
World average value [Uns00]	35	30	400
Present study			
S1-S16	8	7	89
S17-S20	184	22	255

5.2.2 Correlations of Activity Concentration of ^{238}U, ^{232}Th, ^{40}K

Activity correlations of sample S1-S20 for ^{40}K vs ^{232}Th, ^{40}K vs ^{238}U and ^{238}U vs ^{232}Th respectively, are illustrated in Fig 5.48. There is a positive correlation be-

tween ^{238}U vs ^{232}Th and ^{40}K vs ^{238}U with a correlation coefficient of R^2=0.65 and R^2=0.22, respectively. This correlation may be due to a similar indication of soil or sand chemical behaviour and other artificial nuclides being distributed in the environment [Kha01, Elr06, Fuj04]. However, a poor correlation can be observed from ^{40}K vs ^{232}Th with a correlation coefficients of R^2=0.09, the samples concentration of ^{232}Th are associated to soil organic matter. A weak correlation between ^{232}Th and ^{40}K may be caused by a relatively high solubility or high moveable of potassium compared to thorium [Elm04]. The solid line in the figures represents the best fit which is approximately a linear relationship with a correlation coefficient.

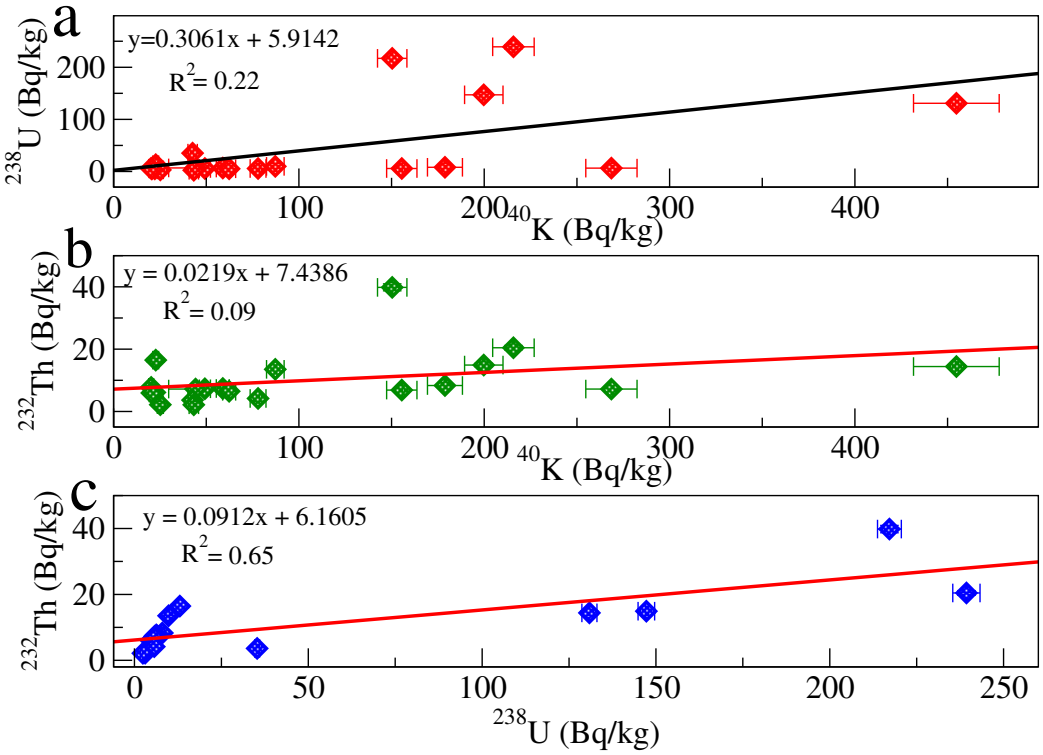

Figure 5.48: Activity correlation between: (a) ^{40}K vs ^{238}U, (b) ^{40}K vs ^{232}Th and (c) ^{238}U vs ^{232}Th.

5.2.3 Radiation Health Risk Assessment

The evaluated radiation hazard indices from the present study are illustrated in Table 5.7. Radium equivalent concentration range from 27-464 Bq/kg while external, internal hazard, AEDE and ELCR range from 0.07-1.24, 0.13-2.38, 0.09-1.65 (mSv/y) and 0.34×10^{-3} to 5.76×10^{-3}, respectively. Some of the samples are far below the permissible average value of 370 Bq/kg for Ra_{equ} as reported in [Uns00] which relate to an effective dose of 1 mSv for the general public [Aja09]. Sample S17 to S20 are relatively higher than the recommended values, this could be due to the fact that the samples were taken in a new dug hole where mining activities are underway. The activity concentration of radium equivalent is used to determine the radiation hazard indices associated with the natural radioactivity (^{226}Ra, ^{232}Th, ^{40}K) as explained in Section 4.4.2, it is assumed that 370 Bq/kg of ^{226}Ra, 259 Bq/kg of ^{232}Th and 4810 Bq/kg of ^{40}K produce the same gamma dose rate [Str76, Kum03].

Before annual effective dose equivalent (AEDE) can be calculated the absorbed dose rate needs to be calculated and apply a conversion factor of 0.7×10^{-6} Sv/Gy and the occupancy for outdoor (D_{out}) and indoor (D_{in}) are 0.2 and 0.8, respectively. The AEDE calculated was used to estimate the ELCR using the equation shown in Subsection 4.4.5. Annual effective dose equivalent (AEDE) average value is less than the recommended value of 1 mSv/y [ICRP91]. Excess lifetime cancer risk (ELCR) values is about 5 times higher than the recommended value of 0.29×10^{-3}, and as a results of this, activities in this area requires regulations to minimise the exposure and subsequently the risk of developing cancer. Figure 5.49 represent the histogram for Ra_{equ}, H_{ext}, H_{int}, AEDE and ELCR $\times10^{-3}$.

Table 5.7: Result of radiological hazard risk factors measured for all samples collected from Southern area of Chad.

Sample	Ra_{equ} (Bq/kg)	H_{ext}	H_{int}	AEDE (mSv/y)	ELCR $\times 10^{-3}$
S1	34.99	0.09	0.16	0.13	0.44
S2	59.02	0.16	0.25	0.22	0.77
S3	38.48	0.10	0.17	0.14	0.49
S4	60.96	0.16	0.26	0.22	0.78
S5	26.85	0.07	0.13	0.09	0.34
S6	33.98	0.09	0.16	0.12	0.43
S7	43.96	0.12	0.20	0.16	0.56
S8	46.42	0.13	0.21	0.17	0.59
S9	42.68	0.12	0.19	0.16	0.55
S10	59.04	0.16	0.25	0.23	0.80
S11	66.19	0.18	0.27	0.27	0.93
S12	59.88	0.16	0.24	0.24	0.85
S13	54.29	0.15	0.23	0.21	0.73
S14	87.39	0.24	0.45	0.31	1.09
S15	38.77	0.10	0.18	0.15	0.51
S16	32.22	0.09	0.16	0.12	0.41
S17	423.06	1.14	2.10	1.51	5.27
S18	289.14	0.78	1.46	1.03	3.62
S19	276.08	0.75	1.34	1.01	3.56
S20	463.71	1.25	2.38	1.65	5.76
World arithmetic mean [Uns00]					
Recommended value	370				0.29
Present study					
Range	27-464	0.09-1.25	0.13-2.38	0.09-1.65	0.34-5.76
Average	111	0.30	0.54	0.41	1.42

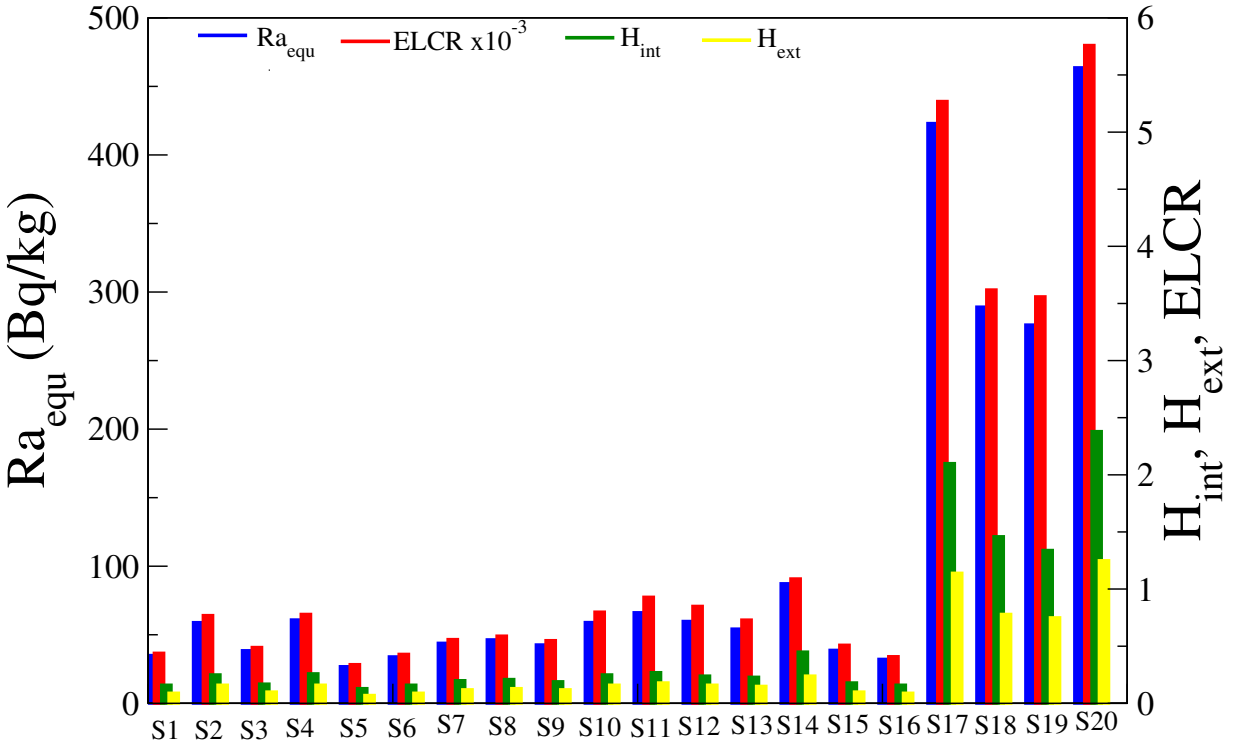

Figure 5.49: Estimated radiation hazard indices showing the Ra_{equ} (blue), ELCR (red), H_{int}(green) and H_{ext} (yellow) for the study area.

5.3 Elemental Concentration: ICP-MS

The selected samples were analysed with ICP-MS in order to determine light, medium and heavy elements that were out of detection limit for HPGe detector. Detailed results from the ICP-MS measurements can be found in Appendix B, Table B.1 and B.2. However, the results present 27 elements (B, V, Cr, Mn, Co, Ni, Cu, Zn, As, Se, Sr, Mo, Cd, Sn, Sb, Ba, Hg, Pb, U, Al, Fe, Ca, K, Ma, Na, P and Si), which are grouped into major elements, essential trace elements, potentially toxic trace elements and toxic trace elements [Ndl16]. Those elements are important since they are capable of reducing crop production due to bio-accumulation

and bio-magnification in the food chain. Also, there is a risk of superficial and underground contamination. Basic knowledge of environmental and associated health effects of the heavy elements is important in order to understand their speciation, remedial options and bio-availability.

Figure 5.50 and 5.51 show the Potentially toxic trace elements and Toxic trace elements concentrations values with their Maximum Allowable Limit (MAL) of the selected samples in mg/kg while the Major elements and Essential elements plots are shown in Appendix B, Figs. B.1 and B.2, respectively. The full details of Trace elements will be discussed in this study. There is a noticeable higher concentration level of Copper (Cu) from sample S17 while other samples are <100 mg/kg. Sample S17 could pose a potential ecological risk factor because of its relatively higher concentration (225 mg/kg) which exceed the maximum allowable limit for agricultural soils (100 mg/kg) recommended by FAO/WHO guidelines [Chi14].

Concentration level of Molybdenum (Mo) for sample S15 and S17 are extremly higher compared to other samples while S4 and S6 are below detection limit. Although Mo is also an essential elements and is needed for different enzymes involving nitrogen fixation, it is only required at low levels where the critical deficiency level is 0.1 mg/kg. In addition, Mo is also potentially toxic trace element for livestocks even when the concentration is low, thus the concentration should be less than 1 mg/kg, which is the normal levels found on a non polluted land [Kab20]. In this result, the average concentration in Mo levels are higher than 1 mg/kg, therefore the soil may be considered unfit for agricultural purposes due to the capability of producing potentially Molybdenum toxic system [Kab20].

The Arsenic (As) Concentrations found in the selected samples ranged from 2 - 6 mg/kg. Some countries in Africa may have naturally higher As concentrations in the soil background, for instance South Africa allowable limit is 5.8 mg/kg [DEA10]. Therefore, the highest As found in the samples could be used as a baseline or MAL for As contaminated soil in Chad.

The distribution of Cobalt (Co), Antimony (Sb), Selenium (Se) and Tin (Sn) were found to be lower in this study. Toxic trace elements Mercury (Hg), Cadmium (Cd) and Lead (Pb) were compared with Maximum Allowable Limit (MAL) of FAO/WHO guidelines which are found to be lower than MAL in some samples. However, there is a noticeable higher concentration in Hg which gave an average concentration of 2 mg/kg compared to MAL given by [Chi14] while sample S17 for Pb is also higher than MAL. High concentration of toxic heavy elements in some individual samples may be traced to high levels of acid mine drainage that dissolves heavy elements into the ground.

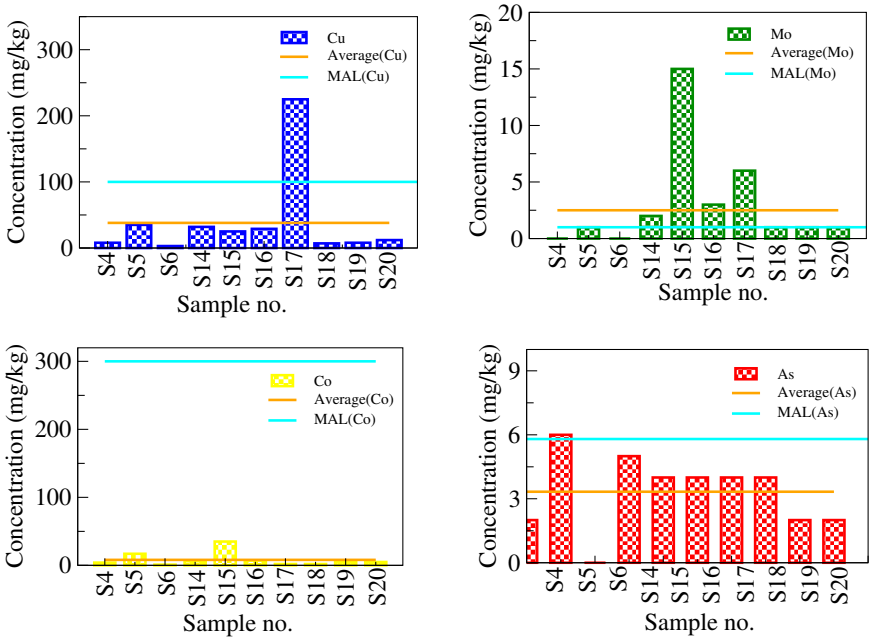

Figure 5.50: The comparison of concentration level of Cu, Mo and As in the selected samples. The horizontal lines represent the average and Maximum Allowable Limit (MAL) from [Kab20, Chi14].

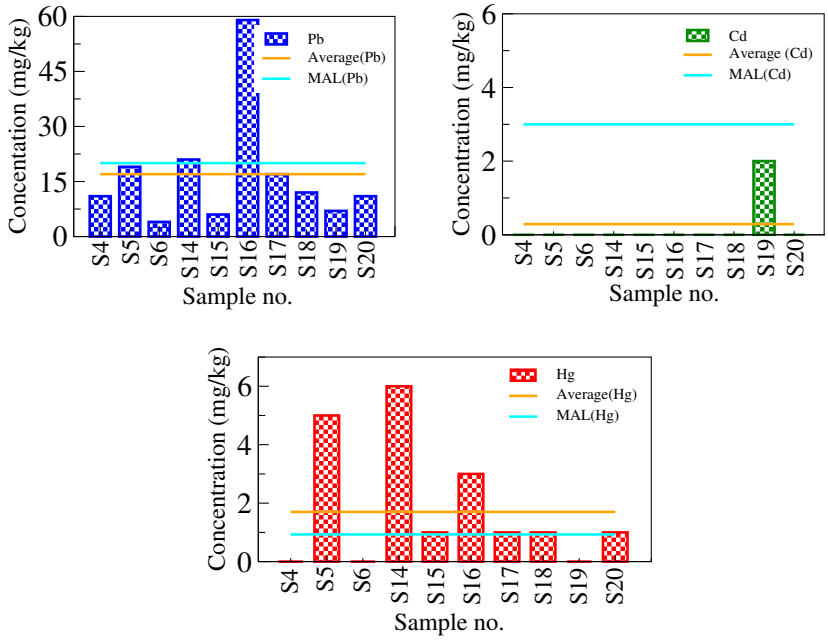

Figure 5.51: Comparison of concentration level of Hg, Cd and Pb in the selected samples. The horizontal lines represent the average and Maximum Allowable Limit (MAL) from [Chi14, DEA10].

5.4 Comparison of ICP-MS and HPGe Data: U and K

Uranium and Potasium found in Trace elements and Major elements were compared with the result obtained with HPGe detector. The results obtained from both HPGe detector and ICP-MS is represented in Figs. 5.52 and 5.53. The ICP-MS concentrations are most commonly expressed as mg/kg which is equivalent to one part per million (ppm). In order for the results to complement each other, the concentrations results for U and K from ICP-MS were converted to Bq/kg

using the following conversion factors [IAEA03]:

$$10000 \text{ ppm K} = 313 \text{ Bq per kg of } {}^{40}\text{K} \tag{5.1}$$

$$1 \text{ ppm U} = 12.35 \text{ Bq per kg of } {}^{238}\text{U} \tag{5.2}$$

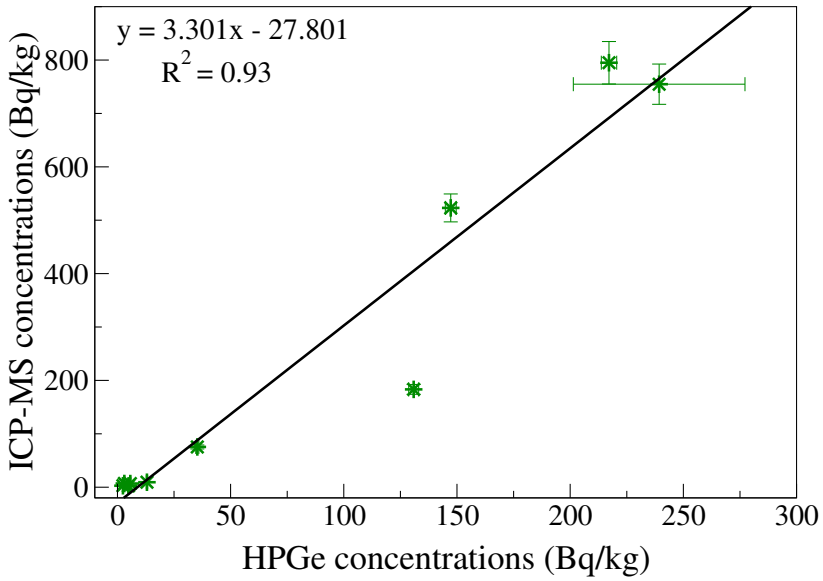

Figure 5.52: Uranium correlations for HPGe and ICP-MS data

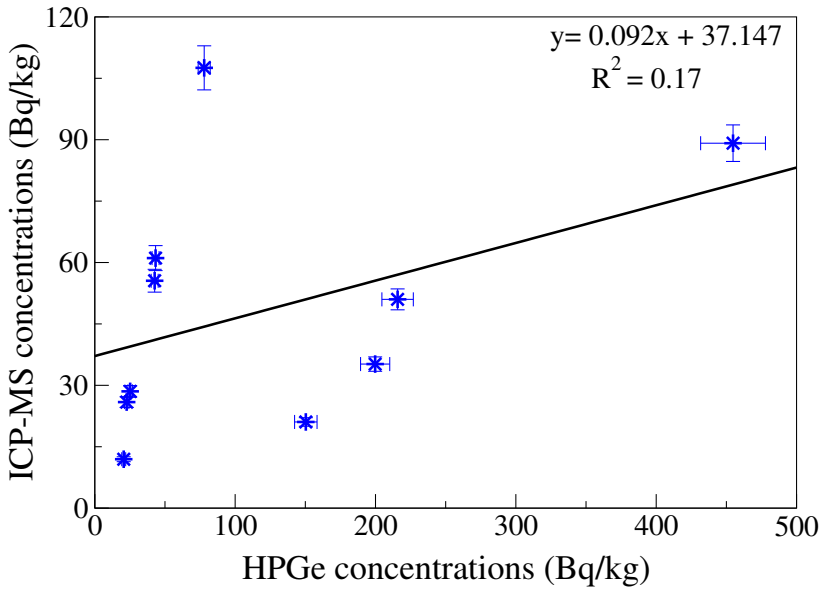

Figure 5.53: Potassium correlations for HPGe and ICP-MS data

Figure 5.52 shows the linearity correlation coefficient for uranium that are determined by HPGe detector and ICP-MS. The result indicated a favourable correlation coefficients with $R^2 = 0.93$. Figure 5.53 indicates the correlation coefficient for potassium which shows a poor correlation with $R^2 = 0.17$. Uranium with strong positive correlations are related linearly, an increase in concentration of one metals leads to increase in concentration of other and vice versa. The correlation result helps in understanding the behaviour and the distribution of each concentration with each other (see Table 5.8). The Limit Of Detection (LOD) values for ICP-MS shown in Table 5.8 represent the lowest metal content value of an element that can quantified in a soil sample. The uncertainties were performed at 95% confidence interval of 0.05.

Table 5.8: Activity concentration and elemental concetration results obtained from HPGe detector and ICP-MS.

Sample	ICP-MS			
	U		K	
	μg/kg	Bq/kg	mg/kg	Bq/kg
LOD	0.17	0.002	50.00	1.60
S4	756.00	9.33 ± 0.47	50.00	26.00 ± 1.30
S5	566.30	7.00 ± 0.35	827.40	29.00 ± 1.43
S6	192.00	2.40 ± 0.12	381.50	12.00 ± 0.60
S14	6104.20	75.40 ± 3.80	1775.00	55.6 ± 2.80
S15	552.00	7.00 ± 0.34	3437.00	107.60 ± 5.40
S16	224.30	3.00 ± 0.14	1951.40	61.10 ± 3.10
S17	64371.24	795.00 ± 40.00	673.00	21.10 ± 1.10
S18	42349.00	523.01 ± 26.20	1121.24	35.20 ±1.80
S19	14835.03	183.21 ± 9.20	2848.40	89.20 ±4.50
S20	61113.10	754.80 ± 38.00	1629.31	51.00 ± 2.60

Sample	HPGe	
	^{238}U (Bq/kg)	^{40}K (Bq/kg)
S4	13.04 ± 0.35	23.00 ± 2.00
S5	3.10 ±0.13	25.22 ± 2.00
S6	4.90 ± 0.17	21.00 ± 1.40
S14	35.30 ± 0.70	43.00 ±3.00
S15	5.70 ± 0.19	78.00 ± 4.30
S16	2.42 ± 0.12	43.30 ±3.00
S17	217.20 ± 3.42	150.40 ± 8.00
S18	147.24 ± 2.40	199.80 ± 10.40
S19	130.90 ± 2.20	454.80 ± 23.12
S20	239.30 ± 4.00	216.00 ± 11.20

Chapter 6

Conclusion and Future Work

6.1 Conclusion

For this study, 20 soil samples were collected from Yapala, located in the Mayo-Dallah in Southern area of Chad in Central Africa. All samples were analyzed using Hyper pure germanium (HPGe) gamma ray detector to identify and quantify radionuclides present in each sample. The concentrations of ^{238}U, ^{232}Th and ^{40}K for sample S1 to S16 ranged between 2.4-35.3, 2.2-16.5, and 20.3-281.8 Bq/kg while S17 to S20 ranged between 130.9-239.3, 14.4-39.8 and 150.4-454.8, respectively. This study revealed that the average activity concentration of ^{238}U for sample S17 to S20 in Mayo-Dallah region is relatively higher than the world average value, while ^{232}Th and ^{40}K are lower. The lowest contributor for the activity concentration of ^{238}U, ^{232}Th and ^{40}K were found in sample S1 to S16. These results show that the activity concentrations of radionuclides (^{214}Bi and ^{214}Pb) are on average lower than radionuclides (^{226}Ra and ^{234m}Pa), which were produced as daughter nuclides prior to the transformation to ^{222}Rn (gas) decay. This means that the assumption of secular equilibrium could not be attained, mainly due to

possible radon-gas leaks in the sealed samples. The measured activity concentration of ^{235}U ranged from 0.8-21.7 Bq/kg while ^{137}Cs ranged between 0.3-3.8 Bq/kg. A good correlation were also observed between ^{40}K vs ^{238}U and ^{238}U vs ^{232}Th activity concentration while poor correlation was observed in ^{40}K vs ^{232}Th.

The radium equivalent activity average value is 111 Bq/kg, and the average external hazard indices, internal hazard indices and annual effective dose equivalent (AEDE) are 0.30, 0.54 and 0.41 (mSv/y) were less than the acceptable limit of unity indicating that the associated gamma radiation level was low, while the excess lifetime cancer risk (ELCR) average is 1.42 $\times 10^{-3}$ which is higher than the recommended value. The main contributor to this dose is from sample S17 to S20, it is therefore recommended not to use soil samples S17 to S20 as building materials.

Ten samples were selected from the Twenty samples collected from Chad for further heavy elemental analysis using Inductively Coupled Plasma-Mass Spectrometry (ICP-MS). The average concentration values in samples are as follows: Cu 38 (within the range 3-225 mg/kg); Mo 3 (within the range 0-15 mg/kg); Co 8 (within the range 1-35 mg/kg); Sn 2 (within the range 0-9 mg/kg); As 3 (within the range 2-6 mg/kg); U 19 (within the range 0-64 mg/kg); Pb 17 (within the range 4-59 mg/kg); Cd 0 (within the range 0-2 mg/kg) and Hg 2 (within the range 0-6 mg/kg), respectively. These results were also compared with Maximum Allowable Limits. Cu, Mo and Hg in some samples were found to be relatively higher in this study while other elements are lower than the Maximum Allowable limit. However, Uranium and Potassium were found with ICP-MS which were

later compared with the one found with HPGe detector and these show a strong correlation of $R^2 = 0.93$ for uranium and a poor correlation of $R^2 = 0.17$ for potassium.

GEANT4 and FLUKA Monte Carlo codes serve as a tool for producing data sets which were used for coincidence summing and efficiency calibration of HPGe detector. Simulation codes accuracy depend on how the detector geometry is modelled. Measurement were done with ^{152}Eu, ^{60}Co, ^{137}Cs, ^{22}Na and ^{40}K standard reference source for efficiency calibration while ^{60}Co and ^{22}Na were used for the coincidence summing. The comparison between the experimental and the simulated spectra provides good agreements. Therefore, it is possible to assume that the simulated spectrum with GEANT4 and FLUKA Monte Carlo codes can be used with calibrating the detector for analysis. The peak efficiency comparison also presented a good agreement between experimental and simulated results with the obtained ratio within 97% confidence.

In addition, an EFFTRAN has been evaluated as a tool for producing data sets which can be used for coincidence summing correction factor of HPGe detector. The accuracy of the EFFTRAN software is heavily dependent on the detector geometry. These results show that there were no statistically significant differences between the correction factor value for the energy range analysed.

6.2 Future Work

Additional regulations are required to enforce and implement corrective measures to mitigate against radiological pollution of the environment. Studies should be

expanded to include radiological assessment of grass/vegetation species for the region and possible transfer mechanism to man-kind. Moreover, further studies on residential area to include building materials (similar to [Pen18]), structures, drinking water quality, etc. is highly recommended. A possible field survey for the area can also be done in order to determine an extensive radiological map of the region which might assist decision making bodies with the implementation of appropriate regulations and policies, as well as identifications of the potentially health risk hotspots.

Appendices

Appendix A

Gamma-ray Transitions and Data Analysis

Table A.1: The gamma-ray transitions used for activity concentration

Uranium series		
Nuclide	Energy (keV)	Decay Probability
^{226}Ra	186.10	0.062
^{214}Pb	295.21	0.184
	351.92	0.358
^{214}Bi	609.31	0.448
	768.36	0.048
	934.06	0.030
	1120.29	0.148
	1238.11	0.059
	1377.67	0.039
	1729.60	0.029
	1764.49	0.154
	2204.21	0.049
^{234}Pa	1001.03	0.008

Table A.1 -continued from previous page		
Thorium series		
Nuclide	Energy (keV)	Decay Probability
^{212}Bi	727.20	0.065
^{228}Ac	338.32	0.113
	794.95	0.043
	911.27	0.266
	968.97	0.162
^{208}Tl	583.19	0.304
	860.56	0.045
	2614.53	0.357
Nuclide	Energy (keV)	Decay Probability
^{40}K	1460.83	0.107
^{235}U	143.80	0.109
^{137}Cs	661.66	0.850

Table A.2: Activity concentration results for sample S1 to S10

Activity concentration (Bq/kg)											
Nuclide	Energy	S1	S2	S3	S4	S5	S6	S7	S8	S9	S10
^{226}Ra	186.10	24.55 ± 1.65	32.97 ± 2.25	25.87 ± 1.74	35.67 ± 2.33	21.81 ± 1.50	23.94 ± 1.63	28.88 ± 1.89	32.21 ± 2.22	28.63 ± 1.94	33.38 ± 2.21
^{214}Pb	295.21	3.79 ± 0.47	11.23 ± 0.78	8.86 ± 0.63	17.68 ± 1.14	10.47 ± 0.73	4.73 ± 0.44	7.98 ± 0.62	6.28 ± 0.67	5.21 ± 0.55	8.14 ± 0.64
	351.92	5.88 ± 0.38	10.56 ± 0.62	7.55 ± 0.45	13.77 ± 0.80	2.83 ± 0.23	5.11 ± 0.33	6.30 ± 0.42	6.32 ± 0.44	5.76 ± 0.39	8.25 ± 0.51
^{214}Bi	609.31	5.22 ± 0.33	9.04 ± 0.52	6.93 ± 0.41	12.14 ± 0.68	3.02 ± 0.23	4.58 ± 0.30	5.64 ± 0.45	5.82 ± 0.40	4.98 ± 0.34	7.18 ± 0.46
	768.36	11.91 ± 1.89	11.99 ± 1.93	5.91 ± 1.37	15.66 ± 2.20	5.08 ± 1.41	7.83 ± 1.65	6.41 ± 1.42	6.03 ± 1.98	6.70 ± 1.52	8.87 ± 1.69
	934.06	1.60 ± 2.30	3.43 ± 14.93	6.37 ± 2.68	6.29 ± 2.02	0.22 ± 0.74	5.99 ± 1.94	0.68 ± 2.76	1.32 ± 1.73	0.83 ± 1.87	0.69 ± 3.63
	1120.29	3.41 ± 0.46	8.62 ± 0.78	5.18 ± 0.54	11.12 ± 0.89	1.79 ± 0.37	3.69 ± 0.48	5.92 ± 0.62	3.27 ± 0.61	4.81 ± 0.55	7.95 ± 0.85
	1238.11	5.64 ± 0.98	8.09 ± 1.88	7.18 ± 1.27	11.08 ± 1.55	1.89 ± 0.97	3.54 ± 1.01	7.97 ± 1.65	8.14 ± 1.68	9.40 ± 1.68	8.44 ± 2.21
	1377.67	2.57 ± 1.18	11.06 ± 2.08	8.11 ± 1.69	14.33 ± 2.40	1.83 ± 1.21	4.54 ± 1.59	11.62 ± 2.44	3.33 ± 1.93	2.32 ± 1.03	7.55 ± 1.73
	1729.60	7.96 ± 7.23	8.39 ± 2.13	8.25 ± 2.47	11.86 ± 2.33	2.79 ± 1.87	6.88 ± 2.02	6.19 ± 1.82	5.71 ± 2.48	6.27 ± 3.00	7.72 ± 1.94
	1764.49	5.35 ± 0.54	8.68 ± 0.74	1.49 ± 0.52	12.83 ± 0.95	3.16 ± 0.42	5.18 ± 0.52	6.73 ± 0.70	5.73 ± 0.67	3.98 ± 0.51	8.18 ± 0.74
	2204.21	5.25 ± 1.27	9.15 ± 1.50	5.85 ± 1.08	12.02 ± 1.83	1.25 ± 0.95	4.85 ± 1.15	6.52 ± 1.27	7.02 ± 1.49	5.53 ± 1.30	6.59 ± 1.35
^{234m}Pa	1001.03	21.12 ± 5.06	33.05 ± 7.72	40.52 ± 7.83	60.60 ± 13.51	29.70 ± 6.75	39.12 ± 7.04	40.45 ± 8.27	63.08 ± 11.02	40.47 ± 9.49	40.38 ± 9.35
^{212}Bi	727.20	7.48 ± 1.09	13.59 ± 1.42	6.88 ± 1.10	15.93 ± 1.55	1.62 ± 1.03	5.14 ± 0.88	8.01 ± 1.10	5.31 ± 1.20	4.49 ± 0.94	7.17 ± 1.36
^{228}Ac	338.32	7.31 ± 0.69	14.33 ± 1.21	8.96 ± 0.80	18.90 ± 1.56	2.84 ± 1.01	5.20 ± 0.59	5.63 ± 0.78	7.75 ± 0.95	6.74 ± 0.76	9.36 ± 0.87
	794.95	0.16 ± 0.66	7.50 ± 1.57	1.85 ± 1.12	8.09 ± 1.49	0.11 ± 1.35	3.37 ± 1.14	2.19 ± 1.28	3.13 ± 1.54	1.16 ± 1.25	2.32 ± 1.16
	911.21	6.74 ± 0.47	13.85 ± 0.83	7.70 ± 0.52	17.37 ± 1.01	1.88 ± 0.24	5.55 ± 0.42	7.28 ± 0.51	6.95 ± 0.57	6.81 ± 0.50	8.42 ± 0.59
	968.97	8.40 ± 0.74	17.91 ± 1.18	10.66 ± 0.83	23.91 ± 1.45	3.58 ± 0.48	8.06 ± 0.67	10.13 ± 0.80	9.66 ± 0.94	8.19 ± 0.77	10.82 ± 0.90
^{208}Tl	583.19	6.13 ± 0.41	13.06 ± 0.76	7.20 ± 0.46	16.34 ± 0.93	1.46 ± 0.20	5.50 ± 0.38	7.83 ± 0.51	6.47 ± 0.50	5.72 ± 0.42	7.66 ± 0.53
	860.56	4.53 ± 1.26	13.70 ± 1.80	7.38 ± 1.34	14.10 ± 2.09	2.50 ± 0.87	3.97 ± 1.22	4.20 ± 1.54	6.62 ± 1.68	2.99 ± 1.70	5.57 ± 1.46
	2614.53	7.37 ± 0.50	12.88 ± 0.80	8.08 ± 0.54	15.58 ± 0.93	4.24 ± 0.36	7.30 ± 0.50	7.85 ± 0.55	8.46 ± 0.62	7.74 ± 0.55	9.73 ± 0.66
^{212}Pb	238.60	9.99 ± 0.55	21.16 ± 1.11	12.54 ± 0.67	27.65 ± 1.43	3.42 ± 0.25	9.33 ± 0.52	12.32 ± 0.66	11.64 ± 0.66	10.06 ± 0.57	13.40 ± 0.73
^{40}K	1460.83	22.25 ± 1.48	87.25 ± 4.75	20.27 ± 1.36	22.71 ± 1.56	25.22 ± 1.63	20.61 ± 1.38	58.91 ± 3.51	49.26 ± 2.98	62.35 ± 3.54	178.79 ± 9.46
^{235}U	143.80	2.11 ± 0.56	2.05 ± 0.70	2.95 ± 0.58	2.50 ± 0.58	0.92 ± 0.29	2.54 ± 0.48	0.93 ± 0.41	1.45 ± 0.44	2.97 ± 0.84	3.04 ± 0.71
^{137}Cs	661.66	0.34 ± 0.10	0.72 ± 0.12	0.45 ± 0.08	0.19 ± 0.12	0.04 ± 0.09	0.61 ± 0.17	1.22 ± 0.13	1.69 ± 0.15	1.33 ± 0.13	0.45 ± 0.20

Table A.3: Activity concentration results for sample S11 to S20

		Activity concentration (Bq/kg)									
Nuclide	Energy	S11	S12	S13	S14	S15	S16	S17	S18	S19	S20
^{226}Ra	186.10	34.20 ± 2.23	28.91 ± 1.97	32.53 ± 2.11	78.93 ± 4.30	26.83 ± 1.75	25.83 ± 1.70	354.53 ± 18.11	252.45 ± 12.99	220.46 ± 11.39	417.85 ± 21.22
^{214}Pb	295.21	7.10 ± 0.62	6.01 ± 0.54	5.28 ± 0.52	40.26 ± 2.13	5.67 ± 0.47	2.16 ± 0.35	260.65 ± 13.14	176.28 ± 8.92	164.73 ± 8.35	293.97 ± 14.80
	351.92	7.17 ± 0.46	6.72 ± 0.43	5.85 ± 0.39	41.94 ± 2.15	6.44 ± 0.40	2.23 ± 0.22	258.05 ± 12.96	166.61 ± 8.39	152.27 ± 7.68	279.28 ± 14.02
^{214}Bi	609.31	6.58 ± 0.43	6.27 ± 0.40	5.44 ± 0.36	34.86 ± 1.80	5.49 ± 0.35	2.36 ± 0.20	206.99 ± 10.40	142.25 ± 7.17	126.65 ± 6.39	237.68 ± 11.94
	768.36	7.91 ± 2.04	11.57 ± 2.58	5.71 ± 1.40	41.96 ± 2.95	9.29 ± 1.63	2.68 ± 0.98	220.56 ± 11.89	150.18 ± 8.35	132.67 ± 7.70	164.68 ± 30.70
	934.06	0.16 ± 3.73	7.80 ± 2.85	3.86 ± 2.51	21.50 ± 2.73	2.25 ± 2.36	0.00 ± 0.85	213.37 ± 12.24	130.70 ± 8.32	102.52 ± 7.07	204.12 ± 11.84
	1120.29	6.03 ± 0.77	4.30 ± 0.63	5.28 ± 0.71	30.21 ± 1.78	5.38 ± 0.59	2.22 ± 0.48	183.37 ± 9.42	133.76 ± 6.95	114.68 ± 6.02	217.87 ± 11.14
	1238.11	2.51 ± 1.31	8.59 ± 2.61	11.46 ± 2.02	30.90 ± 2.33	3.15 ± 1.12	1.56 ± 0.90	191.37 ± 10.33	127.84 ± 7.22	132.38 ± 7.60	211.62 ± 11.37
	1377.67	1.71 ± 1.42	3.80 ± 1.45	4.20 ± 1.65	33.56 ± 2.90	0.09 ± 0.89	1.81 ± 1.25	225.39 ± 12.52	144.92 ± 8.55	125.57 ± 7.63	246.68 ± 13.62
	1729.60	6.40 ± 2.22	9.35 ± 2.68	6.48 ± 2.70	37.40 ± 3.47	3.78 ± 1.39	8.45 ± 5.52	224.33 ± 12.91	160.73 ± 9.77	143.78 ± 9.01	258.68 ± 14.66
	1764.49	6.33 ± 0.67	6.87 ± 0.68	5.40 ± 0.61	32.67 ± 1.92	6.22 ± 0.61	2.90 ± 0.42	202.67 ± 10.41	141.92 ± 7.38	123.32 ± 6.47	227.74 ± 11.66
	2204.21	11.28 ± 1.79	5.32 ± 1.37	6.49 ± 1.40	32.28 ± 2.57	5.12 ± 1.06	3.43 ± 1.08	198.72 ± 10.96	128.31 ± 7.46	112.14 ± 6.83	214.85 ± 11.74
^{234m}Pa	1001.03	44.20 ± 9.76	22.87 ± 6.80	46.11 ± 10.49	51.87 ± 9.29	44.01 ± 8.06	31.70 ± 7.90	408.77 ± 27.68	226.77 ± 19.38	167.62 ± 18.19	329.35 ± 24.45
^{212}Bi	727.20	6.82 ± 1.36	6.98 ± 1.27	6.59 ± 1.14	2.00 ± 0.70	0.14 ± 0.51	1.60 ± 0.54	37.68 ± 2.91	21.03 ± 2.06	11.24 ± 2.11	18.83 ± 2.29
^{228}Ac	338.32	7.97 ± 0.93	8.40 ± 0.91	7.97 ± 0.82	31.39 ± 1.82	4.72 ± 0.67	0.89 ± 0.59	40.83 ± 2.56	6.01 ± 1.18	9.03 ± 1.27	14.03 ± 2.48
	794.95	7.56 ± 1.86	9.11 ± 4.64	2.37 ± 1.54	8.32 ± 1.44	0.23 ± 0.93	1.07 ± 0.71	31.96 ± 6.87	9.68 ± 2.32	8.65 ± 3.18	13.63 ± 2.86
	911.21	7.37 ± 0.56	6.45 ± 0.51	6.73 ± 0.50	3.27 ± 0.34	3.82 ± 0.34	1.91 ± 0.26	46.77 ± 2.49	16.69 ± 1.04	15.76 ± 1.01	23.85 ± 1.38
	968.97	7.95 ± 0.79	9.75 ± 0.94	8.87 ± 0.83	3.87 ± 0.59	4.89 ± 0.56	2.94 ± 0.56	64.85 ± 3.55	25.24 ± 1.66	22.05 ± 1.56	34.24 ± 2.13
^{208}Tl	583.19	6.26 ± 0.47	6.04 ± 0.44	6.31 ± 0.44	2.61 ± 0.30	3.71 ± 0.30	1.73 ± 0.22	38.40 ± 2.04	15.95 ± 0.94	14.32 ± 0.88	20.56 ± 1.19
	860.56	3.36 ± 1.99	3.63 ± 1.55	3.00 ± 1.40	0.13 ± 0.78	3.80 ± 1.18	3.92 ± 1.65	31.35 ± 3.41	10.01 ± 2.83	12.43 ± 2.99	9.52 ± 2.61
	2614.53	7.99 ± 0.56	8.15 ± 0.56	7.53 ± 0.54	5.02 ± 0.40	5.82 ± 0.43	3.80 ± 0.34	33.23 ± 1.81	16.22 ± 0.96	14.20 ± 0.87	18.78 ± 1.09
^{212}Pb	238.60	11.84 ± 0.65	10.09 ± 0.57	10.53 ± 0.58	11.28 ± 0.63	6.76 ± 0.39	3.13 ± 0.22	105.31 ± 5.31	57.49 ± 2.95	50.14 ± 2.56	81.38 ± 4.12
^{40}K	1460.83	281.79 ± 14.50	268.60 ± 13.82	155.51 ± 8.18	42.63 ± 2.53	77.94 ± 4.26	43.28 ± 2.53	150.35 ± 7.93	199.75 ± 10.37	454.76 ± 23.12	215.74 ± 11.20
^{235}U	143.80	1.86 ± 0.73	0.80 ± 0.34	1.92 ± 0.54	3.48 ± 0.59	1.14 ± 0.42	1.76 ± 0.58	16.27 ± 1.62	12.56 ± 1.38	7.82 ± 1.06	21.67 ± 1.94
^{137}Cs	661.66	0.03 ± 0.06	0.07 ± 0.08	0.19 ± 0.19	0.46 ± 0.09	0.05 ± 0.07	0.26 ± 0.10	2.43 ± 0.20	1.56 ± 0.15	1.82 ± 0.19	3.83 ± 0.27

Appendix B

Elemental Analysis Data

Table B.1: Elemental concentrations

Major Elements (mg/kg)												
	LOD	S4	S5	S6	S14	S15	S16	S17	S18	S19	S20	Sample average
Ca	50.00	275	375	964	1236	43739	1699	7900	3701	12476	8112	8048
Fe	5.00	14951	36773	3053	16379	75993	16880	22820	15912	17510	19684	23996
Al	15.00	40138	7920	4204	8602	34400	8967	10289	7619	12668	11047	14586
K	50.00	827	911	381	1775	3437	1951	673	1124	2848	1629	1556
Mg	50.00	429	304	175	713	22573	851	2085	1154	2472	3752	3451
Na	50.00	BDL	BDL	BDL	BDL	2405	BDL	196	254	121	502	348
P	50.00	124	58	136	110	2456	112	550	165	1281	326	532
Si	50.00	5959	6659	5169	4652	4603	6252	5890	6542	6032	6051	5781
Essential Elements (mg/kg)												
Zn	0.35	13	16	13	20	97	15	276	116	87	126	79

Table B.1 -continued from previous page												
Essential Elements (mg/kg)												
	LOD	S4	S5	S6	S14	S15	S16	S17	S18	S19	S20	Sample average
Cr	0.05	26	15	13	14	17	16	3	13	11	5	13
Ni	0.04	14	5	2	5	31	5	90	3	6	7	17
Mn	0.05	130	1966	113	590	1218	491	260	264	691	362	609
Ba	0.01	31	502	28	161	89	123	32	31	65	42	110
Sr	0.01	12	6	10	11	217	14	30	21	72	35	77
B	1.35	6	4	BDL	2	BDL	BDL	BDL	BDL	16	2	3
Cu	0.35	8	35	3	32	25	29	225	7	8	12	38
Mo	0.01	0.47	1.15	0.15	1.69	15.50	3.00	5.60	1.32	0.96	0.75	2.50
V	0.01	33	83	9	33	115	34	16	12	28	23	39
Co	0.004	4	17	1	6	35	7	2	2	5	5	8
Se	0.01	0.31	0.07	0.06	0.10	0.13	0.18	0.04	0.08	0.44	0.04	0.15

Table B.2: Elemental concentrations

Potential Toxic Trace Elements (mg/kg)												
	LOD	S4	S5	S6	S14	S15	S16	S17	S18	S19	S20	Sample average
Cu	0.35	8	35	3	32	25	29	225	7	8	12	38
Mo	0.01	0.47	1.15	0.15	1.69	15.50	3.00	5.60	1.32	0.96	0.75	2.50
Co	0.003	4	17	1	6	35	7	2	2	5	5	8
Sb	0.001	BDL	0.60	BDL	0.24	0.08	0.23	0.08	0.17	1.01	0.02	0.24
Se	0.01	0.31	0.07	0.06	0.10	0.13	0.18	0.04	0.08	0.44	0.04	0.15
Sn	0.01	1.29	0.35	0.29	0.46	3.95	0.35	8.89	3.73	2.09	4.32	2.77
As	0.01	1.74	6.09	0.41	5.22	4.15	4.07	3.95	3.87	1.61	2.15	3.33
U	0.0002	0.76	0.57	0.19	6.10	0.55	0.22	64.37	42.35	14.84	61.11	19.03
Toxic Trace Elements (mg/kg)												
Pb	0.01	11	19	4	21	6	59	17	12	7	11	17
Cd	0.001	0.004	0.025	0.009	0.026	0.116	0.027	0.415	0.096	1.896	0.253	0.286
Hg	0.003	0.069	4.886	0.070	5.572	0.671	3.483	0.687	0.747	0.477	0.796	1.746

Figure B.1: Bar charts of elemental concentration for major elements.

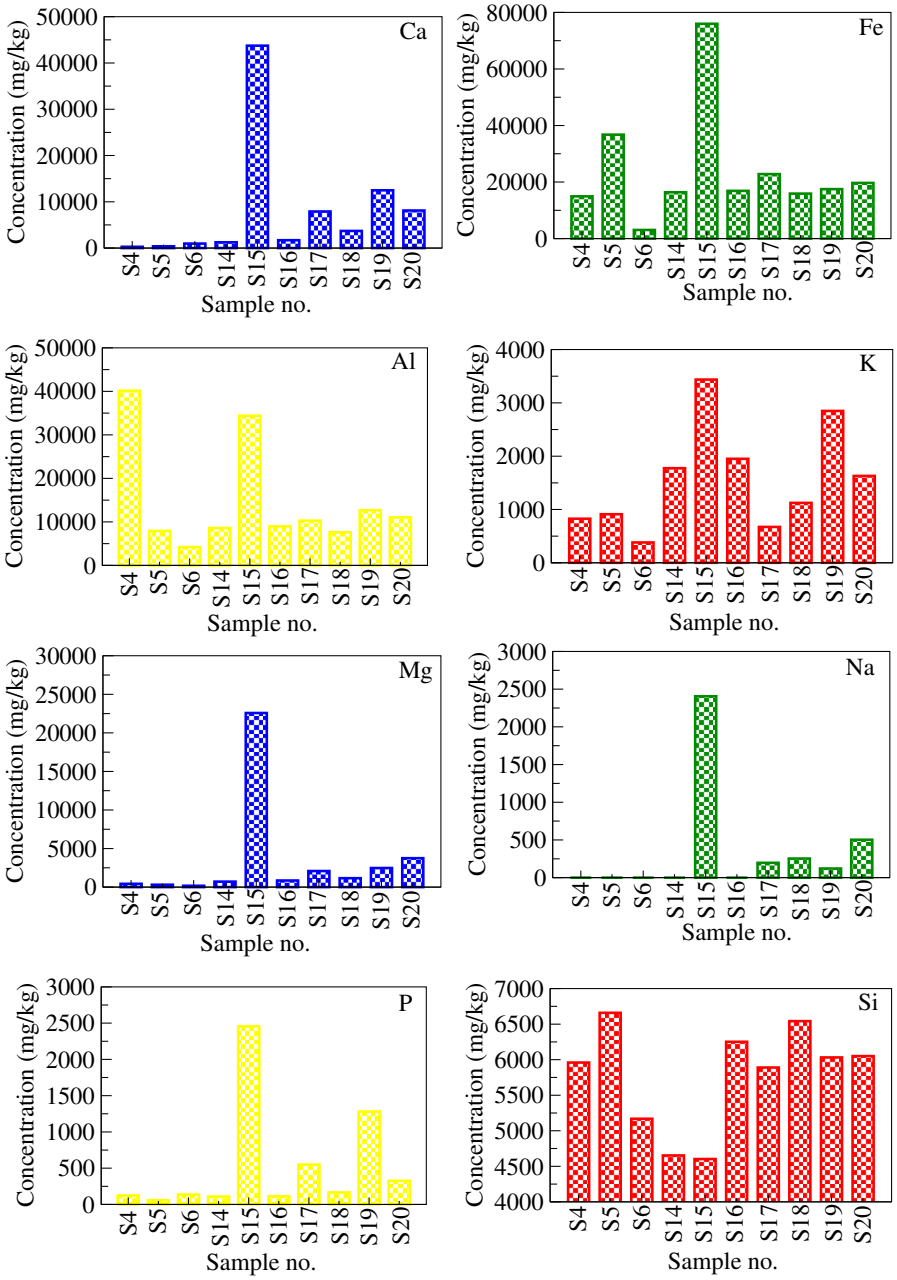

Figure B.2: Bar charts of elemental concentration for Essential trace elements.

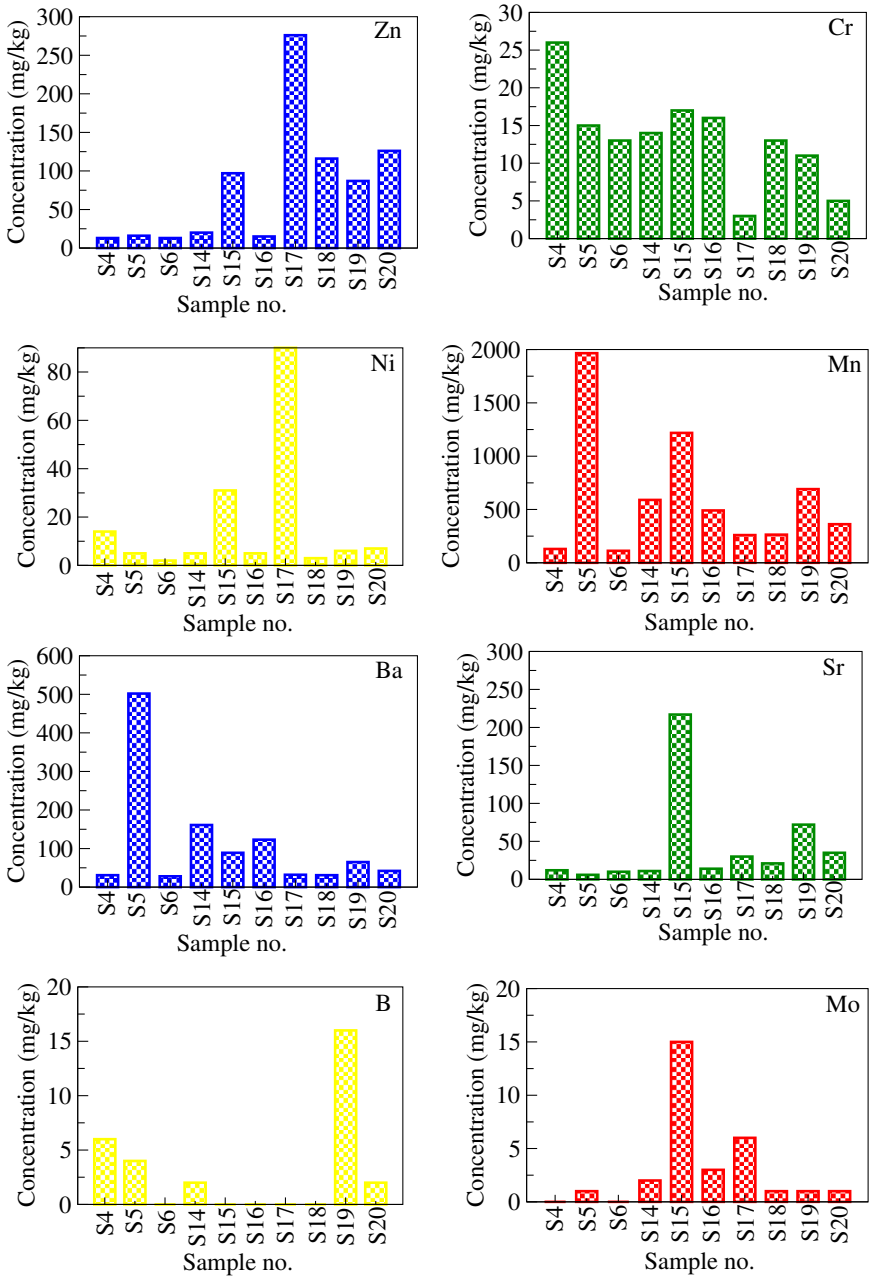

Bibliography

[Aga11] C. Agarwal, S. Chaudhury, A. Goswami, and M. Gathibandhe. *True coincidence summing corrections in point and extended sources*. Journal of Radioanalytical and Nuclear Chemistry, co-published with Springer Science + Business Media BV, 773-780, 2011.

[Ago03] S. Agostinelli, J. Allison, K. al Amako, J. Apostolakis, H. Araujo, P. Arce, M. Asai, D. Axen, S. Banerjee, G. Barrand and others. *GEANT4 simulation toolkit*. Nuclear instruments and methods in physics research section A: Accelerators, Spectrometers, Detectors and Associated Equipment, 250-303, 2003.

[Ahm14] N. Ahmad, M. S. Jaafar, M. Bakhash, M. Rahim. *An overview on measurements of natural radioactivity in Malaysia*. Journal of Radiation Research and Applied Sciences, 136-141, 2015.

[Aja20] M. B. Ajani, P. P. Maleka, I. T. Usman, S. Penabei. *Assessment of environmental radiation exposure from soil radioactivity around the Southern area of Chad*. Radiation Protection and Environment, 0972-0464, 2020.

[Aja09] O. S.Ajayi. *Measurement of activity concentrations of* ^{40}K, ^{226}Ra *and* ^{232}Th *for assessment of radiation hazards from soils of the southwestern region of*

Nigeria. Radiation and Environmental Biophysics, Springer, 323-332, 2009.

[Ala14] D. Al-Azmi. *Gamma Dose Rate Measurements in Kuwait Using a Car-Borne GPS Integrated Dosimetric System*. World Journal of Nuclear Science and Technology, Scientific Research, 7, 2014.

[Ali08] F. A. Ali *Measurements of Naturally Occurring Radioactive Materials (NORM) in Environmental Samples*. University of Surrey, 2008.

[Alm12] B.A. Almayahi, A.A. Tajuddin and M.S. Jaafar. *Radiation hazard indices of soil and water samples in Northern Malaysian Peninsula*. Applied Radiation and Isotopes, 2652-2660, 2012.

[Alv38] L. W. Alvarez. *The capture of orbital electrons by nuclei*. Physical Review, 486, 1938.

[Ama05] K. Amako, S. Guatelli, V. N. Ivanchencko,M. Maire, B. Mascialino, K. Murakami, P. Nieminen, L. Pandola, S. Parlati, M. G Pia, and others. *Comparison of Geant4 electromagnetic physics models against the NIST reference data*. IEEE Transactions on Nuclear Science, 910-918, 2005.

[Arn04] D. Arnold and O. Sima. *Application of GESPECOR software for the calculation of coincidence summing effects in special cases*. Applied Radiation and Isotopes, 167-172, 2004.

[Baj15] A.D. Bajoga, N. Alazemi, P.H. Regan, and D.A. Bradley. *Radioactive investigation of NORM samples from Southern Kuwait soil using high-resolution gamma-ray spectroscopy*. Radiation Physics and Chemistry, 305-311, 2015.

[Bas19] Bash(4.2.42).*Free Software Foundation*, Unix shell program. Accesses [18.11.19]. https://www. fsf.org.

[Bat10] H. Bateman. *The solution of a system of differential equations occurring in the theory of radio-active transformations*. Proc. Cambridge Phil. Soc., 423-427, 1910.

[Bei81] A. Beiser. *Concepts of Modern Physics*. McGraw-Hill, 9780070044739, 1981.

[Bos08] J. Boson, G. Gren and L. Johansson. *A detailed investigation of HPGe detector response for improved Monte Carlo efficiency calculations*. Nuclear Instruments and Methods in Physics Research Section A: Accelerators, Spectrometers, Detectors and Associated Equipment, 304-314, 2008.

[But72] D.K. Butt and A.R. Wilson. *A study of the radioactive decay law.*Journal of Physics A: General Physics, IOP Publishing, 1248, 1972.

[Cet06] J. Cetnar. *General solution of Bateman equations for nuclear transmutations*. Annals of Nuclear Energy, 640-645, 2006.

[Cem08] H. Cember and T. E. Johnson. *Introduction to Health Physics*. Medical Physics, 5959, 2008.

[Chi14] T. M. Chiroma, R. O. Ebewele, F.K. Hymore. *Comparative Assessement Of Heavy Metal Levels In Soil, Vegetables And Urban Grey Waste Water Used For Irrigation In Yola And Kano*. International Refereed Journal of Engineering and Science (IRJES), ISSN (Online) 2319-183X, 2014.

[Cho12] Qi, Chong and Liotta, RJ and Wyss, Ramon. *Generalization of the Geiger-Nuttall law and alpha clustering in heavy nuclei*, Journal of Physics: Conference Series, 012-131, 2012.

[Cho14] Qi, Chong and Andreyev, AN and Huyse, Mark and Liotta, Roberto J and Van Duppen, Piet and Wyss, Ramon. *On the validity of the Geiger–Nuttall alpha-decay law and its microscopic basis*. Physics Letters B, 203-206, 2014.

[Col12] Collaboration, Geant. *Geant4 User's Guide for Application Developers*. Accessible from the GEANT4 web page [1] Version geant4, 2012. http://ftp.uni-frankfurt.de/gentoo/distfiles/BookForAppliDev-4.9.6.pdf

[Cro70] C.E. Crouthamel, F. Adams, R. Dams. *Applied gamma-ray spectrometry*. Pergamon press, 1970.

[Cut83] N. H. Cutshall, I. L. Larsen and C. R. Olsen. *Direct analysis of 210Pb in sediment samples: self-absorption corrections*. Nuclear Instruments and Methods in Physics Research, 309-312, 1983.

[Dam95] R. F. J. Dams, J. Goossens and L. Moens *Spectra and non spectral interferences in inductively coupled plasma-mass spectrometry*. Mikrochim, Acta , 119-277, 1995.

[DEA10] Department of Environmental Affairs *The Framework for the Management of Contaminated Land, South Africa*, 2010. Assessed [20.07.2020]. http://sawic.environment.gov.za/documents/562.pdf.

[Deb88] K. Debertin and R. G. Helmer. *Gamma-and X-ray spectrometry with semiconductor detectors*. 1988.

[Eis97] M. Eisenbud and T. F. Gesell. *Environmental Rasioactivity from Natural, Industrial & Military Sources*. Califonia , USA: Accademic Press, Fourth ed. 1997.

[Elk08] S. U. El-Kameesy, S. ABD El-Ghany, S. M. El-Minyawi, Z. Miligy and E. M. El-Mabrouk. *Natural radioactivity of beach sand samples in the Tripoli Region, Northwest Libya*. The Scientific and Technological Research Council of Turkey, 245-251, 2008.

[Elm04] M.H. El Mamoney, A.E.M. Khater. *Environmental characterization and radio-ecological impacts of non-nuclear industries on the Red Sea coast*. Journal of Environmental Radioactivity, 151-168, 2004.

[Elr06] H. I. El-Reefy, T. Sharshar, R. Zaghloul and H. M. Badran. *Distribution of gamma-ray emitting radionuclides in the environment of Burullus Lake: I. Soils and vegetations*. Journal of Environmental Radioactivity, 148-169, 2006.

[Ens20] ENSDF. *Evaluated Nuclear Structure Data File*. Assessed [15.02.2020]. https://www.nndc.bnl.gov/

[Eur19] European nuclear society. *decay chains, natural*. Technical Reports Series. Assessed [15.12.2019]. http://www.euronuclear.org/info/encyclopedia/decaybasinnatural.htm.

[Fer00] C. Ferguson.*General Purpose Source Particle Module for GEANT4/SPARSET: User Requirement Document*. Uos-rep-07. reat. space. qinetiq, 2000.

[Fer05] A. Ferrari, P. R. Sala, A. Fasso, J. Ranft. *Fluka: a multi-particle transport code*. CERN European Organisation for Nuclear Research, 2005.

[Fir96] R.B. Firestone , S.Y.F. Chu , C.M. Baglin and J. Zipkin *Table of Isotopes*. Ed. Shirley V.S, John Wiley & Sons, 1996.

[Fuj04] R. Fujiyoshi and S. Sawamura. *Mesoscale variability of vertical profiles of environmental radionuclides (40K, 226Ra, 210Pb and 137Cs) in temperate forest soils in Germany*. Science of the Total Environment, 177-188, 2004.

[Gen95] M. Genet. *The Discovery of Uranic Rays: A Short Step for Henri Becquerel but a Giant Step for Science*. Radiochimica Acta, 3-12, 1995.

[Ger] Germanium Detectors. *User's Manual*. Canberra Industries, 9231358B.

[Gil08] G.R.Gilmore. *Practical Gamma-ray Spectroscopy*. Wiley, ISBN: 978-0-470-86196-7, 2008.

[Has19] A. Hastings, J. r. Smith, and L. Marcia. *Gamma-Ray Detectors*. Accessed [15.08.19]. https://fas.org/sgp/othergov/doe/lanl/docs1/00326398.pdf

[Hen02] P. H. G. M Hendriks, M. Maucee, R. J. de Meijer. *MCNP modelling of scintillation-detector gamma-ray spectra from natural radionuclides*. Applied Radiation and Isotopes, 449-457, 2002.

[Hus17] H. Husain and L. Sakhnini. *Radiological impact of NORM generated by oil and gas industries in the kingdom of Bahrain*. Journal of environmental radioactivity, 127-133, 2017.

[IAEA03] International Atomic Energy Agency (IAEA).*Extent of Environmental Contamination by Naturally Occurring Radioactive Material (NORM) and Technological Options for Mitigation*. Technical Reports Series No. 419. International Atomic Energy Agency, Vienna, 2003.

[IAEA20] International Atomic Energy Agency. *The Environmental Behaviour of Radium: Revised Edition*. Accessed [29.04.20]. http://www-pub.iaea.org/books/IAEABooks/10478/.

[ICRP91] International Commission on Radiological Protection (ICRP). *Recommendation of the international Commission on radiological protection*. Pergamon Press, Oxford, Annals of ICRP 2103, 1991.

[Ins19] Institut national de la statistique, des tudes conomiques et dmographiques (INSEED). *Deuxime recensement gnral de la population et de l habitat* . RGPH2. Accessed [29.10.2019]. http://www.ambtchad-altun.com.

[Jod06] P. Jodlowski. *Self-absorption correction in gamma-ray spectrometry of environmental samples-an overview of methods and correction values obtained for the selected geometries*. Nukleonika, 21-25, 2006.

[Jon19] G. Jonkers, F. A. Hartog, W. A. I. Knaepen and P. F. J. Lancee *Characterisation of NORM in the oil and gas production (E & P) industry. Proceedings of international symposium on radiological problems with Natural Radioactivity in the Non- Nuclear Industry*. Technical Reports Series, Amsterdam, the Netherlands, accesses [14.05.19].

[Kat98] R. L. Kathren. *NORM sources and their origins*. Wiley-Interscience, Applied radiation and isotopes, 149-168, 1998.

[Kab20] A. Kabata-Pendias. *Trace Elements in Soils and Plants (Fourth Edi)*. Taylor and Francis Group. Accessed [12.03.20]. https://doi.org/10.1201/b10158-25.

[Kha01] A. E. M. Khater, R. H. Higgya, M. Pimpl. *Radiological impacts of natural radioactivity in Abu-Tartor phosphate deposits, Egypt*. Journal of Environmental Radioactivity, 255-267, 2001.

[Kle82] A. W. Klement. *CRC Handbook of Environmental Radiation*. Florida: CRC Press, 1982.

[Kno99] G.F. Knoll. *Radiation Detection and Measurement*. Third edition, John Willey and Sons, Inc, 1999.

[Kor93] M. Korun and R. Martin. *Coincidence summing in gamma and X-ray spectrometry*. Nuclear Instruments and Methods in Physics Research Section A: Accelerators, Spectrometers, Detectors and Associated Equipment, 478-484, 1993.

[Kos03] J. Kosler and P. J. Sylvester. *Preset Trends and the Future of Zircon in Geochronology: Laser Ablation ICPMS*. Mineral Geochem, 243-275, 2003.

[Kri81] R. Krieger. *Radioactivity of construction materials*. Betonwerk Fertigteil Techn, 468, 1981.

[Kra88] K. S. Krane. *Introductory Nuclear Physics*. John Wiley and Sons, second edition, 1988.

[Kum03] A Kumar, M Kumar, B Singh, S Singh. *Natural activities of 238U, 232Th and 40K in some Indian building materials*. Radiation measurements, 465-469, 2003.

[Lab92] A. Lambrechts, L. Foulquier, and J. Garnier-Laplace. *Natural radioactivity in the aquatic components of the main French rivers*. Oxford University Press, 253-256, 1992.

[Lan13] S. Landsberger and Brabec, C and Canion, B and Hashem, J and Lu, C and Millsap, D and George, G. *Determination of ^{226}Ra, ^{228}Ra and ^{210}Pb in NORM products from oil and gas exploration: problems in activity underestimation due to the presence of metals and self-absorption of photons.*Journal of environmental radioactivity, 0265-931X, 23-26, 2013.

[Leo87] W. R. Leo. *Techniques for nuclear and particle physics experiments: a how-to approach*. Springer Science & Business Media, 1987.

[Lil01] J. S. Lilley. *Nuclear Physics: Principles and Applications*. pp. 412. ISBN 0-471-97935-X. Wiley-VCH, June 2001.

[Lot17] P. Lotfalinezhad, S. Kashian, M. S Kotahi1, A. A. Fathivan. *Estimation of natural radioactivity and radiation exposure in environmental soil samples of Golestan, Iran*. Iranian Journal of Medical Physics, 98-103, 2017.

[Mal14] F. Malik. *Natural radioactivity in sand samples collected along the bank of river Indus in the area spanning over Gilgit to Lowarian, Pakistan: assessment of its radiological hazards*. Journal of Radioanalytical and nuclear Chemistr, 373-379, 2014.

[Met56] N. Metropolis and H. A. Meyer. *Symposium on Monte Carlo Methods*. New York, John Wiley & Sons, 29-36, 1956.

[Mey56] Meyer, Herbert Albert and others. *Symposium on Monte Carlo Methods*. Wiley, 1956.

[Mil18] M. O. Miller. *The impact of coincidence summing corrections in the gamma-ray spectrometry analysis of uncontaminated surface soils*. SDRP Journal of Earth Science and Environmental Studies, 2472-6419, 2018.

[Muh10] M. A. Muhammad, I. F. Idris, P. M. Simon and S. A. Arabi. *Distribution of gamma-emitting radionuclides in soils around the centre for energy research and training (CERT) Ahmadu Bello University, Zaria, Zaria-Nigeria*. Journal of American Science, 995-1001, 2010.

[Nao97] P. Naomi. *Marie Curie and the Science of Radioactivity*. Oxford University Press: A perspective on Industrial Contributions. IAEA Bulletin #2.

[Ndl16] N.B. Ndlovu. *Elemental analysis of Mosses and Lichens from the Western Cape (South Africa) using INAA and ICP-MS*. A dissertation presented for the degree of Doctorate of Philosophy in Physics, Stellenbosch University, 2016.

[New08] R.T. Newman, R. Lindsay, K.P. Maphoto, N.A. Mlwilo, A.K. Mohanty,D.G. Roux,R.J. De Meijer and I.N. Hlatshwayo. *Determination of soil, sand and ore primordial radionuclide concentrations by full-spectrum analyses of high-purity germanium detector spectra*. Applied Radiation and Isotopes, 855-859, 2008.

[Oya20] B. Oyamta, D. Bayang, D. Mianyo. *tude sur les Ressources minires et ptrolires dans le Mayo Kebbi Ouest Tchad*. Accessed [06.01.20]. https://www. peacere-sources.net/les/docs/publications/Rapport_Etude_Ressource_ mines_MKO_25-06-2013.pdf.

[Pai13] R. Paira, B. Sahu. *New form of Geiger-Nuttall law in α -radioactivity*. DAE Symp. Nucl. Phys,214-215, 2013.

[Pel08] D.B. Pelowits. *MCNPX Users Manual*. Los Alamos National Laboratory, (2008).

[Pen18] S. Penabei, D. Bongue, P. Maleka, T. Dlamini, Sadou , C.J. Guembou Shouop , Y.I. Halawlaw, A. Ngwa Ebongue and M.G. Kwato Njock. *of natural radioactivity levels and the associated radiological hazards in some*

building materials from Mayo-Kebbi region, Chad. Radioprotection, 265-278, 2018.

[Pra13] J. Pradler. *On an unverified nuclear decay and its role in the DAMA experiment*. Physics Letter B, 399-404, (2013).

[Rad95] D. C. Radford. *Background subtraction from in-beam HPGe coincidence data sets*.Nuclear Instruments and Method A, 297-306, 1995.

[Rob09] E. Robu and C. Giovani *Gamma-ray self-attenuation corrections in environmental samples*.Romanian Reports in Physics, 295-300, 2009.

[Sha97] T. Sharshar, T. Elnimr, F. A. El-Husseiny and A. El-Abd. *Efficiency calibration of HPGe detectors for volume-source geometries*. Applied radiation and isotopes, 695-697, 1997.

[Sim92] O. Sima. *Photon attenuation for samples in Marinelli beaker geometry: an analytical computation*. Health physics, 445-449, 1992.

[Sim97] O. Sima and C. Dovlete. *Matrix effects in the activity measurement of environmental samplesimplementation of specific corrections in a gamma-ray spectrometry analysis program*. Applied Radiation and Isotopes, 59-69, 1997.

[Sim01] O. Sima and D. Arnold and C. Dovlete. *GESPECOR: a versatile tool in gamma-ray spectrometry*. Journal of Radioanalytical and Nuclear Chemistry, 359-364, 2001.

[Str76] E. Stranden. *Some aspects on radioactivity of building materials*. Physica Norvegica, 163-167, 1976.

[Tho98] A. Thompson and others. *Environmental Geology in Land Use Planning: A Guide to Good Practice*. Transport and the Regions, Symonds Travers Morgan, East Grinstead, 80, 1998.

[Tra20] B. Traci and M. Nicole. *Inductively Coupled Plasma*. Accessed [08.06.2020]. www.cee.vt.edu/ewr/environmental/teach/smprimer/icp/icp.html.

[Ula87] S. M. Ulam. *Stanislaw Ulam, 1909-1984*. Los Alamos National Laboratory, 1987.

[Uns00] Unscear, Sources. *effects of Ionizing Radiation*. United Nations, New York, 2000.

[Ven15] Y. Venegas-Argumedo and M, E. Montero-Cabrera *True coincidence summing corrections for an extended energy range HPGe detector*. AIP Conference Proceedings, 030004, 2015.

[Vid05] T. Vidmar and A. Likar. *Calculation of total efficiencies of extended samples for HPGe detectors*. Nuclear Instruments and Methods in Physics Research Section A: Accelerators, Spectrometers, Detectors and Associated Equipment, 251-254, 2005.

[Vla09] V. Vlachoudis and others. *FLAIR: a powerful but user friendly graphical interface for FLUKA*.Proc. Int. Conf. on Mathematics, Computational Methods & Reactor Physics), Saratoga Springs, New York, 3, 2009.

[Wey08] S. Weyer, A.D. Anbar, A. Gerdes, G.W. Gordon, T.J. Algeo and E.A. Boyle. *Natural fractionation of 238U/235U*. Geochimica et Cosmochimica Acta, 345-359, 2008.

[Wil98] T. Williams and C. Kelley. *Gnuplot*. An Interactive Ploting Program: Version 3.7, 1998.

[WNA19] World Nuclear Association. *Naturally-Occurring Radioactive Materials (NORM)*. Accessed [22.08.19]. www.world-nuclear.org/info/info30.html

[Zie99] R. A. Zielinski, J. K. Otton. *Naturally Occurring Radioactive Materials (NORM) in Produced Water and Oil-Field Equipment An Issue for the Energy Industry*. U. S. Geological Survey, 1999.